NASA CR-72792
UTC-2359

FINAL REPORT

DETERMINATION OF THE EFFECTS OF LIQUID INJECTANTS ON NOZZLE ABLATIVE PERFORMANCE

by L. G. Ross and C. A. Le Febvre

UNITED TECHNOLOGY CENTER
1050 E. Arques Avenue
Sunnyvale, California 94088

prepared for

NATIONAL AERONAUTICS AND SPACE ADMINISTRATION

December 31, 1970

CONTRACT NAS-3-13304

NASA Lewis Research Center
Cleveland, Ohio
J. J. Notardonato, Project Manager
Solid Rocket Technology Branch
Chemical Rocket Division

CONTENTS

ILLUSTRATIONS

ILLUSTRATIONS (Continued)

ILLUSTRATIONS (Continued)

ILLUSTRATIONS (Continued)

TABLES

ABBREVIATIONS

BDC	bottom dead center
d_p	port diameter
F_a	axial force
F_s	side force
ID	inside diameter
I_{sp}	specific impulse
I_{sp_s}	side force specific impulse
L	length
LITVC	liquid injectant thrust vector control
NASA	National Aeronautics and Space Administration
OD	outside diameter
PBAN	polybutadiene-acrylic acid-acrylonitrile
PM	manifold pressure
P/N	part number
S/N	specification number
TDC	top dead center
TVC	thrust vector control
W_a	propellant flow rate
W_s	injectant flow rate
ϵ or E	area ratio
ϵ_i or E_i	injection area ratio

ABSTRACT

The objective of this program was to evaluate the effect of liquid injectants on the ablative performance of low-cost nozzle materials.

Four candidate low-cost nozzle materials and a standard material were tested with two liquid injectants to determine liquid injectant thrust vector control (LITVC) ablation performance. Ten motor firings were successfully conducted, utilizing a 3.5-in. (0.089 m) throat diameter with average chamber pressures of 600 and 700 psia (4.5×10^6 N/m^2).

Conclusions are that the low-cost silicas, double thickness and vacuum bag cured, performed similarly to the higher cost standard material and are suitable for both thrust vector control (TVC) and non-TVC affected areas.

Liquid injection with low-cost materials, other than silica-based materials, increased the ablation severely to the point of non-use in TVC areas. In non-TVC areas, the materials also showed greater ablation at the higher test pressures due to the increased heat flux. The nonsilica-based materials are only suitable for greater expansion area ratios well downstream of injectant effects and at lower heat fluxes.

DETERMINATION OF THE EFFECTS OF LIQUID INJECTANTS ON NOZZLE ABLATIVE PERFORMANCE

By L. G. Ross and C. A. LeFebvre
United Technology Center

SUMMARY

The objectives of this program were to determine the effect of liquid injection on the ablative performance of low-cost nozzle materials, to measure TVC performance of the fluids used for injection, and to predict the 260-in. motor nozzle performance using LITVC with the best three nozzle materials evaluated.

To accomplish these objectives, 10 motor firings were conducted to evaluate the following nozzle materials and injectant fluids:

Materials

FM-5272	Crepe paper phenolic
KF-418[a]	Canvas duck phenolic
SP-8030-96	High silica double-weight phenolic
MXS-198	Silica epoxy novalac
FM-5504	High silica phenolic

Injectant Fluids

N_2O_4	Nitrogen tetroxide
CCL_2F-$CCLF_2$	Freon 113 grade TF

The nozzle materials were selected based upon previous promising performances on tests without LITVC. The highly reactive N_2O_4 and inert Freon injectants that were selected offered a wide range in performance based upon previous usage. They provide a range of ablation data suitable for interpolation with other TVC fluids.

All 10 tests were completed successfully, and all program objectives were accomplished.

The test motor employed a throat diameter of 3.5 in. (0.089 m), an expansion ratio of 6:1, an average pressure of 600 to 700 psia (4.5×10^6 N/m^2), a duration of 21 to 25 sec, and a PBAN propellant containing 16% aluminum. TVC injection was accomplished at area ratios of 2.5 and 3.5, at injectant to motor flow ratios

[a]Fiberite Corp. now refers to this material as MXK-418.

(W_s/W_a) from 0.011 to 0.045. These parameters were selected to provide meaningful scale-up data for larger size motors such as the 260-in.-diameter solid motor.

The candidate materials were screened with both N_2O_4 and Freon during the first six tests. The FM-5504 material, which is used for the exit cone of the UTC 120-in.-diameter motor nozzles, was tested under the same conditions to serve as a basis for comparison. Three materials were selected from the screening tests, FM-5272, SP-8030-96, and MXS-198. The KF-418 canvas duck phenolic was eliminated from further testing because of high chemical attack by the N_2O_4 injectant, poor ablation, and inconsistent erosion patterns.

The three remaining materials were then tested with N_2O_4 at a higher W_s/W_a of 0.045 at injection area ratios of 2.5 and 3.5. Also, one test was conducted with injection at two pressures to evaluate the effects of injection pressure on ablation.

TVC impulse performance was determined for both Freon and N_2O_4. Results agreed generally with published performance data for both fluids. At high injection flow rates with N_2O_4, a lower performance than expected was observed. This is attributed to the short length of the nozzle and incomplete reaction of the N_2O_4.

The ablation data from these tests were evaluated as a function of heat flux in the nozzle. Several important improvements were made in the analysis techniques to correlate the subscale data with 120-in. nozzle data. By accounting for the addition of rubber from the aft closure insulation, correlation with the standard silica material for this 3.5-in. (0.089 m)-diameter throat nozzle and the 37.7-in. (0.96 m)-diameter throat 120-in. motor nozzle was within 0.5 mil/sec (1.27×10^{-5} m/sec) rms for the non-TVC ablation.

Results of the non-TVC correlation are summarized in figure 1, indicating good performance of the selected silica-based material. Poor performance was observed with both FM-5272 and KF-418. Previous NASA results of these materials were satisfactory but they were obtained under lower heat flux (lower pressure) conditions. They could be suitable materials in larger expansion ratio (low heat flux) areas of large nozzles.

The TVC affected ablation results for the candidate materials showed that the low-cost silica materials, SP-8030-96 and MXS-198, are comparable to the standard silica, FM-5504, and that the crepe paper FM-5272 has approximately 3 times greater ablation and the canvas duck, KF-418, has approximately 10 times greater ablation. Predictions of the 260-in.-diameter nozzle employing these materials and using the LITVC duty cycle and baseline nozzle design presented in NASA Contract No. NAS 3-12040, resulted in the following:

FM-5504 - high silica (standard)	No increase in baseline nozzle liner thickness
SP-8030 - double weight silica	No increase in baseline nozzle liner thickness
MXS-198 - epoxy novalac silica	No increase in baseline nozzle liner thickness
FM-5272 - crepe paper phenolic	No increase in baseline nozzle liner thickness for area ratios above 5:1
KF-418 - canvas duck phenolic	Not acceptable for LITVC

The optimum 260-in. nozzle materials based on LITVC use would be MXS-198 from an area ratio of 2.5 to 5, and FM-5272 from 5 to 8.515.

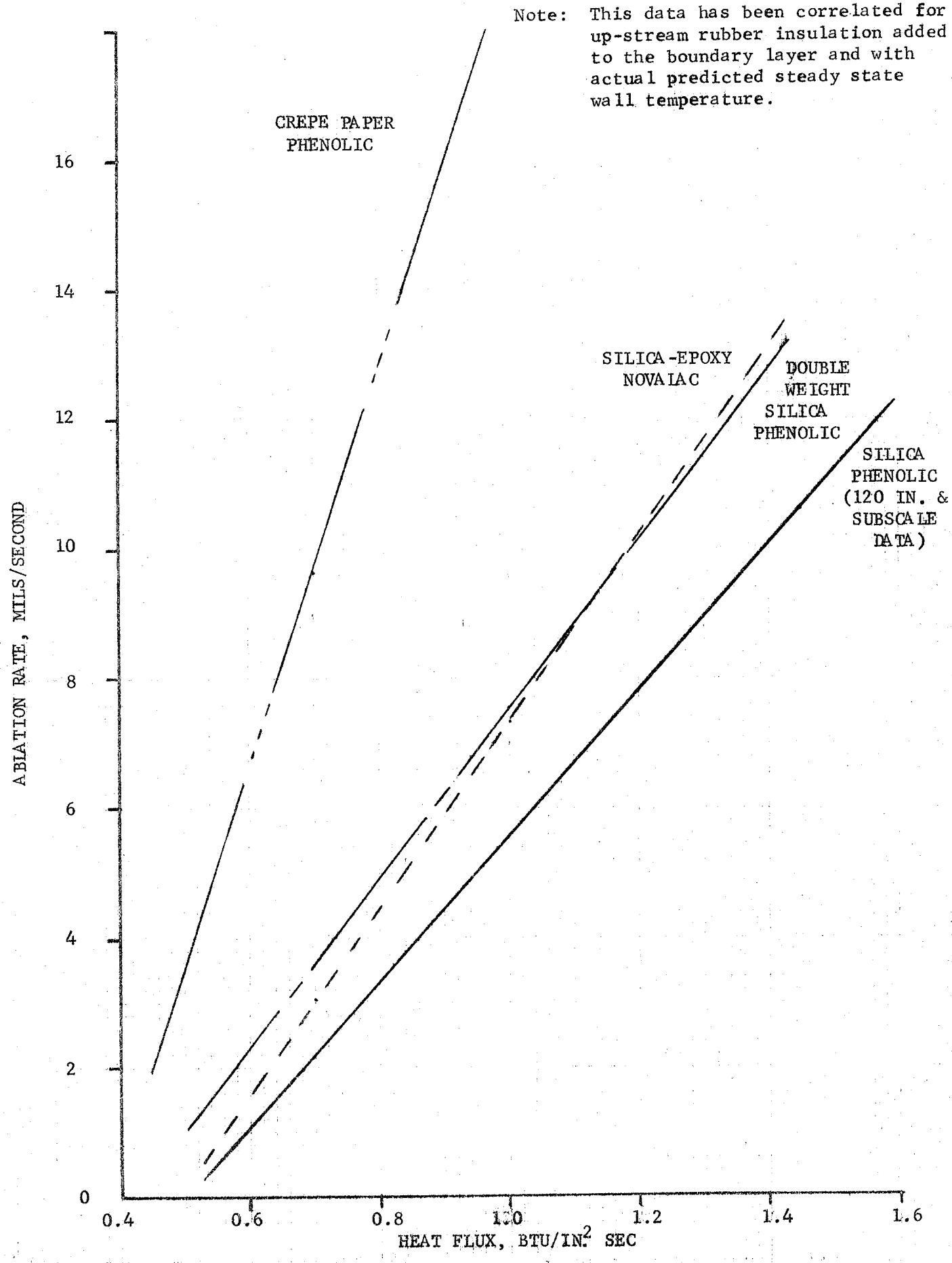

Figure 1. - Comparison of Non-TVC Ablation Rate

INTRODUCTION

The possibility of using LITVC for the 260-in.-diameter solid motor with new low-cost nozzle materials requires an accurate determination of LITVC performance, nozzle material ablation, and compatibility. A low-cost nozzle design study with LITVC must consider these effects on each of the candidate materials to allow accurate weight/cost tradeoffs to be made. The determination of the effects of liquid injectants on nozzle ablative performance was the prime objective of this program.

This contract, directed by NASA/Lewis Research Center, utilized candidate low-cost nozzle materials selected from previous NASA work for characterization with LITVC. The materials selected were (1) FM-5272 crepe paper-phenolic, (2) KF-418 canvas duck phenolic, (3) SP-8030 high silica double-weight phenolic, and (4) MXS-198 silica epoxy novalac.

The crepe paper phenolic and canvas duck phenolic were selected because of their low material costs. The high silica double-weight phenolic was selected because of the reduced wrapping time for large nozzles. The silica epoxy novalac cure system was selected because of its vacuum bag cure capability, eliminating the need for large autoclaves for a 260-in.-diameter motor nozzle. MXA-6012 asbestos phenolic was also considered but rejected based upon prefire erosion predictions.

To provide a correlation with large solid motor nozzle ablation with LITVC, FM-5504 high silica phenolic, a standard silica material currently used on the UTC 120-in.-diameter motor nozzle, was also specified for test.

Two injectants, N_2O_4 and Freon, were selected on the basis of a tradeoff study. The reactive N_2O_4 was selected because of high TVC performance and the availability of scale-up data from 120-in.-diameter motor firings. Inert Freon represented the minimum in expected ablation and TVC performance. These data allow interpolation of expected performance for other TVC fluids.

The program was conducted in two tasks: (1) Task I - Effects of Liquid Injectants on Ablative Performance and (2) Task II - Data Analysis.

Subtask 1.1 - Design and fabrication. - The test motor and nozzle were designed to meet the contract requirements. Fabrication of the test hardware was completed during this subtask.

Subtask 1.2 - Screening tests. - Each ablative material was evaluated with Freon and N_2O_4 to select the best three materials for further testing. To minimize the number of tests required to accomplish the program objectives, two separate materials were used in opposing 180° (3.14 rad) segments during the screening tests. Injection was accomplished in the center of each segment; flow rates were low enough to ensure that shock interactions did not occur with the opposite side of the nozzle. Side-force data were measured by staggering the flow time periods on opposite sides of the nozzle.

Subtask 1.3 - Material Verification Tests. - Three materials were evaluated with injection in two nozzle area ratios at higher injectant flow rates. Based on results from the first six tests, the materials selected for tests 7, 8, and 9 were SP-8030-96 high silica double-weight phenolic, MXS-198 silica epoxy novalac, and FM-5272 crepe paper phenolic. The injectant was N_2O_4.

The canvas duck phenolic material was eliminated from testing because of excessive chemical attack in the injection port areas and general excessive erosion. The N_2O_4 was selected as the remaining injectant based upon test results and a study considering side-force performance, cost, density, and compatibility with the nozzle materials.

An additional reduction in the number of tests required was accomplished by injecting in two areas ratios during the material verification tests. This resulted in a total of nine tests.

A tenth test was conducted to evaluate the effects of injection pressure on ablative performance. The material, injectant, and injection area ratio for the tenth test were FM-5272 crepe paper phenolic, N_2O_4, and 2.5, respectively. FM-5272 was selected because it was the lowest cost remaining material.

The test program requirements, including the selection of materials and injectants, are presented in table I. In the later tests, pressures were reduced to the minimum level specified for the 260-in.-diameter motor because of severe erosion experienced with KF-418 and FM-5272 in the higher heat fluxes of the early tests.

TEST CONFIGURATION

The test configuration consisted of a standard UTC 3-TM-3A test motor utilizing a fully developed PBAN propellant, a subscale nozzle based on 260-in. design criteria and a large solid-type TVC configuration. A description of each major area is presented in the following sections.

Motor Design

The following requirements for the solid motor-nozzle combination were selected to provide meaningful subscale data applicable to the 260-in.-diameter motor:

		SI units
Throat diameter, in.	3.5 minimum	0.0889 m
Expansion ratio	6:1	6:1
Chamber pressure, average, psig	600±50	4,136,880 N/m^2
Action time, sec	25 minimum	25 sec
Propellant aluminum content	15±1% (wt)	15%
Propellant combustion temperature, °F	5,800±200	3,477°K
Propellant type	PBAN	PBAN

Test No.	Nozzle exit cone material		Injectant fluid	Injectant flow rate to motor flow rate		Injectant area ratio		Injectant pressure psi (N/m^2)		Average chamber pressure psi (N/m^2)
	Quad I	Quad III		Quad I	Quad III	Quad I	Quad III	Quad I	Quad III	
6101	FM-5505	FM-5504	Freon 113	0.0136	0.0246	2.5	2.5	765 (5.25×10^6)	730 (5.02×10^6)	681 (4.7×10^6)
6102	FM-5272	KF-418	Freon 113	0.0130	0.0121	2.5	2.5	765 (5.25×10^6)	760 (5.2×10^6)	695 (4.77×10^6)
6103	MXS-198	SP-8030	Freon 113	0.0135	0.0118	2.5	2.5	780 (5.36×10^6)	770 (5.3×10^6)	692 (4.77×10^6)
6104	FM-5504	FM-5504	N_2O_4	0.0135	0.0240	2.5	2.5	830 (5.7×10^6)	810 (5.58×10^6)	685 (4.71×10^6)
6105	KF-418	FM-5272	N_2O_4	0.0135	0.0123	2.5	2.5	828 (5.7×10^6)	825 (5.67×10^6)	689 (4.75×10^6)
6106	MXS-198	SP-8030	N_2O_4	0.0135	0.0120	2.5	2.5	820 (5.65×10^6)	810 (5.58×10^6)	691 (4.77×10^6)
6107	SP-8030	SP-8030	N_2O_4	0.0447	0.0426	2.5	2.5	735 (5.05×10^6)	725 (5×10^6)	603 (4.15×10^6)
6108	MXS-198	MXS-198	N_2O_4	0.0435	0.0449	2.5	2.5	732 (5.05×10^6)	708 (4.88×10^6)	608 (4.17×10^6)
6109	FM-5272	FM-5272	N_2O_4	0.0435	0.0457	2.5	2.5	730 (5.02×10^6)	718 (4.95×10^6)	604 (4.15×10^6)
6110	FM-5272	FM-5272	N_2O_4	0.0137	0.0137	2.5	2.5	720 (4.95×10^6)	280 (1.93×10^6)	606 (4.16×10^6)

TABLE I. - TEST CONDITION SUMMARY

The test motor selected to meet these requirements utilized standard heavyweight hardware with a fully developed propellant, UTP-3096. The characteristics of this propellant are presented in table II.

The test hardware consists of heavyweight steel cases and end closures, designated TM-3. A three-segment grain was designed to attain the required pressure and burning time with a 3.5-in. (0.0889 m)-diameter throat. The grain consists of a cylindrical, radially slotted, internal-burning geometry with a bore diameter of 8 in. (0.2 m). The predicted pressure-time history is slightly progressive-regressive. The two radial slots in the grain with one face restricted offsets the progressivity of the internal-burning cylinder.

The test motor design is shown in figure 2. Ignition of the test motor was accomplished using a standard TM-3 bag igniter containing 125 g of $BKNO_3$ pellets with dual 207A squibs. The igniter was installed in the center of the motor on the grain surface.

The motor cases were insulated with silica-loaded Buna-N rubber, sized for two firings to reduce processing costs. The forward closures were insulated with Gen Gard V-61 and were used for two firings without reprocessing. The aft closures utilized ORCO-9250, a silica/asbestos Buna-N rubber insulation, and were refurbished for each firing.

The propellant grain design was stress analyzed for loads arising during environmental extremes. The resulting stress-strain fields were compared with time- and temperature-dependent failure criteria based on measured allowables. The resulting margins of safety are ample, as would be expected from the grain stress integrity observed in previous TM-3 firings with identical grain configurations. The lowest margin of safety is 3.09, which is associated with bore cracking at midgrain during firing at 40°F (278°K).

LITVC Nozzle Design

The subscale LITVC nozzle was designed to simulate exit cone conditions of a full-scale 260-in.-diameter nozzle. This design utilized the required materials and full-scale nozzle fabrication techniques in addition to nozzle geometry to ensure that LITVC ablation can be scaled to a 260-in.-diameter nozzle design. The subscale nozzle is shown in figure 3. Expansion area ratios and nozzle half angle of 17.5° (3.27 rad) from the throat extension to the exit plane have been utilized as planned in the full-scale 260-in.-diameter motor nozzle to allow TVC performance scaleup of the measured data.

A throat with a 3.5-in. (0.0889 m)-diameter was used, which provides adequate subscale data and allows UTC to utilize a proven subscale test motor. A heavyweight nozzle shell was used to maintain ablative plastic structural loads or strain levels at relatively low levels which are typical of large nozzles; i.e., less than 0.0015 in./in.

TABLE II. - CHARACTERISTICS OF UTP-3096 PROPELLANT

Composition, wt %		
		SI Units
Aluminum	16	-
AP	68	-
PBAN	16	-
Ballistic properties		
Burning rate (1,000 psi), in./sec	0.217	0.0055 m/sec
Pressure exponent	0.18	-
Pressure sensitivity to temperature, $\%^{o}F$	0.13	-
Flame temperature, ^{o}F	5,600	3,367^{o}K
Characteristic velocity, ft/sec	5,050	1,539 m/sec
Density, $lb/in.^3$	0.063	17,100 N/m^3
Specific impulse (standard), sec	246	-

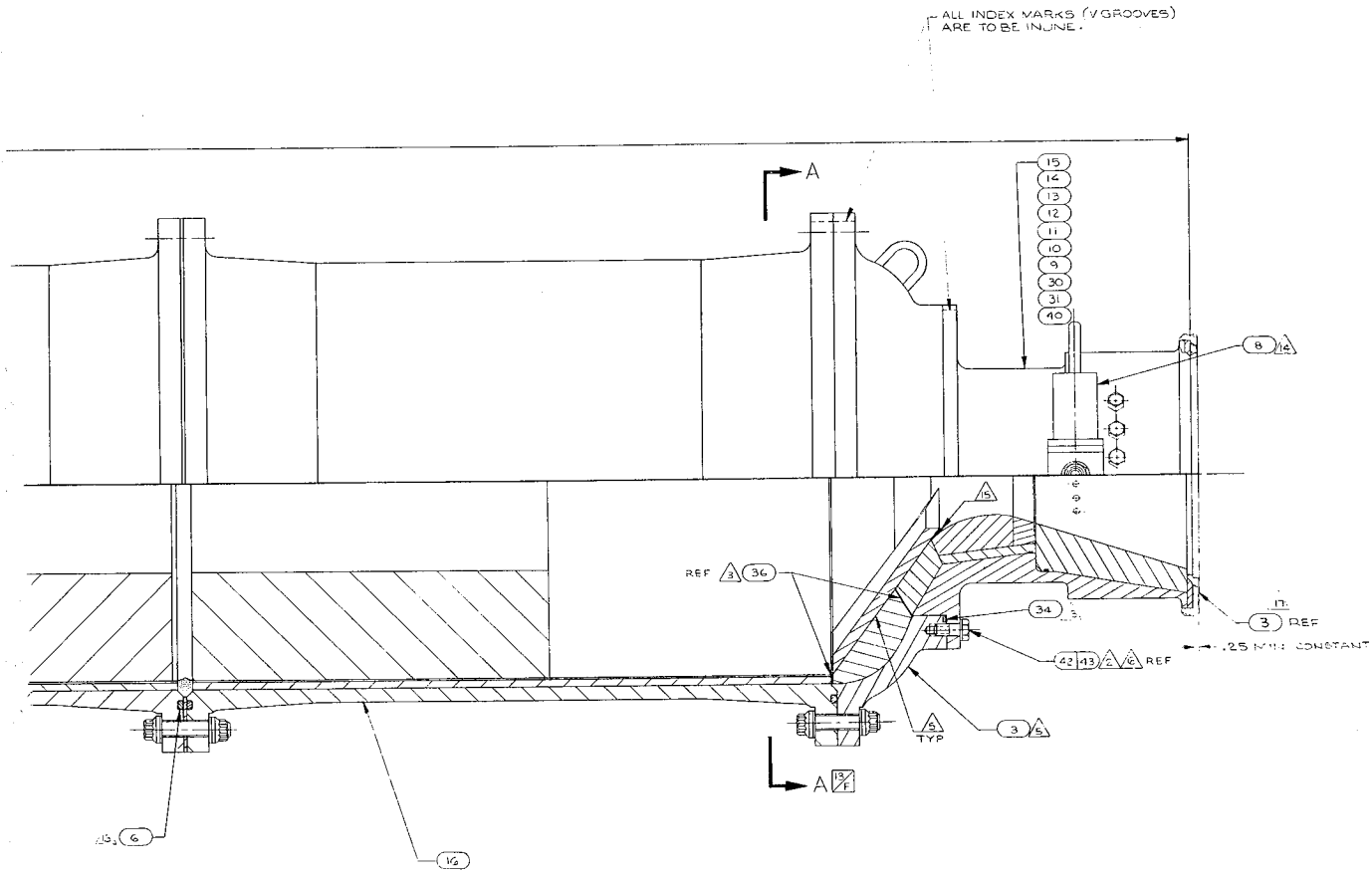
ALL INDEX MARKS (V GROOVES) ARE TO BE IN LINE.
A
15
14
13
12
11
10
9
30
31
40
8
14
15
REF
3
36
34
3
17
3
REF
42
43
C
V6
REF
.25 MIN CONSTANT
6
TYP
3
5
A
13
F
13
6
16

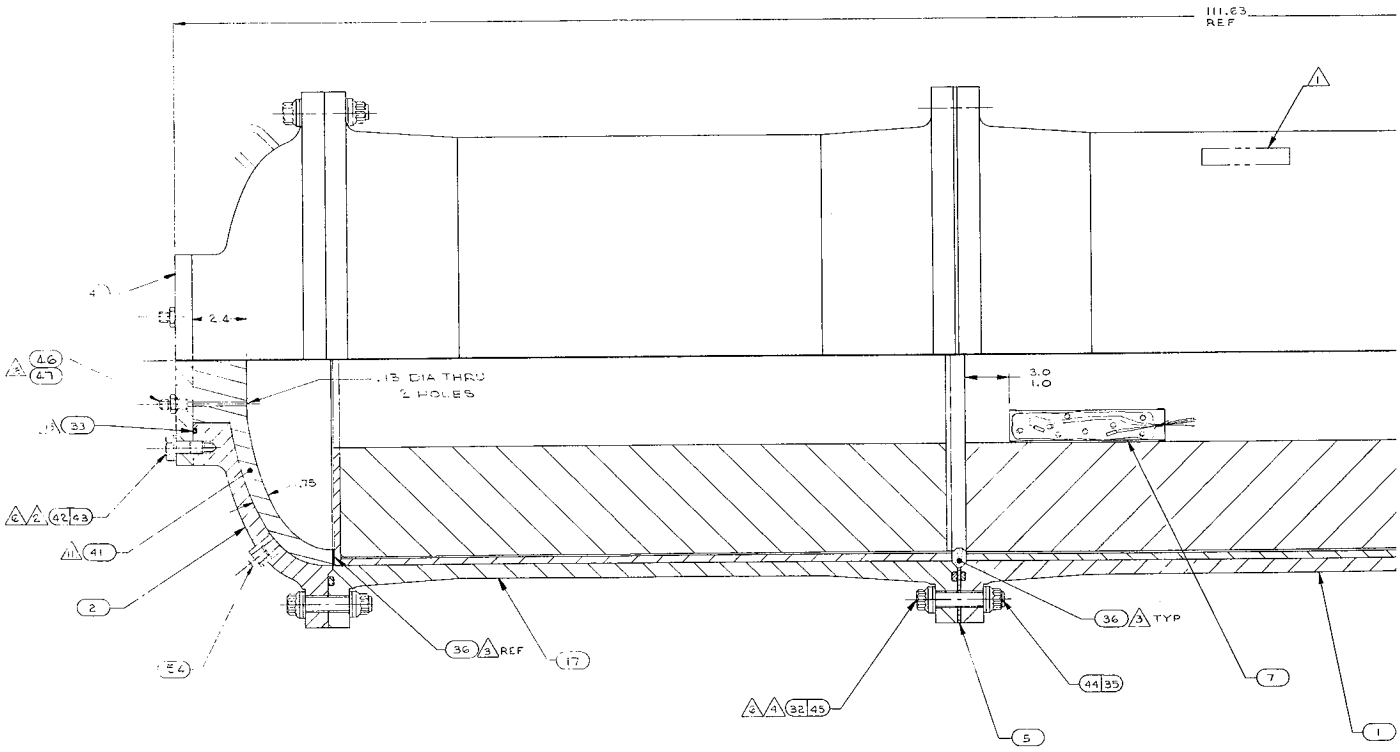

Figure 2. - 3-TM-3A Test Motor

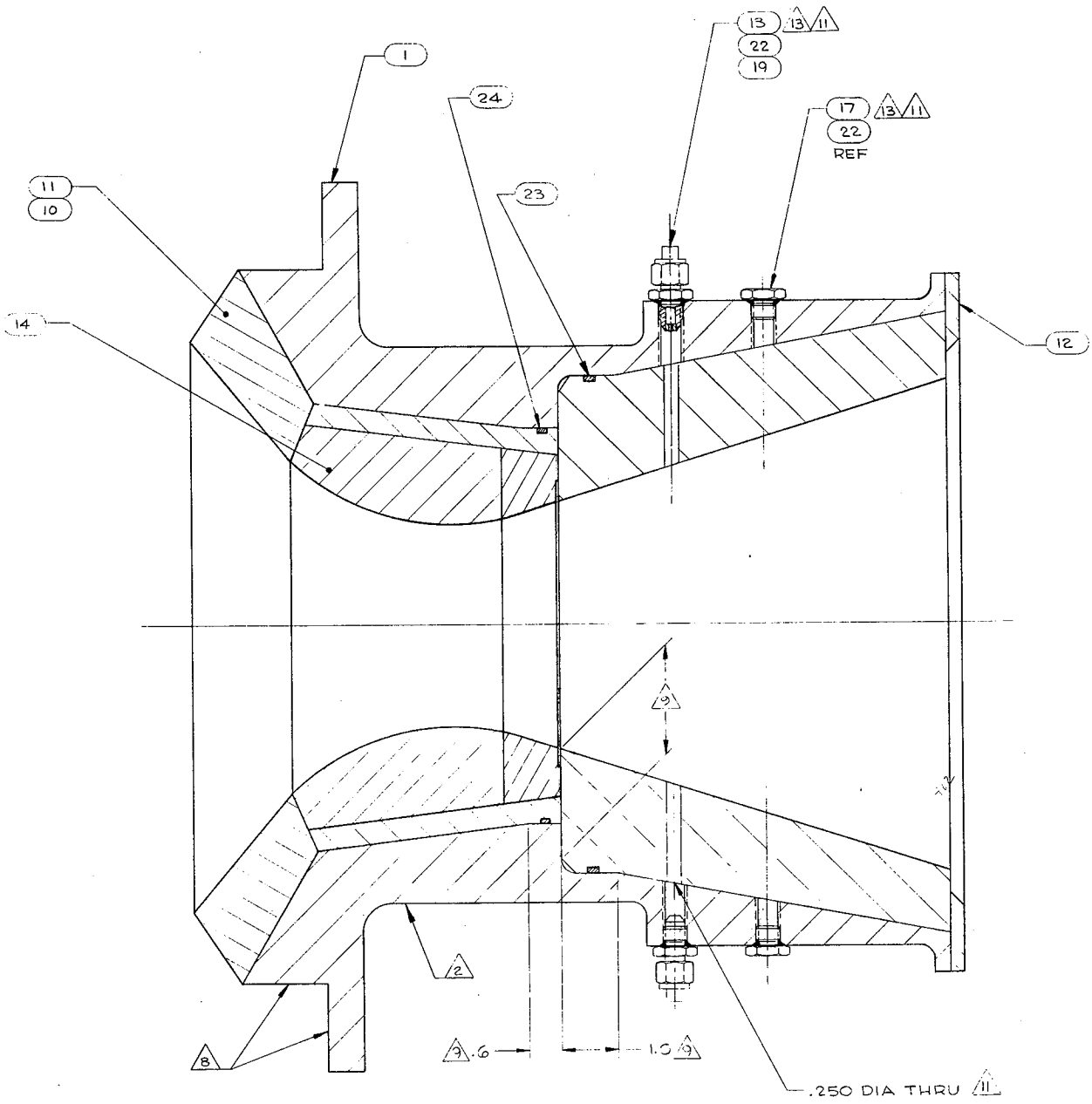

Figure 3. - LITVC Subscale Nozzle

The subscale nozzle utilizes a silica phenolic entrance cap, graphite throat, carbon phenolic throat extension, silica phenolic throat backup, and the candidate material exit cones.

The nozzle entrance is insulated with molded MX-2625 0.5- by 0.5-in. (0.0127- by 0.0127 m) chopped squares of high silica phenolic molding compound. The nozzle entrance insulator, which provides the housing with a thermo and ablative protection, covers an area ratio of 10.1:1 to 3.3:1 (subsonic).

An ablative throat was considered; however, a molded Speer 8882 graphite material was used because of the problems in fabricating a small bias-wrapped structure indicative of the full-scale design.

A throat extension ring using full-scale materials (MX-4926) carbon phenolic and flat-laminate fabrication techniques were used to simulate the full-scale flow conditions and interface into the exit cone liners.

The exit cone liner test section of interest extended from an expansion area ratio of 1.5 to 6. All exit cone liners were tapewrapped parallel to centerline to provide ablation results comparable to full-scale nozzles.

The material which was used as a standard of comparison in the exit cone was FM-5504 high silica phenolic in accordance with UTC specification 4MDS-40722. This material was selected because of extensive use in the UTC 120-in.-diameter LITVC motor firings. The four candidate low-cost materials utilized for exit cones are as follows:

Material	Manufacturer	UTC Specification No.
MXS-198 silica epoxy novalac	Fiberite Corp.	SE0308
SP-8030-96 high silica double-weight phenolic	Armor Co.	SE0302
FM-5272 crepe paper phenolic	U.S. Polymermic Co.	SE0301
KF-418 canvas duck phenolic	Fiberite Corp.	SE0300

The exit cone liner thickness design was based on the predicted ablation when experiencing the severest liquid injection condition as shown in figure 4.

One low-cost candidate exit cone material, MXA-6012 asbestos phenolic, was eliminated from testing because early analysis of this material, based upon results from Contract No. NAS 3-10288, revealed that the erosion rate would be of such high magnitude that it would be impractical to design with it as an ablative exit cone liner. The predicted ablation with LITVC is shown in figure 5.

To conserve the number of test firings and amount of hardware used while still obtaining required data for evaluation, the candidate exit cone liners were split along centerline at TDC and BDC; the prefinished half cones of

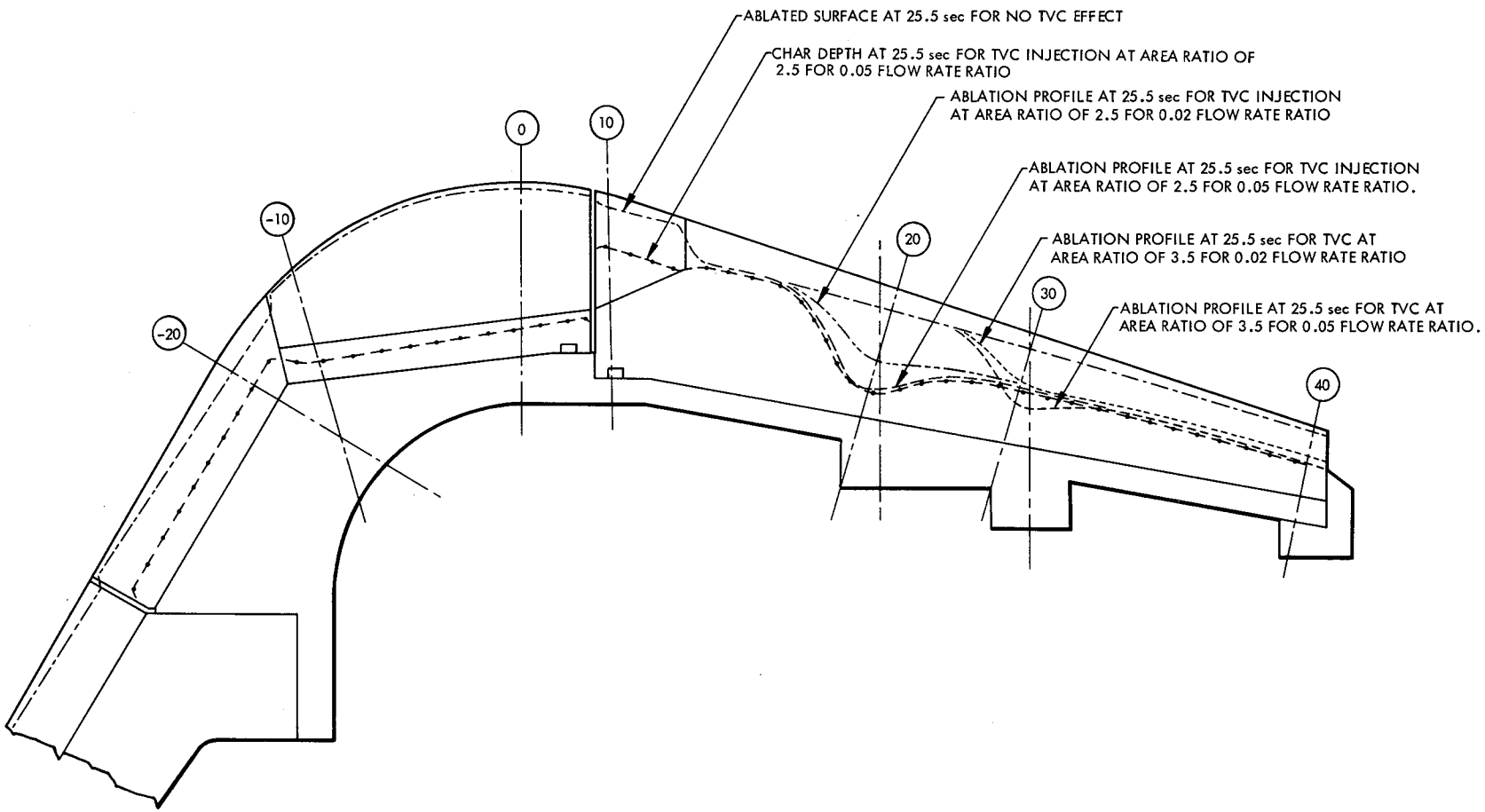

Figure 4. - Predicted Nozzle Ablation Profiles

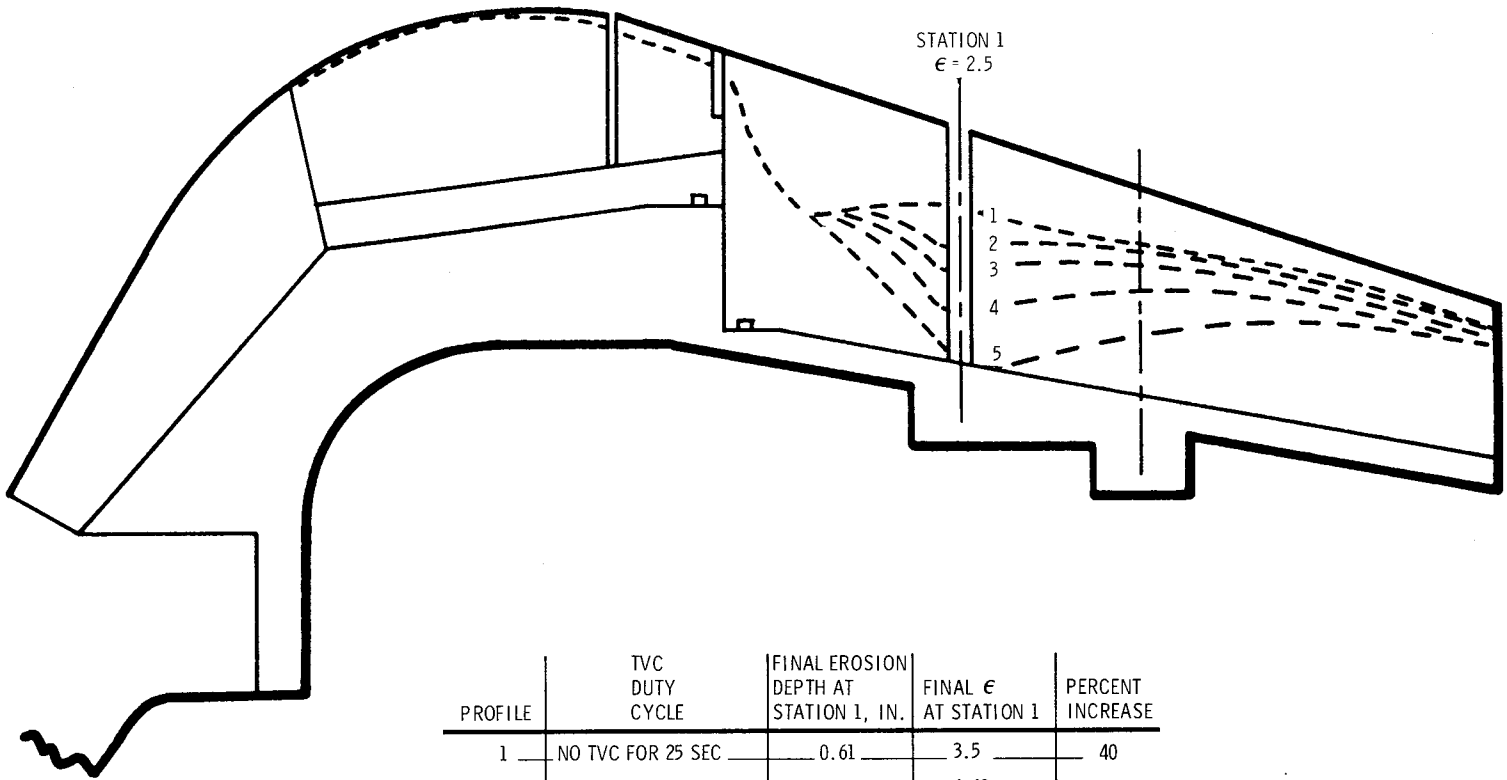

PROFILE	TVC DUTY CYCLE	FINAL EROSION DEPTH AT STATION 1, IN.	FINAL ϵ AT STATION 1	PERCENT INCREASE
1	NO TVC FOR 25 SEC	0.61	3.5	40
2	0.01 W_s/W_a FOR 10 SEC	0.94	4.43	77
3	0.02 W_s/W_a FOR 10 SEC	1.13	4.90	96
4	0.01 W_s/W_a FOR 25 SEC	1.42	5.70	128
5	0.02 W_s/W_a FOR 25 SEC	1.93	7.0 (MATERIAL REMOVED TO SHELL WALL)	180

Figure 5. - Predicted Ablation of MXA-6012 Asbestos Phenolic

different candidate materials were reassembled, bonded together, and final machined in the following parts: (1) MXS-198 silica epoxy novalac/SP-8030-96 high silica double-weight phenolic and (2) FM-5272 crepe paper phenolic/ MXK-418 canvas duck phenolic.

The nozzle/aft closure housing was designed with 1018-1030 low-carbon steel. The walls of the housing were designed to be extra thick to allow for refurbishing and reuse without any warpage or deformaties taking place during firing or disassembly. The exit cone portion of the housing completely supports the exit cone liner and is flanged at the exit plane to utilize a retaining ring.

TVC System Design

The test nozzle LITVC configuration was designed to simulate the injectant flow conditions which are characteristic of large rocket motor LITVC systems. The test nozzle design employed a 17.5° (0.327 rad) half angle, 6:1 expansion nozzle, and TVC injection at expansion area ratios of 2.5 and 3.5.

To utilize empirical scale-up criteria developed by UTC, the same successful injection geometry configuration that was used for the 120-in.-diameter motor was used on this program. This includes six equally spaced injection ports located in a 75° (1.31 rad) quadrant section with an injectant supply pressure of 750 psia ($5{,}170{,}500$ N/m^2). Two injection area ratios, 2.5 and 3.5, were used to allow extrapolation of performance to other injection area ratios, if needed.

The injection port characteristics were designed in accordance with common practice utilized on previous subscale and full-scale programs at UTC. The flow of injectant is regulated by calibrated orifices made from standard AN 815 unions (see figure 6). The orifices were reamed and deburred to assure uniform flow and good stream solidity characteristics. All orifices were precalibrated at a given ΔP to verify desired flow rate, equivalent flow from all orifices, and adequate flow solidity which is important in determining quadrant TVC performance.

The port sizing downstream of the injectant orifices was selected to simulate orifice-to-nozzle entrance port area ratios, port diameters, and L/dp ratios equivalent to that used in 120-in.-diameter motors and subscale configuration. Orifice diameters were calculated to provide the desired test flow rate ratios of table III, where W_s is the average injectant rate and W_a is the average propellant flow rate. An average W_a of 37.8 lb/sec (17.12 kg/sec) and an average aft stagnation chamber pressure of 610 psia (4.2×10^6 N/m^2) were used. Isentropic nozzle pressures at $\epsilon = 2.5$ and $\epsilon = 3.5$ are 53.0 and 32.7 psia (2.5×10^5 N/m^2), which results in a gas specific heat ratio of 1.18. The pressure increase due to TVC at the test values of W_s/W_a was calculated from the characteristic nozzle backpressure functions developed during the 120-in.-diameter motor program. Actual flow rates were measured during the tests using flow meters and were as predicted.

TABLE III. - TVC GEOMETRY SUMMARY

Injection Orifice Diameters			
		Orifice diameter	
Fluid	W_s/W_a	in.	m
Freon	0.013	0.028	0.0007
Freon	0.025	0.038	0.00096
N_2O_4	0.013	0.028	0.0007
N_2O_4	0.025	0.038	0.0096
N_2O_4	0.045	0.055	0.0014

L/dp ratio		
Nozzle injection	Injectant port L/dp	
	T=0	T=25 sec
2.5	5.6	2.0
3.5	5.0	2.5

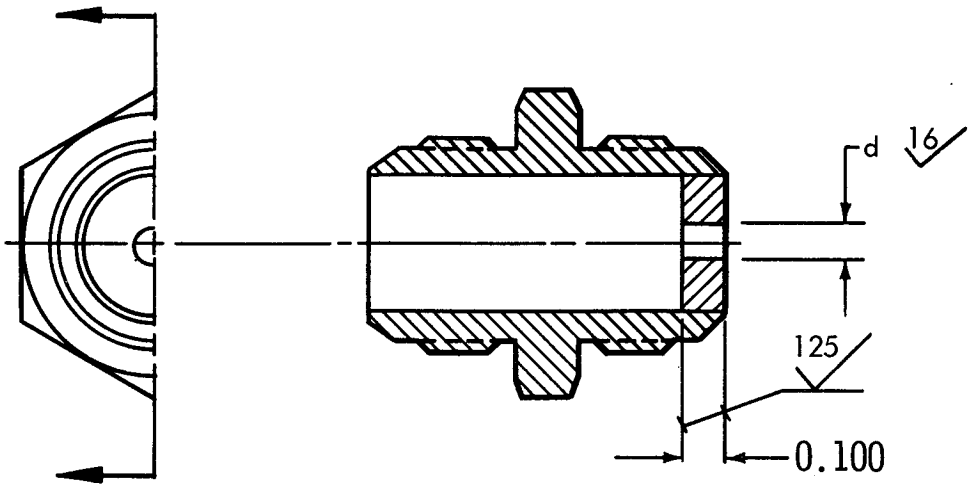

Figure 6. - LITVC Subscale Injectant Orifice

The resultant injectant port L/dp varies as the liner ablates and brackets the 120-in.-diameter motor nozzle values of 4.7 to 3.2.

FABRICATION

All test hardware, except the nozzle exit cones, were fabricated by UTC according to design requirements and standard propellant processing procedures. Fabrication of the exit cones was performed by recognized nozzle manufacturers who have demonstrated experience with similar materials. Because determining the ablative performance of the candidate materials was the prime objective of the program, fabrication details for the exit cones are presented.

Specifications for each candidate were prepared for both material and fabrication to ensure controlled conditions for fabrication. The standard material was procured and fabricated in accordance with its 120-in.-diameter motor specification. The detailed specifications are presented in table IV.

Two sources of exit cones were used during the program. The liners for the screening test nozzles were fabricated by Swedlow, Inc., Garden Grove, California. The liners for the material verification tests were fabricated by Edler Industries, Costa Mesa, California. Both suppliers used the same material and fabrication specifications and the same tooling.

TABLE IV. - EXIT CONE FABRICATION SPECIFICATIONS

Specification	Title
UTC SE0300	Tape, Canvas Duck, Phenolic Resin Impregnated
UTC SE0306	Insulation, Canvas Duck Reinforced Plastic, Fabrication of
UTC SE0301	Tape, Creped Kraft Paper, Phenolic Resin Impregnated
UTC SE0303	Insulation, Kraft Paper Reinforced Plastic, Fabrication of
UTC SE0302	Tape, Doubleweight High-Silica Cloth, Phenolic Resin Impregnated
UTC SE0304	Insulation, High-Silica Doubleweight Reinforced Plastic, Fabrication of
UTC SE0308	Tape, Silica Cloth, Epoxy-Novalac Resin Impregnated
UTC SE0305	Insulation, Silica Tape Reinforced Epoxy-Novalac Plastic, Fabrication of
4MDS-40722	Tape, High Silica Cloth, Phenolic Resin Impregnated
UTC SE0062	Insulation, High-Silica Reinforced Plastic, Fabrication of

Fabrication of Liners for Screening Test Nozzles
By Swedlow Inc.

FM-5504 high silica phenolic 7-in. (0.178 m)-wide tape. - This material, the standard for this program, was used to fabricate the liner in accordance with existing UTC specifications. Warp tape was wrapped on a solid steel conical mandrel parallel to centerline with sufficient material overage for tag-end properties testing. A test panel was layed up after completion of the wrapping procedure, and prepared with the wrapped preform for a 1,000-psi (6,894,000 N/m^2) hydroclave cure. After completion of the cure cycle, the preform was stripped of the rubber bags and bleeder cloth and sent to the machine shop for final machining.

MXS-198 silica epoxy novalac 7-in. (0.178 m)-wide tape. - Warp tape material was wrapped parallel to centerline on a solid steel conical mandrel, with controlled billet temperature of 90° to 110° (308°K). After wrapping, bleeder cloth was applied, and the assembly was encased in a vacuum bag and cured with a previously layed-up test panel in an air circulating oven.

KF-418 canvas duck phenolic 7-in. (0.178 m)-wide tape. - This material was purchased and fabricated in accordance with UTC specifications. Moderate tape temperature achieved good tack during the wrapping procedure, and billet temperature was held to 90° to 110° (308°K) without additional external cooling systems. After completion of the wrap, the preform and a layed-up test panel was vacuum bag cured in an autoclave. The material machined easily but appeared porous. This phenomenon was attributed to the canvas duck reinforcement, since the alcohol test did not reveal any discrepancies such as cracks, delaminations, or voids. After tag-end and test panel results were obtained, the liner was accepted.

FM-5272 crepe paper phenolic 7-in.- (0.178 m)-wide tape. - The complete lack of tack inherent in this material did not affect the wrapping procedures in the fabrication of an exit cone liner preform. However, the low material thickness increased the wrapping time considerably more than standard silica products and was very time-consuming when compared to the double-weight silica. After the wrap was completed and the test panel prepared, both items were vacuum bag cured in an autoclave.

Because of a high coefficient of thermal expansion, the preform was removed from the mandrel at a high temperature (180° to 200°) (357°K) to prevent freezing to the mandrel and cracking due to material shrinkage. The preform was immediately placed in an oven set at 200°F (360°K) and allowed to cool to room temperature by reducing the temperature 20° (264°K) per hour. Upon acceptance of tag-end and test panel results, the liner was accepted.

SP-8030-96 high silica double-weight phenolic 7-in. (0.178 m)-wide tape. - This material was easy to handle and wrapped without difficulty using moderately low temperature to produce proper tack. Wrapping speed can be increased over conventional materials without hindering product quality. The increased wrapping speed did not produce distortions in the fabric as expected, but seemed to smooth out any anomaly that attempted to start. The preform along with a test

panel was cured in an autoclave. Upon acceptance of tag-end and test panel results, the liner was accepted.

UTC considers that all materials processed satisfactorily and are suitable for large solid rocket nozzle manufacture. However, several of the low-cost materials did not perform as well as expected in non-TVC areas. To obtain representative data of the candidate materials as fabricated, similar to large motor nozzles, Edler Industries was selected to manufacture the remaining four nozzles. Edler Industries was selected because of their suggested modified cure cycles and their previous experience with the materials involved.

Fabrication of Liners for Material Verification Tests By Edler Industries

SP-8030-96 high silica double-weight phenolic. - No problems were encountered in the fabrication of the preform billet with this material. Wrapping speed changes during the fabrication process had no effect on tacking or material handling. The preform and the test panel were vacuum bag autoclave cured. The short cure cycle did not affect physical or mechanical properties of this material.

FM-5272 crepe paper phenolic. - This material was wrapped without difficulty. The preform and the test panel were vacuum bag autoclave cured. To prevent the preform from freezing to the mandrel or cracking during cooldown, the preform was removed at a higher temperature (180° to 200°F) (357°K) and placed in an oven for a long-duration cooldown to room temperature. The short cure cycle did not affect physical or mechanical properties requirements.

MXS-198 silica epoxy novalac. - This material posed no problems during the fabrication process. However, the short time period (2 hr at 210°F) (370°K) to drive off volatiles appeared to be insufficient and some delaminations occurred at the forward end of the liner. New material was ordered but it contained a higher volatile content which was not in accordance with UTC specifications. There was insufficient time to reorder new material to specification and remake the part; consequently the original liner was used.

Cure cycles used by Swedlow Inc. and Edler Industries are summarized in table V. The screening nozzle physical test summary is presented in table VI, and the material verification nozzle physical summary is presented in table VII.

TESTING

Ten tests were conducted in two phases to evaluate the LITVC effects on material ablation in the nozzle. The first phase consisted of six screening tests to evaluate each material with N_2O_4 and Freon at low injection flow rates. The best three materials were then tested in the second phase with N_2O_4 at higher flow rates and two injection area ratios. All testing was conducted in test bay ST 1-3 at the UTC Development Center, Coyote, California. The test

TABLE V. - EXIT CONE CURE CYCLES

Material	Cure temperature		Cure duration, hr	Cure pressure	
	^{o}F	^{o}K		psi	N/m^2
SWEDLOW, INC.					
KF-418	180 300	325 418	3.5 4.5	225	1,550,000
FM-5272	180 325	352 432	4.0 4.0	225	1,550,000
MXS-198	180 325	352 432	2.0 3.0	Vacuum bag pressure	
SP-8030-96	180 225 250 340	352 377 390 440	3.0 2.0 3.0 1.5	225	1,550,000
FM-5504	180 310 310	352 424 424	2.0 1.5 4.0	1,000	6,894,000
EDLER INDUSTRIES					
FM-5272	210 310	368 424	2.0 3.0	225	1,550,000
MXS-198	210 310	368 424	2.0 3.0	Vacuum bag pressure	
SP-8030-96	210 310	368 424	2.0 3.0	225	1,550,000

P/N C06300-01-01 S/N SWU 104 FM-5504 Test 6101		
Test	Requirement	Actual Value
Tensile strength	10,000 psi min (6.89×10^7 N/m^2)	14,640 (10^8 N/m^2)
Degree of cure	> 99.5%	99.796%
Density	105 lb/ft^3 min (1,689 kg/m^3)	106.5 lb/ft^3 (1,704 kg/m^3)
P/N C06300-01-01 S/N SWU 105 FM-5504 Test 6104		
Test	Requirement	Actual Value
Tensile strength	10,000 psi min (6.89×10^7 N/m^2)	16,030 (11×10^7 N/m^2)
Degree of cure	> 99.5%	99.775%
Density	105 lb/ft^3 min (1,689 kg/m^3)	107.7 lb/ft^3 (1,723 kg/m^3)
P/N C06300-06-01 S/N SWU 101 KF-418/FM-5272 Test 6102		
KF-418		
Test	Requirement	Actual Value
Tensile strength	5,000 psi min (3.44×10^7 N/m^2)	6,846 (4.7×10^7 N/m^2)
Degree of cure	> 99.5%	99.33%
Density	81 lb/ft^3 (1,296 kg/m^3)	78.8 lb/ft^3 (1,260 kg/m^3)
FM-5272		
Test	Requirement	Actual Value
Tensile strength	8,000 psi min (5.5×10^7 N/m^2)	13,223 (9×10^7 N/m^2)
Degree of cure	> 99.5%	99.566%
Density	82 lb/ft^3 (1,312 kg/m^3)	82.4 lb/ft^3 (1,318 kg/m^3)
P/N C06300-06-01 S/N SWU 102 KF-418/FM-5272 Test 6105		
KF-418		
Test	Requirement	Actual Value
Tensile strength	5,000 psi min (3.44×10^7 N/m^3)	13,500 (9×10^7 N/m^2)
Degree of cure	> 99.5%	99.398%
Density	81 lb/ft^3 (1,296 kg/m^3)	82 lb/ft^3 (1,312 kg/m^3)

TABLE VI. - PHYSICAL PROPERTIES SUMMARY

(Screening Nozzle Physical Test Summary)

FM-5272		
Test	Requirement	Actual Value
Tensile strength	8,000 psi min (5.5×10^7 N/m^2)	8,720 (6×10^7 N/m^2)
Degree of cure	> 99.5%	99.471%
Density	87 lb/ft^3 (1,312 kg/m^3)	82 lb/ft^3 (1,312 kg/m^3)
P/N C06300-07-01 S/N SWU 102 SP-8030/MXS-198 Test 6103		
SP-8030		
Test	Requirement	Actual Value
Tensile strength	10,000 psi min (6.89×10^7 N/m^2)	12,378 (8.5×10^7 N/m^2)
Degree of cure	> 99.5%	99.530%
Density	105 lb/ft^3 (1,680 kg/m^3)	103.5 lb/ft^3 (1,656 kg/m^3)
MXS-198		
Test	Requirement	Actual Value
Tensile strength	15,000 psi min (10^8 N/m^2)	18,150 (1.2×10^8 N/m^2)
Degree of cure	> 99.5%	99.735%
Density	93.6 lb/ft^3 (1,497 kg/m^3)	98.6 lb/ft^3 (15N kg/m^3)
P/N C06300-07-01 S/N SWU 103 SP-8030/MXS-198 Test 6106		
SP-8030-96		
Test	Requirement	Actual Value
Tensile strength	10,000 psi min (6.89×10^7 N/m^2)	13,188
Degree of cure	> 99.5%	99.782%
Density	105 lb/ft^3 (1,680 kg/m^3)	104 lb/ft^3 (1,664 kg/m^3)
MXS-198		
Test	Requirement	Actual Value
Tensile strength	15,000 psi min (10^8 N/m^2)	18,150
Degree of cure	> 99.5%	99.735%
Density	93.6 lb/ft^3 (1,497 kg/m^3)	98.6 lb/ft^3 (1,577 kg/m^3)

TABLE VI. - PHYSICAL PROPERTIES SUMMARY (Continued)

P/N C06300-04-01 S/N E-0033-0-1 SP-8030-96 Test 6107		
Test	Requirement	Actual Value
Tensile strength	10,000 psi min (6.89×10^7 N/m^2)	10,543 (7.23×10^7 N/m^2)
Acetone extraction	.5% max	.43%
Density	105 lb/ft^3 (1,689 kg/m^3)	109.2 lb/ft^3 (1,747 kg/m^3)
P/N C06300-05-01 S/N E-0034-0-1 MXS-198 Test 6108		
Test	Requirement	Actual Value
Tensile strength	15,000 psi min (10^8 N/m^2)	15,351 (1.06×10^8 N/m^2)
Acetone extraction	.5% max	.11%
Density	93.6 lb/ft^3 (1,497 kg/m^3)	93.6 lb/ft^3 (1,497 kg/m^3)
P/N C06300-03-01 S/N E-032-0-1 FM-5272 Test 6109		
Test	Requirement	Actual Value
Tensile strength	8,000 psi min (5.5×10^7 N/m^2)	8,006 (5.5×10^7 N/m^2)
Acetone extraction	.5% max	.5%
Density	82 lb/ft^3 (1,312 kg/m^3)	82 lb/ft^3 (1,312 kg/m^3)
P/N C06300-03-01 S/N E-0032-0-2 FM-5272 Test 6110		
Test	Requirement	Actual Value
Tensile strength	8,000 psi min (5.5×10^7 N/m^2)	8,110 (5.6×10^7 N/m^2)
Acetone extraction	.5% max	.41%
Density	82 lb/ft^3 (1,312 kg/m^3)	82 lb/ft^3 (1,312 kg/m^3)

TABLE VII. - MATERIAL VERIFICATION NOZZLE PHYSICAL TEST SUMMARY

facility consists of a multicomponent test stand, a portable fluid supply system, and associated data recording and controls. Instrumentation used during the tests is described in table VIII.

Test Facility

Force stand. - The motors were test fired in a six-component force stand instrumented to measure three force components: axial, forward side, and aft side. The vertical legs of the stand were flexured to allow motor movement during the test. The test motor is shown installed in the stand in figures 7 and 8. The side force and the axial force load cells are shown. Capability for calibrating the stand is provided in both the axial direction and side plane.

The forward and aft sections of the stand are connected by a lightweight cradle which maintains alignment from test to test. The motor is installed by attaching the forward closure to the axial thrust pylon and setting the aft closure in a clamp at the aft end.

Alignment of the stand is necessary only once, allowing the testing of three motors per day during the test program.

Fluid supply system. - The fluid supply system used for the LITVC tests is portable and was originally built for subscale 120-in.-diameter motor TVC tests at AEDC, Tennessee. The system has two fluid tanks and associated pressurization and controls. Figure 9 presents a schematic of this system. Installation in test cell ST-3 is shown in figure 10.

The fluid feed system to the test nozzle consisted of a 0.5-in. (0.0127 m) tube section with two separate lines at the aft end of the stand. Each of the two lines had a flow meter, flex tube connection to the nozzle, and isolation hand valve. Injectant temperature was measured in the feedline upstream of the two separate lines.

Screening Tests

Six tests were conducted to evaluate the four candidate low-cost materials plus the standard silica material with N_2O_4 and Freon injection at an area ratio of 2.5. The results for these six tests are presented in tables IX and X.

Freon injectant tests. - The first three tests (6101, 6102, and 6103) were conducted using Freon 113 grade TF as the injectant. This was done to allow reevaluation of the TVC duty cycle if needed for more reactive N_2O_4 tests. An injectant flow rate was selected to obtain a flow rate ratio W_s/W_a of 0.013, which is indicative of large solid motor requirements. Each candidate material was fabricated in half of the nozzle exit liner, which made it possible to obtain the test results with fewer tests. The standard material was used in both halves of one nozzle, and a higher injectant flow rate was utilized in the extra quadrant. This provided intermediate data between the screening tests and the material verification tests.

TABLE VIII. - INSTRUMENTATION

Parameter	Symbol	Range	SI units
Axial force - 1	FA-1	25,000 lb_f	111,250 N
Axial force - 2	FA-2	25,000 lb_f	111,250 N
Aft side force - 1	FSA-1	1,000 lb_f	4,450 N
Aft side force - 2	FSA-2	1,000 lb_f	4,450 N
Forward side force - 1	FSF-1	500 lb_f	2,225 N
Forward side force - 2	FSF-2	500 lb_f	2,225 N
Chamber pressure - 1	PC-1	1,000 psig	6.89×10^6 N/m^2
Chamber pressure - 2	PC-2	1,000 psig	6.89×10^6 N/m^2
Manifold pressure, quad I	PM-1	1,000 psig	6.89×10^6 N/m^2
Manifold pressure, quad II	PM-3	1,000 psig	6.89×10^6 N/m^2
Injectant flow rate, quad I	Q-1	5 to 15 gpm[a]	1 to 3 m^3/sec
Injectant flow rate, quad III	Q-3	5 to 15 gpm[a]	1 to 3 m^3/sec
Injectant temperature	TI	0 to 140 ^oF	250^o to 330 ^oK
Instrumentation accuracy, ±3% nominal			

[a]Flow range adjusted for test conditions
5-gpm maximum range for tests 1 through 6
15-gpm maximum range for tests 7 through 10

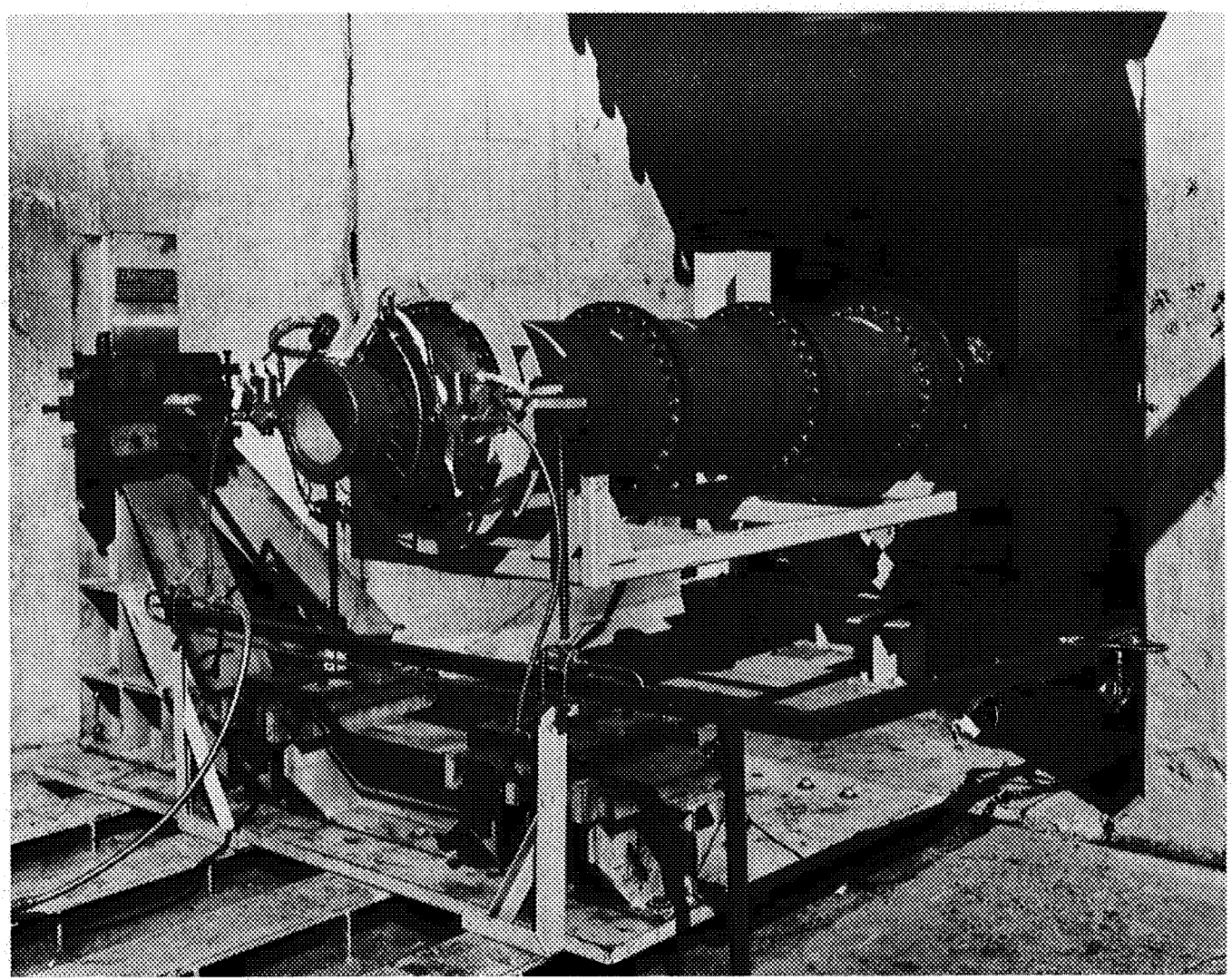

Figure 7. - LITVC Test Motor Installation

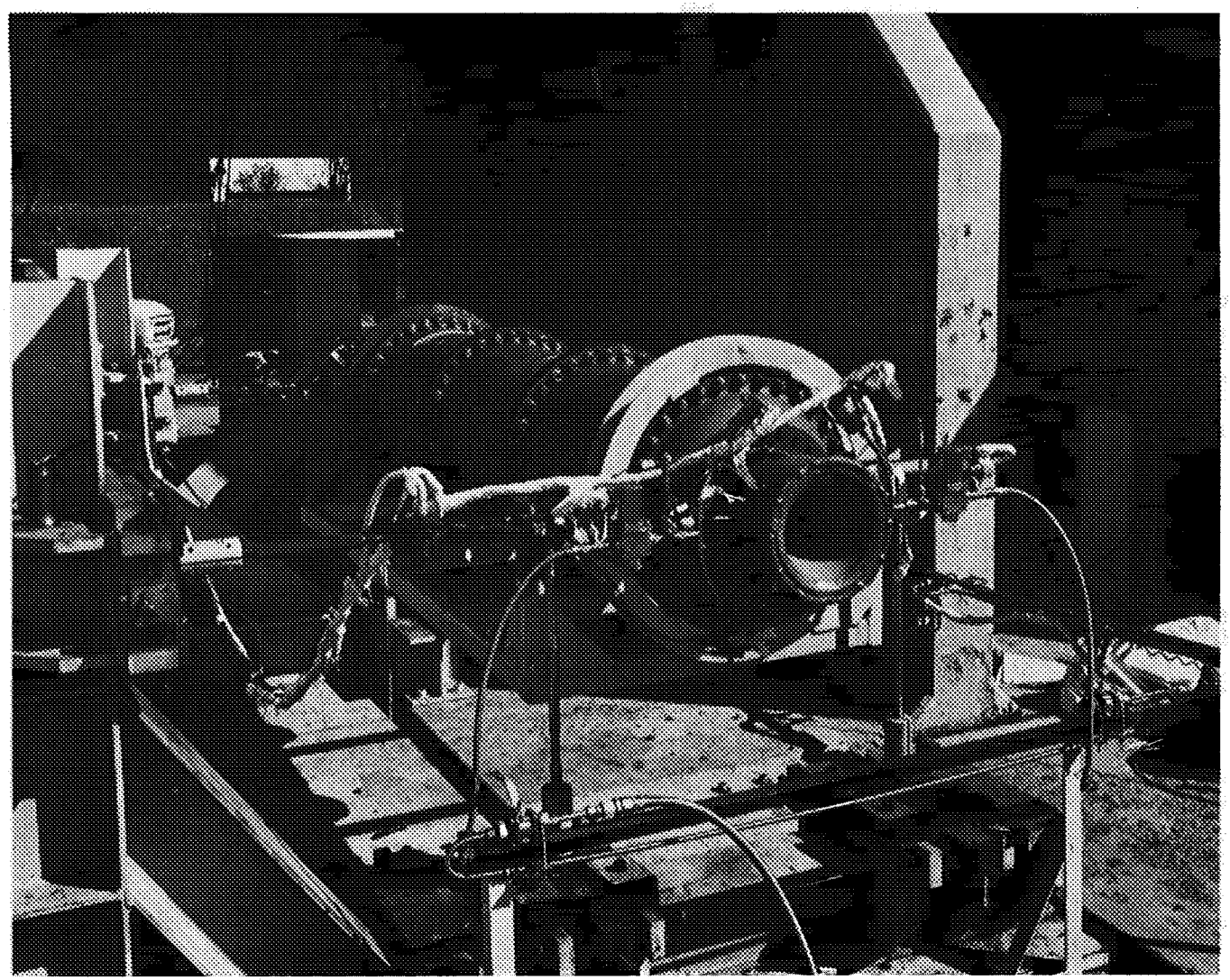

Figure 8. - Test Facility Force Measurement Configuration

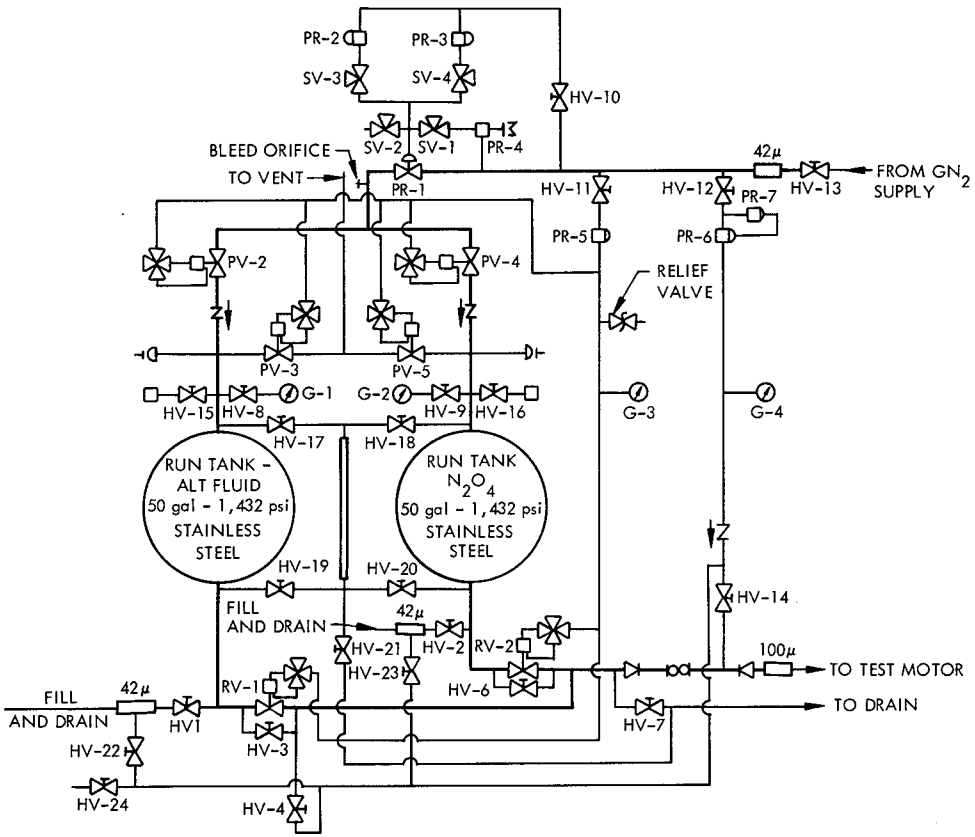

HAND VALVES (HV)

HV-1. ALT TANK FILL
2. INJECTANT TANK FILL
3. ALT TANK AUXILIARY BYPASS
4. MAIN LINE DRAIN
6. INJECTANT TANK AUXILIARY BYPASS
7. MAIN LINE DRAIN
8. ALT TANK GAGE ISOLATION
9. INJECTANT TANK GAGE ISOLATION
10. SECONDARY PRESSURE REGULATOR ISOLATION DOME
11. VALVE ACTUATION REGULATOR ISOLATION
12. PURGE REGULATOR ISOLATION
13. GN_2 SUPPLY
14. PURGE ISOLATION
15. 16. TANK TRANSDUCER ISOLATION
17. 18. 19. 20. SIGHT GAGE ISOLATION
21. SIGHT GAGE DRAIN
22. 23. FILL AND DRAIN PURGE ISOLATION
24. FIELD ISOLATION

SOLENOID VALVES (SV)

SV-1. PRIMARY PRESSURE DOME ISOLATION
2. DOME VENT
3. SECONDARY PRESSURE DOME ISOLATION
4. SECONDARY PRESSURE DOME ISOLATION

PRESSURIZATION VALVES (PV)

PV-2. ALT TANK PRESSURE
3. ALT TANK VENT
4. INJECTANT TANK PRESSURE
5. INJECTANT TANK VENT

PRESSURE REGULATORS (PR)

PR-1. MAIN PRESSURE
2. SECONDARY PRESSURE DOME
3. SECONDARY PRESSURE DOME
4. MOTOR LOADER
5. VALVE ACTUATION
6. PURGE
7. PURGE DOME HAND LOADER

REMOTE VALVES (RV)

RV-1. ALT TANK AUXILIARY
2. INJECTANT TANK AUXILIARY

PRESSURE GAGES (G)

G-1. ALT TANK
2. INJECTANT TANK
3. VALVE ACTUATION
4. PURGE

Figure 9. - TVC Fluid Supply Schematic

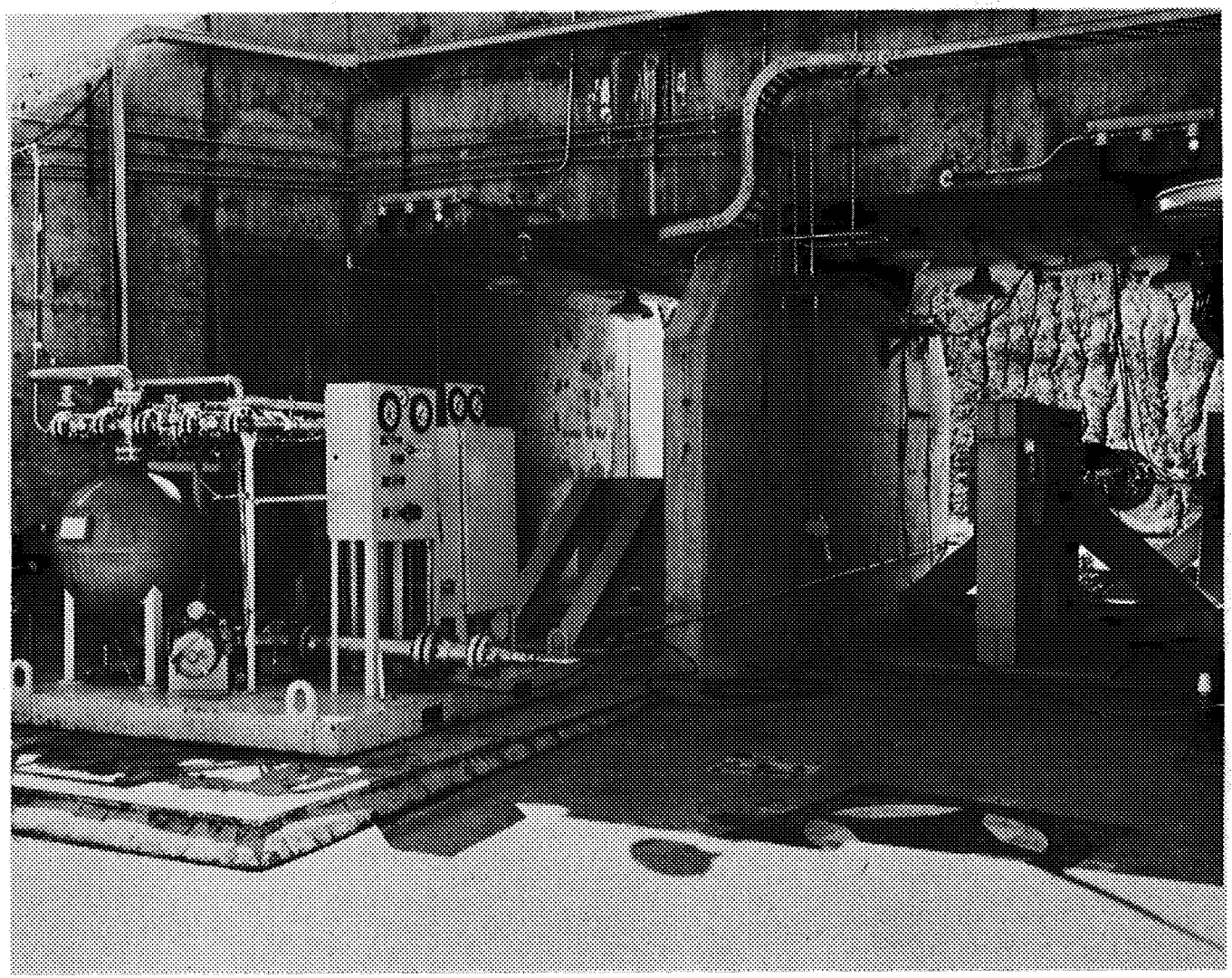

Figure 10. - Fluid Supply Installation

	6101	6102	6103
TVC injectant fluid	Freon 113 'TF' (CCL_2F-$CCLF_2$)	Freon 113 'TF' (CCL_2F-$CCLF_2$)	Freon 113 'TF' (CCL_2F-$CCLF_2$)
TVC injectant area ratio			
Quadrant I	2.5	2.5	2.5
Quadrant III	2.5	2.5	2.5
TVC injectant flow rate, lb/sec (kg/sec)			
Quadrant I	0.577 (0.257)	0.560 (0.253)	0.581 (0.262)
Quadrant III	1.043 (0.472)	0.523 (0.236)	0.508 (0.230)
TVC injectant pressure, psia (N/m^2)			
Quadrant I	765 ($5.25x10^7$)	765 ($5.25x10^7$)	780 ($5.36x10^7$)
Quadrant III	730 ($5.02x10^7$)	760 ($5.22x10^7$)	770 ($5.3x10^7$)
TVC injection duration, sec			
Quadrant I	17.2	17.3	17.5
Quadrant III	17.2	17.3	17.4
Motor duration, sec (action time)	21.7	21.2	21.5
Motor average pressure, psia (N/m^2) (action time)	681 ($4.7x10^7$)	695 ($4.78x10^7$)	692 ($4.75x10^7$)
Motor average flow rate, lb/sec (kg/sec)	42.36 (19.2)	43.23 (19.6)	43.04 (19.5)
Average flow rate ratio, (W_s/W_a)			
Quadrant I	0.0136	0.0130	0.0135
Quadrant III	0.0246	0.0121	0.0118
Nozzle Materials			
Quadrant I	FM-5504	FM-5272	MXS-198
Quadrant III	FM-5504	KF-418	SP-8030
TVC on			
Quadrant I	1.15	1.10	1.15
Quadrant III	3.11	3.08	3.10
TVC off			
Quadrant I	18.30	18.40	18.65
Quadrant III	20.25	20.35	20.55
Throat diameter, in. (m)			
Pretest	3.508 (0.089)	3.508 (0.089)	3.508 (0.089)
Posttest	3.574 (0.091)	3.574 (0.091)	3.574 (0.091)
TVC injection orifice diameter, in. (m)			
Quadrant I	0.028 (0.00071)	0.028 (0.00071)	0.028 (0.00071)
Quadrant III	0.038 (0.00097)	0.028 (0.00071)	0.028 (0.00071)

TABLE IX. - SUMMARY OF LITVC TESTS 6101, 6102, AND 6103

	6104	6105	6106
TVC injectant fluid	N_2O_4	N_2O_4	N_2O_4
TVC injection area ratio			
Quad I	2.5	2.5	2.5
Quad III	2.5	2.5	2.5
TVC injectant flow rate, lb/sec (kg/sec)			
Quad I	0.577 (0.261)	0.579 (0.262)	0.579 (0.262)
Quad III	1.021 (0.462)	0.527 (0.238)	0.515 (0.233)
TVC injectant pressure, psia (N/m^2)			
Quad I	830 ($5.7x10^7$)	828 ($5.7x10^7$)	820 ($5.65x10^7$)
Quad III	810 ($5.6x10^7$)	825 ($5.68x10^7$)	810 ($5.6x10^7$)
TVC injection duration, sec			
Quad I	17.2	10.2	16.9
Quad III	17.2	17.0	16.85
Motor duration, sec (action time)	21.2	21.1	20.7
Motor average pressure, psia (N/m^2) (action time)	685 ($4.7x10^7$)	689 ($4.75x10^7$)	691 ($4.76x10^7$)
Motor average flow rate, lb/sec (kg/sec)	42.61 (19.3)	42.86 (19.4)	42.98 (19.5)
Average flow rate ratio (W_s/W_a)			
Quad I	0.0135	0.0135	0.0135
Quad III	0.0240	0.0123	0.0120
Nozzle materials			
Quad I	FM-5504	KF-418	MXS-198
Quad III	FM-5504	FM-5272	SP-8030
TVC on			
Quad I	1.10	7.90	1.15
Quad III	3.10	3.10	3.10
TVC off			
Quad I	18.3	18.10	18.05
Quad III	20.30	20.10	19.95
Throat diameter, in. (m)			
Pretest	3.508 (.089)	3.508 (.089)	3.508 (.089)
Posttest	3.580 (.091)	3.578 (.091)	3.576 (.091)

TABLE X. - SUMMARY OF LITVC TESTS 6104, 6105, AND 6106

The initial six tests were run at an average chamber pressure of 695 psia (4.77×10^6 N/m^2). This pressure correlated well with previous subscale and 120-in.-diameter motor firing results. However, non-TVC area ablation on several low-cost candidates was more severe than expected. Consequently, a lower burning rate was used on the remaining four tests to yield an average pressure of 604 psi (4.15×10^5 N/m^2) with lower heat fluxes suitable for the 260-in.-diameter nozzle. The chamber pressures for all 10 tests are shown in figure 11.

The postfire condition of the test nozzles is described in the following sections. These nozzles utilized the same LITVC injection geometry as the 120-in.-diameter motor nozzle which is shown in figure 12. The same ablation patterns are presented for the test nozzles as exhibited by the 120-in.-diameter motor nozzle. A ridge is formed downstream of the injection port, with eroded valleys around the port extending downstream. There are some slight differences in ablation patterns between the test nozzles and the 120-in.-diameter motor nozzle which are due to the physical distance between injection ports. Figure 13 shows the ablation of the 120-in.-diameter nozzle due to each injection shock with separate erosion patterns for each injection port. The shock for each injection port on the smaller contract nozzles interact due to the closer physical spacing, and only one groove is formed between the ports.

The light areas upstream of the ports on the 120-in.-diameter motor nozzle, which are not present on the test nozzles, are caused by N_2O_4 leakage after the test. The leakage is due to the nozzle-up configuration of the test.

Test 6101. - The standard material nozzle was used with FM-5504 high silica phenolic throughout the nozzle liner. Quadrant I flow rate ratio was 0.0136, and quadrant III flow rate ratio was 0.0246. The posttest condition of quadrants I and III are shown in figures 14 and 15, respectively.

Only slight erosion has occurred in the TVC port valleys for the 0.013 and 0.024 flow ratios. At the higher expansion ratios near the exit, the valleys are smoothed and not evident.

Test 6102. The materials used in this nozzle were FM-5272 crepe paper phenolic in quadrant I and KF-418 canvas duck phenolic in quadrant III. The injectant flow rate ratio was 0.013 in quadrant I and 0.012 in quadrant III.

The postfire condition of the FM-5272 crepe paper phenolic material is shown in figure 16. Severe gouging is evident in the TVC port, as well as the non-TVC, areas. The TVC quadrant is well described by the grooves extending to the exit for each TVC port. This erosion is in sharp contrast to the standard material used in test 6101.

The posttest condition of KF-418, the canvas duck phenolic material, is shown in figure 17. Excessive gouging and grooving is present in the TVC and non-TVC areas. The bondline between the two materials is washed out at the nozzle exit, which may have contributed to some of the excessive erosion at the bond interface. This material appears to be worse than FM-5272 crepe paper phenolic.

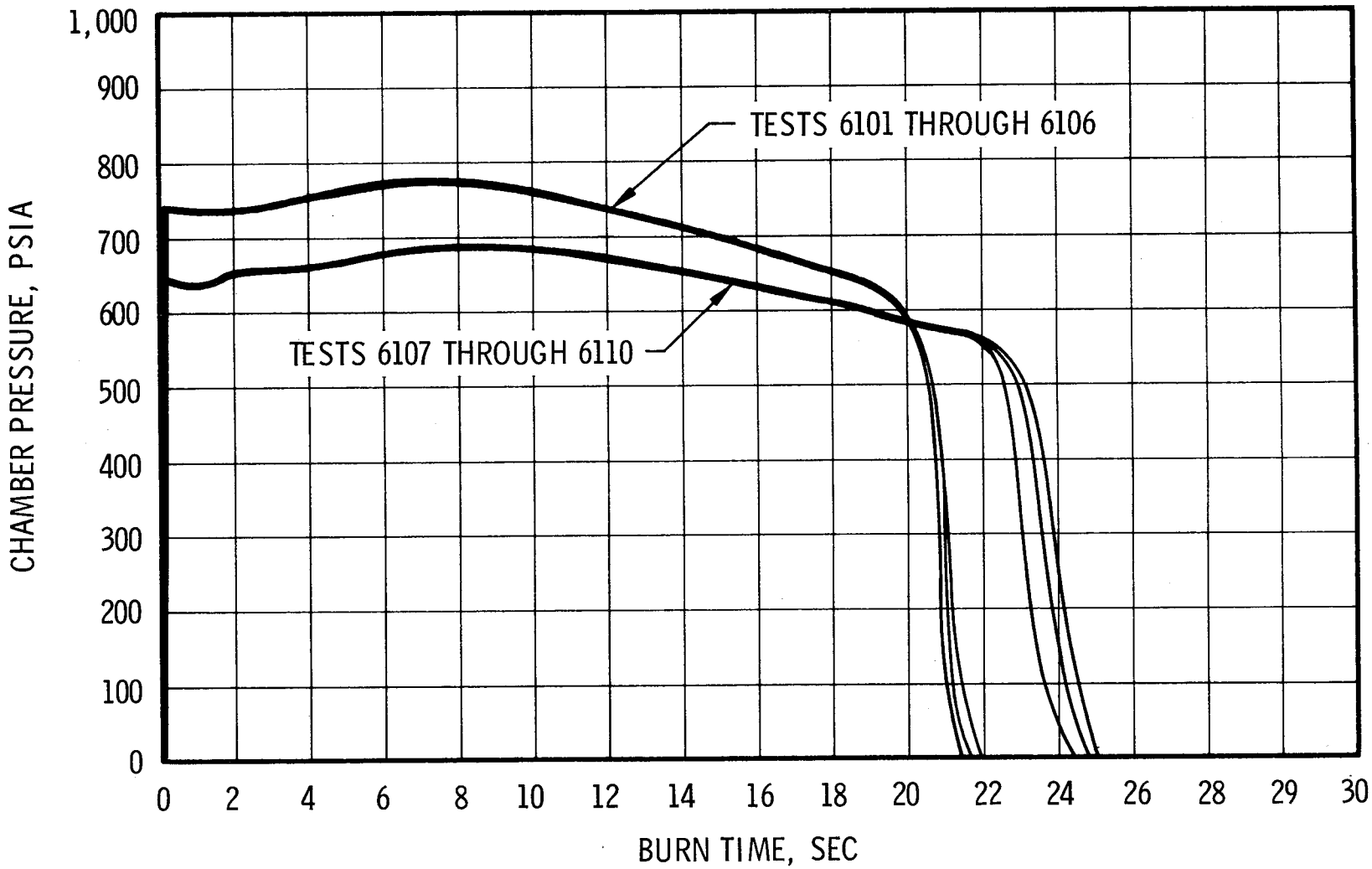

Figure 11. - Test Motor Pressure History

Figure 12. - 120-in. Nozzle Posttest Condition

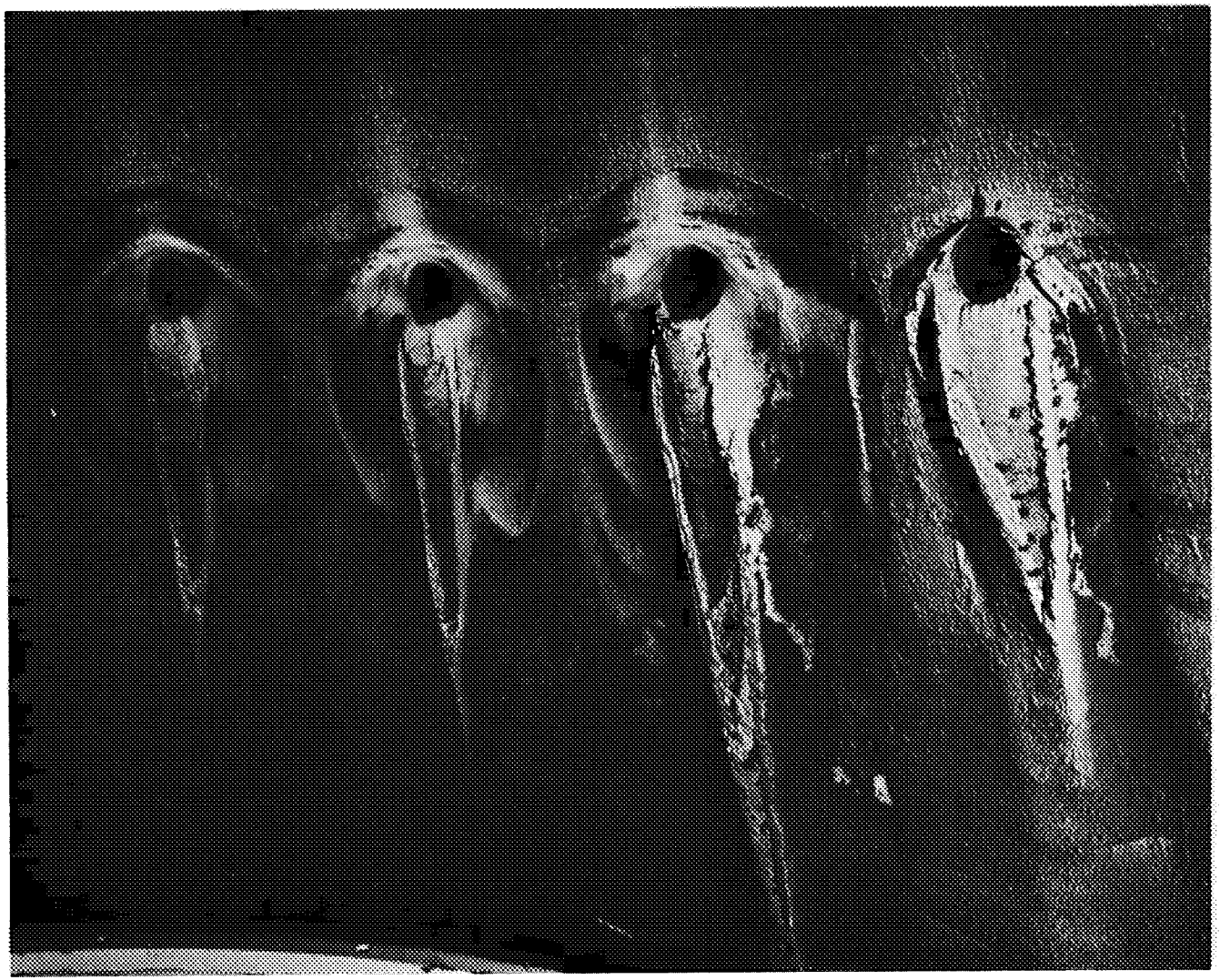

Figure 13. - 120-in.-Diameter Nozzle TVC Ablation

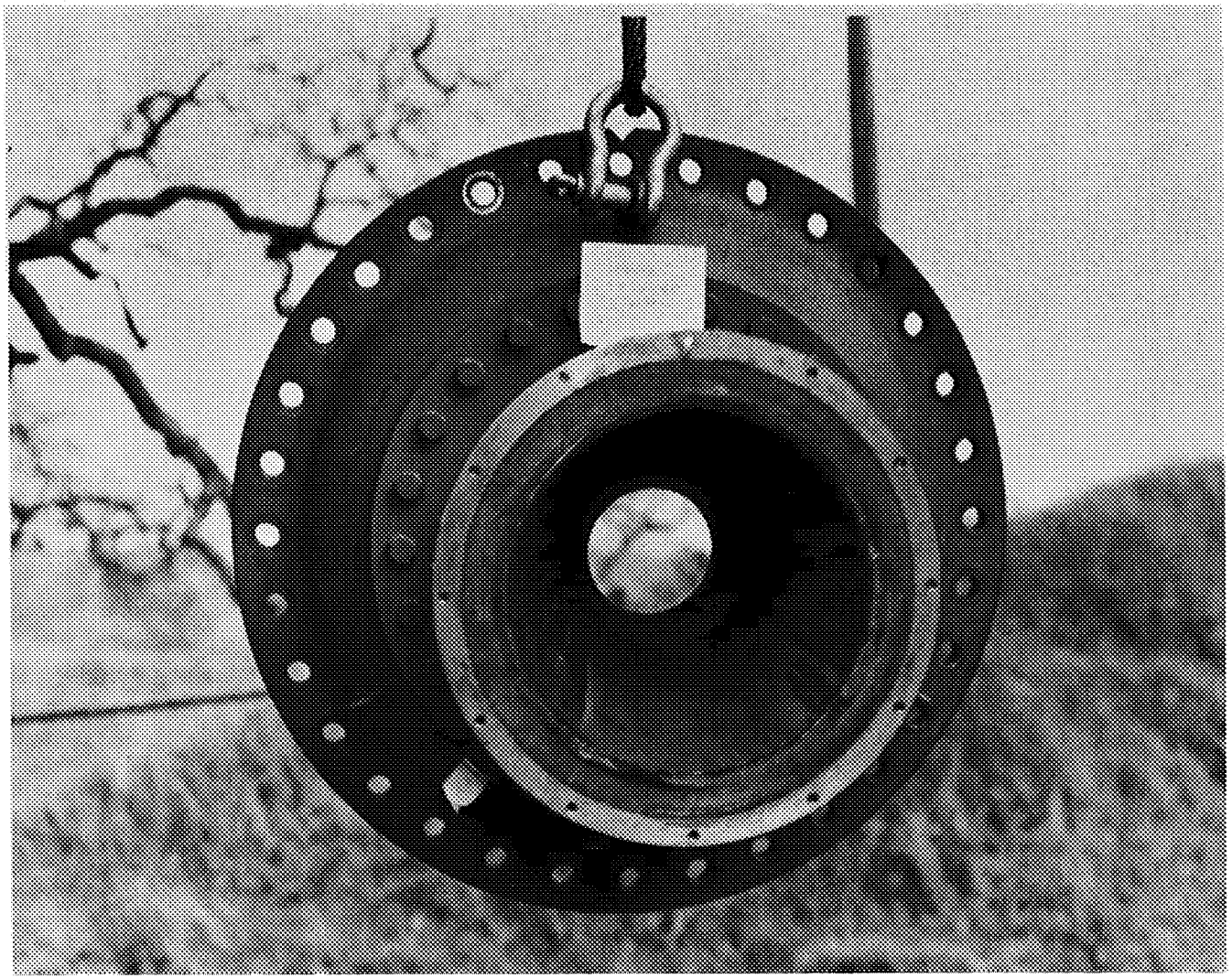

Figure 14. - Nozzle Condition, Quad I, Test 6101

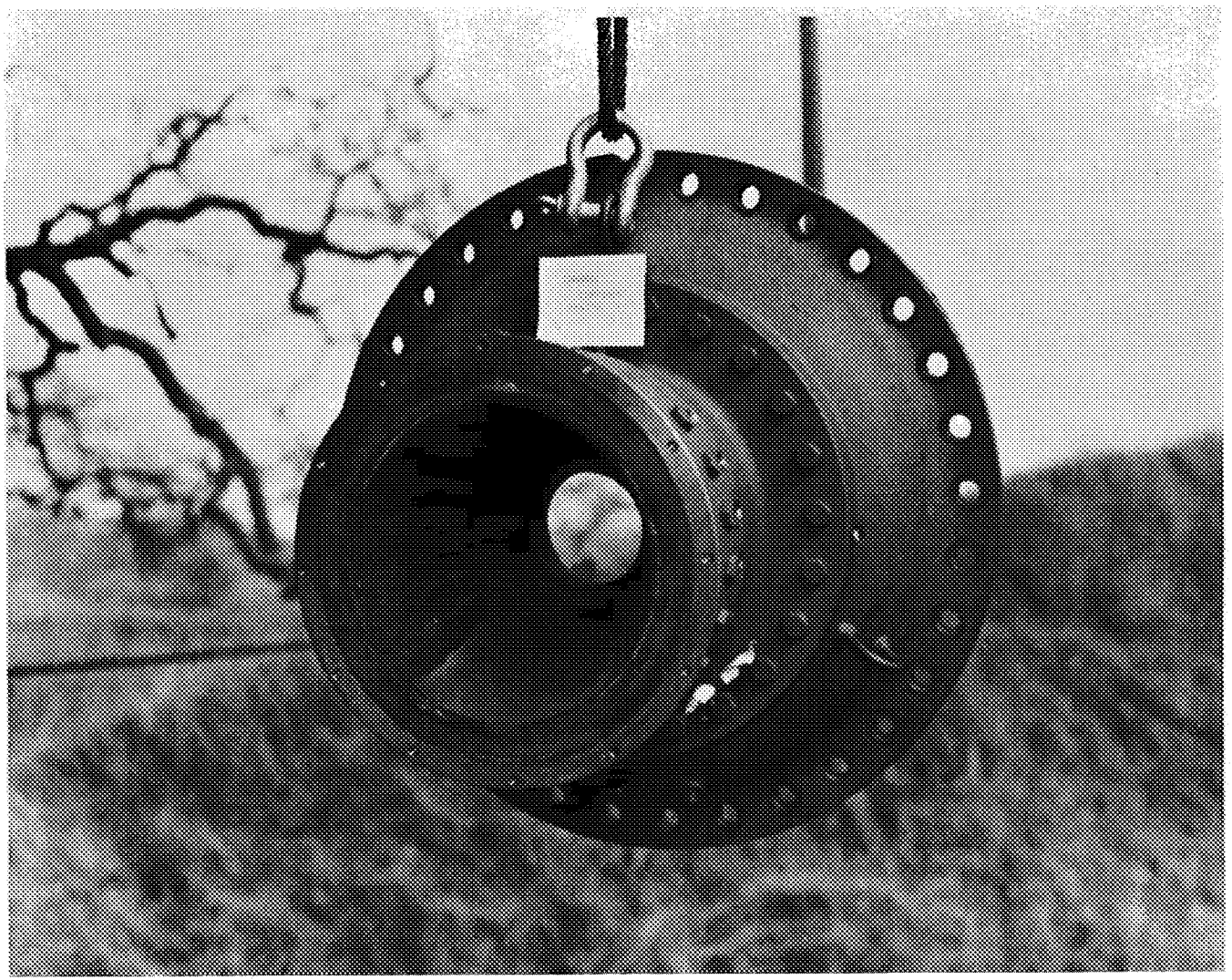

Figure 15. - Nozzle Condition, Quad III, Test 6101

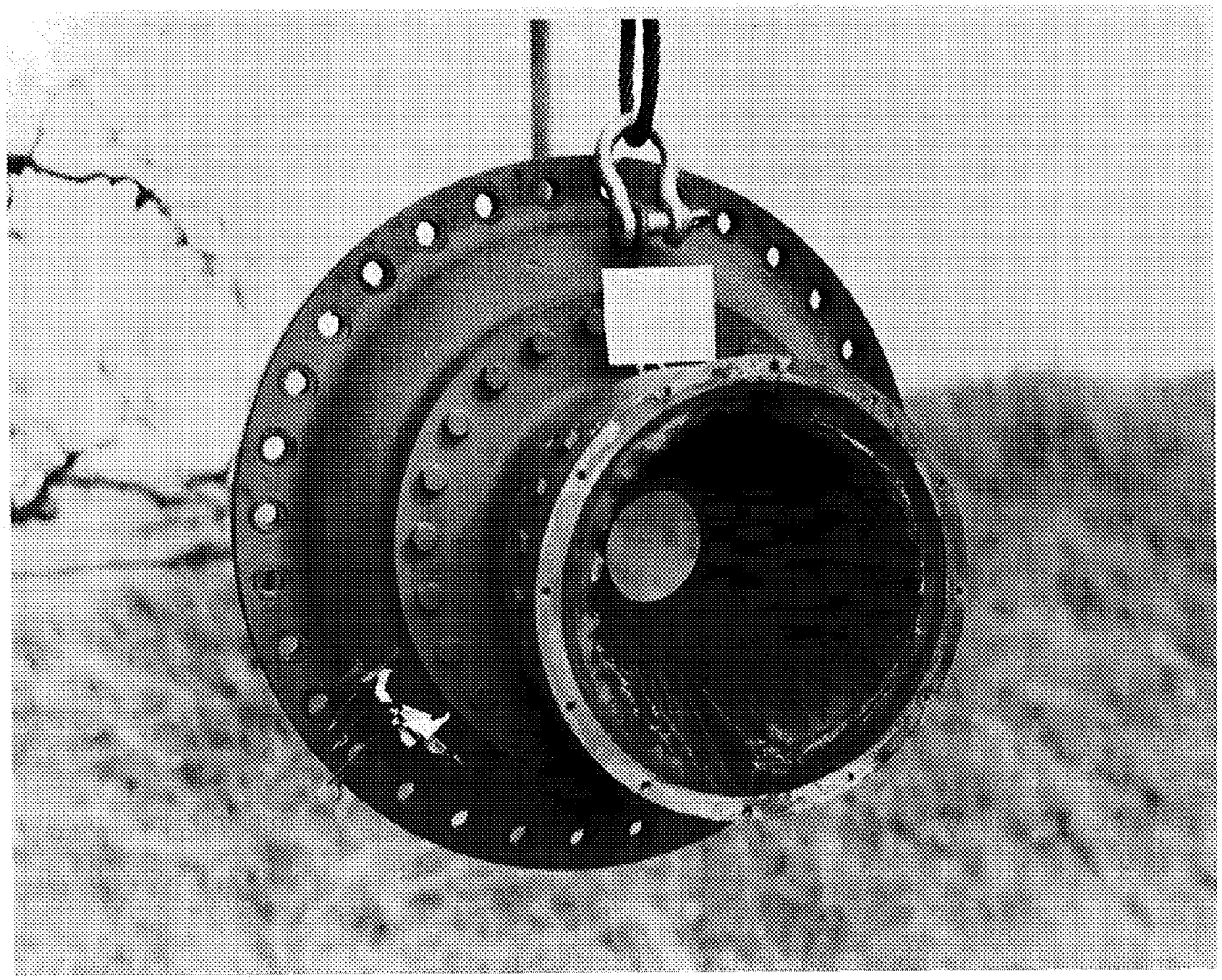

Figure 16. - Nozzle Condition, Quad I, Test 6102

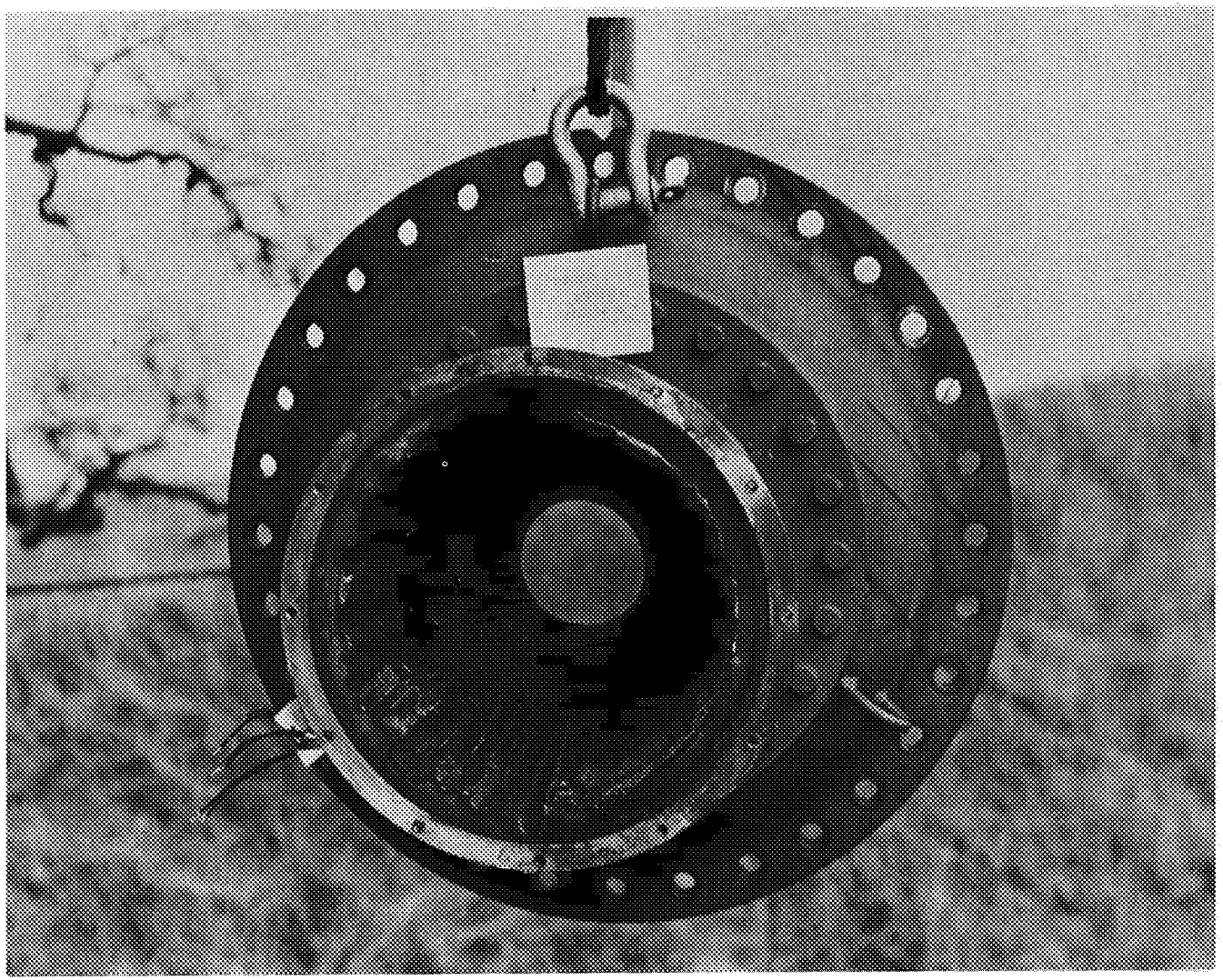

Figure 17. - Nozzle Condition, Quad III, Test 6102

Test 6103. - This nozzle utilized MXS-198 silica epoxy novalac in quadrant I and SP-8030-96 double-weight silica phenolic in quadrant III. The injectant flow rate ratios were 0.0135 in quadrant I and 0.0118 in quadrant III.

The posttest condition of the MXS-198 silica epoxy novalac is shown in figure 18. The TVC ports are clearly evident by the raised ridge, as seen with the standard material in test 6101. There is no gouging in the non-TVC areas, and the erosion is similar to that found in the standard material.

Figure 19 shows the SP-8030-96 double-weight silica phenolic material following the test. The ridges are present at each TVC port, and again erosion is similar to the standard material. The bondline has a slight gouge at the forward section of the nozzle but is intact at the exit.

N_2O_4 injectant tests. - The same nozzle materials were tested with N_2O_4 at similar flow rate ratios. The TVC duty cycles were the same except for the canvas duck material which was the poorest material with Freon. The duty cycle for this material was shortened from 17 to 10 sec to prevent excessive erosion.

Test 6104. - The standard material nozzle was used with injectant flow rate ratios of 0.0135 in quadrant I and 0.024 in quadrant III. Figures 20 and 21 show the conditions of quadrants I and III, respectively. The ridges are present at each TVC port and extend to the nozzle exit. The erosion is greater than experienced with Freon at the same flow rate; however, the non-TVC areas are similar.

Test 6105. - This nozzle used KF-418 canvas duck phenolic in quadrant I and FM-5272 crepe paper phenolic in quadrant III. Injectant flow rate ratios were 0.0135 in quadrant I and 0.0123 in quadrant III. The TVC injection duration in quadrant I was only 10 sec, as discussed previously.

The KF-418 canvas duck phenolic material is shown in figure 22. The non-TVC gouging is present as seen in test 6102; however, the TVC area appears to be quite different. The injection ports are eroded from the initial size of 0.250 in. (0.0062 m) to over 0.750 in. (0.019 m). Also, there are no distinctive ridges behind the TVC ports as exhibited by the silica materials. The ablation in the non-TVC area is less with this exit cone than with the similar part used in test 6102, which indicates a nonreproducible behavior in the material. The excessive erosion of the TVC ports with N_2O_4 precludes use of this material with N_2O_4 liquid injection, and the canvas was eliminated from further testing.

Figure 23 shows the FM-5272 crepe paper phenolic material following the test. The gouging in the non-TVC areas is similar to that experienced in test 6102; however, the total ablation is less. The ridges behind the TVC port are not as large as with Freon, which is due to the N_2O_4 reacting in the nozzle downstream of the ports. The effect is less cooling with N_2O_4 behind the injectant stream. There was no chemical attack of N_2O_4 upon FM-5272, crepe paper phenolic, and this material was selected for further testing. A room temperature cure technique was utilized to bond the exit cone liner in the steel shell to avoid shrinkage stresses at the bondline between the two halves of the exit

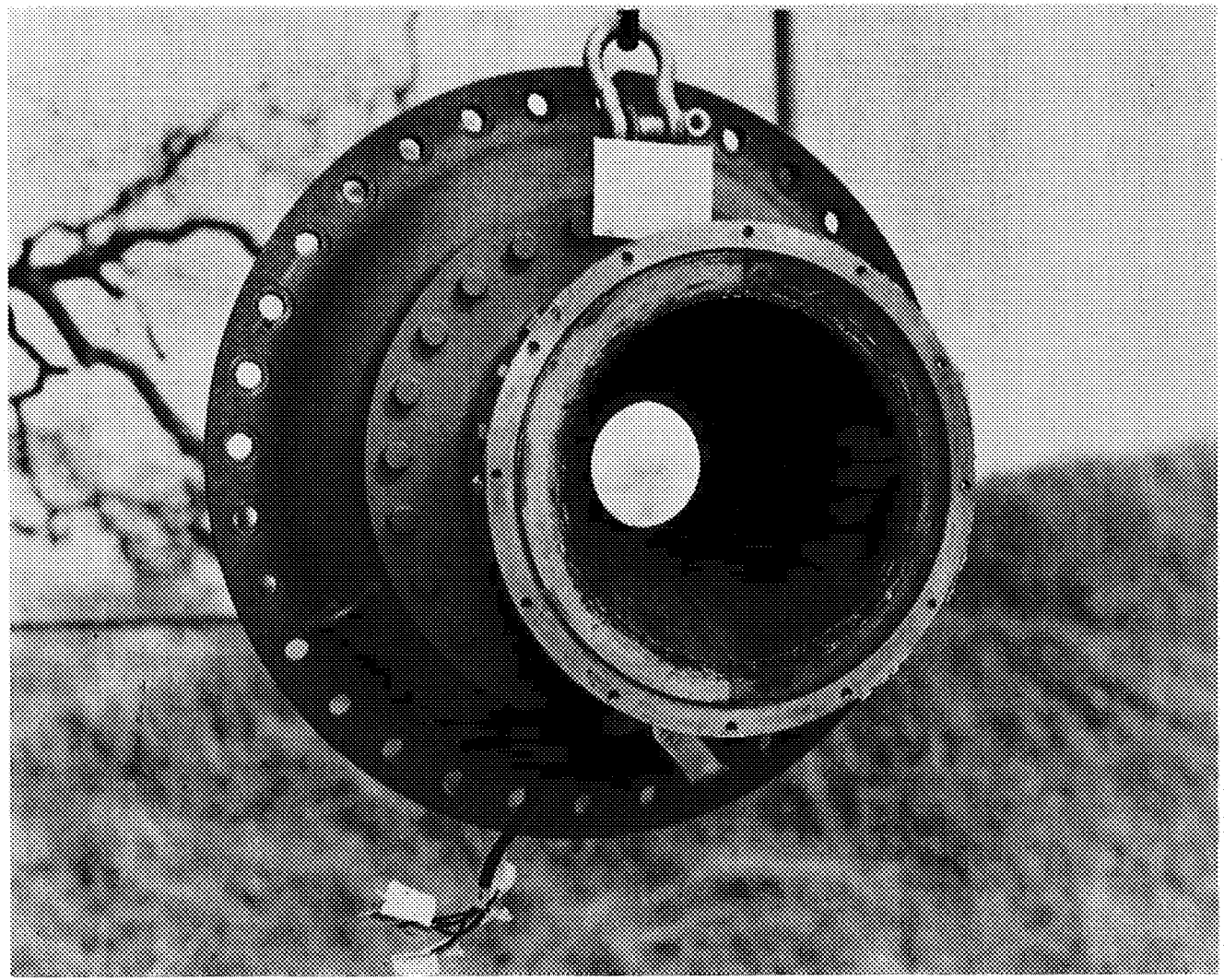

Figure 18. - Nozzle Condition, Quad I, Test 6103

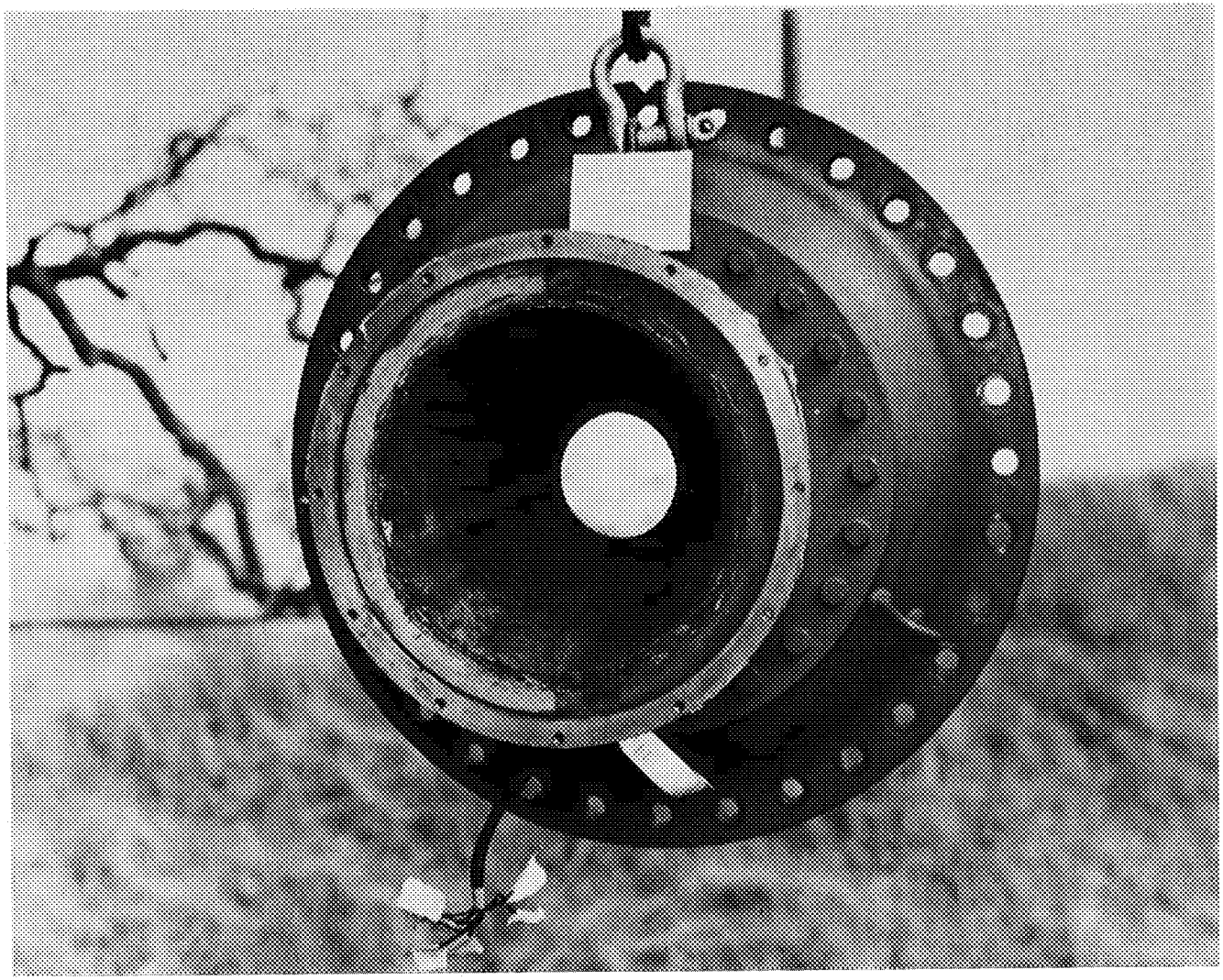

Figure 19. - Nozzle Condition, Quad III, Test 6103

Figure 20. - Nozzle Condition, Quad I, Test 6104

Figure 21. - Nozzle Condition, Quad III, Test 6104

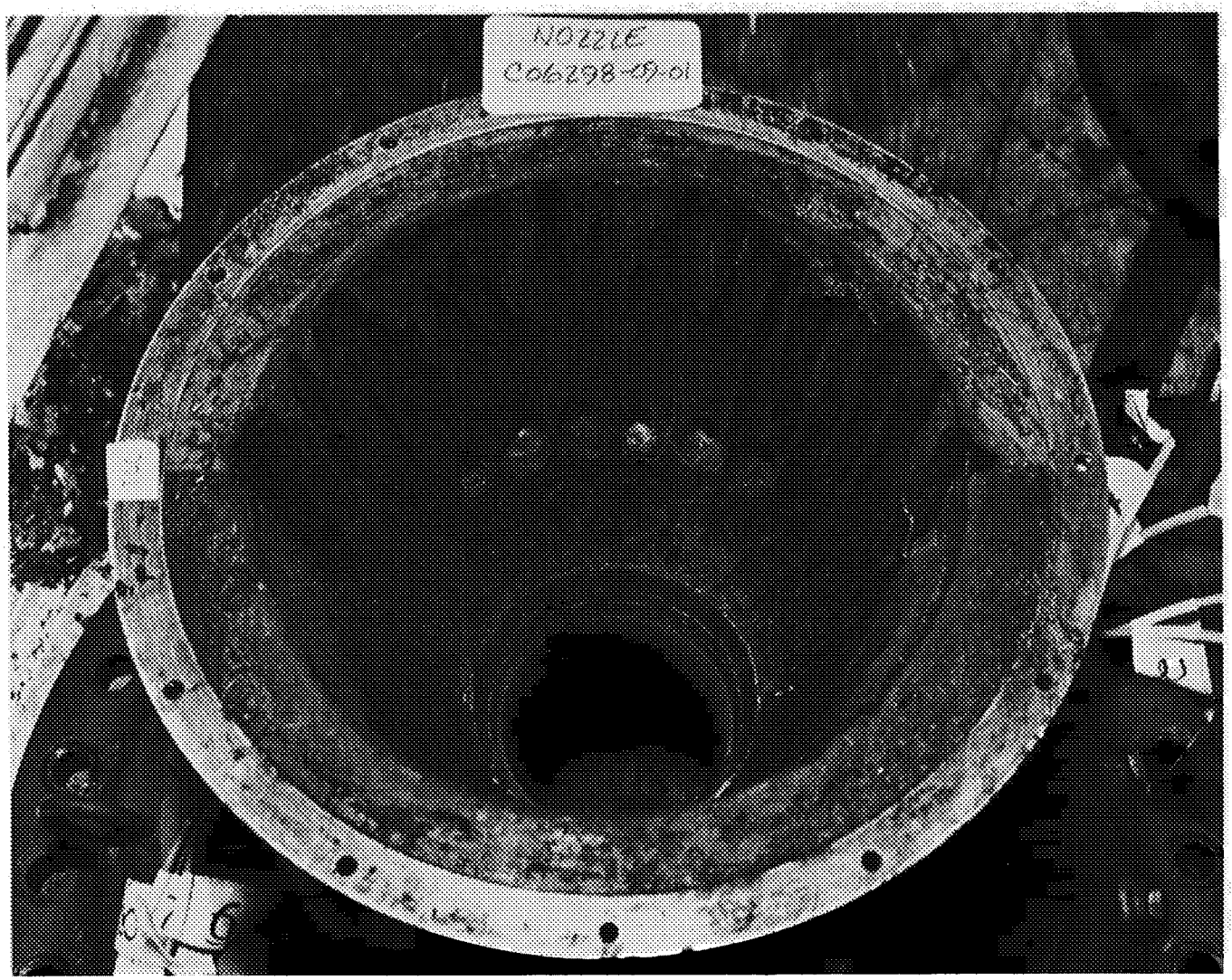

Figure 22. - Nozzle Condition, Quad I, Test 6105

Figure 23. - Nozzle Condition, Quad III, Test 6105

cone liners. The bondline erosion was not as severe as test 6102 and probably reduced the material ablation at the interface.

Test 6106. - The nozzle for this test used MXS-198 silica epoxy novalac in quadrant I with a flow rate ratio of 0.0135 and SP-8030-96 double-weight silica phenolic in quadrant III with a flow rate ratio of 0.0120.

The posttest conditions of these materials are shown in figures 24 and 25. Both materials have similar results as the standard material in test 6104 and hence they were selected for further testing.

Material Verification Tests

Four tests were conducted to evaluate MXS-198 silica epoxy novalac, SP-8030-96 double-weight silica phenolic, and FM-5272 crepe paper phenolic with N_2O_4 injection at area ratios of 2.5 and 3.5. One of the tests with the FM-5272, crepe paper phenolic material evaluated the effect of injection pressure by injecting the same flow rate in each quadrant at an area ratio of 2.5 but with different pressures. The results of these four tests are presented in table XI. The nozzle material results are discussed below.

Test 6107. - The SP-8030-96 double-weight silica phenolic material was used for this nozzle with injectant flow ratios of 0.0447 in quadrant I and 0.0426 in quadrant III. Figure 26 shows the condition for injection at $\epsilon = 2.5$, and figure 27 shows the condition for injection at $\epsilon = 3.5$. The ridges behind the TVC ports are similar in shape for both quadrants; however, the injection at $\epsilon = 2.5$ has decreased the effect of the ridge near the exit due to less cooling as the N_2O_4 reacts in the nozzle. All other areas in the nozzle appear good, and the ablation performance is equal to that of previous tests.

Test 6108. - The MXS-198 silica epoxy novalac material was evaluated during this test at injectant flow ratios of 0.0435 in quadrant I and 0.0449 in quadrant III. Figures 28 and 29 present the condition of the two quadrants, respectively. The exit cone liner had delaminations prior to test as a result of a short cure cycle. These delaminations caused the forward portion of the liner to be ejected during the test, which can be seen in the above figures but did not seem to obscure the test area. The aft portion of the liner was similar in performance to the SP-8030-96 double-weight silica phenolic liner except for laminate separations throughout the nozzle, also due to the cure cycle.

Test 6109. - FM-5272 crepe paper phenolic was used at injectant flow ratios of 0.0435 and 0.0457 in quadrants I and III, respectively. Figures 30 and 31 present the condition of the two quadrants. A similar effect on the TVC port ridge as with the SP-8030-96 double-weight silica nozzle is noticed in this nozzle. The boundary of the TVC shock can be seen in each quadrant where the deeper grooves are located at the edge of the TVC ports. Ablation in the non-TVC areas is similar to previous FM-5272 tests, and gouging is still present.

Figure 24. - Nozzle Condition, Quad I, Test 6106

Figure 25. - Nozzle Condition, Quad III, Test 6106

	6107	6108	6109	6110
TVC injectant fluid	N_2O_4	N_2O_4	N_2O_4	N_2O_4
TVC injectant area ratio				
Quad I	2.5	2.5	2.5	2.5
Quad III	3.5	3.5	3.5	2.5
TVC injectant flow rate, lb/sec (kg/sec)				
Quad I	1.675 (0.753)	1.646 (0.745)	1.636 (0.740)	0.515 (0.233)
Quad III	1.596 (0.721)	1.699 (0.768)	1.717 (0.775)	0.515 (0.233)
TVC injectant pressure, psia (N/m^2)				
Quad I	735 (5.05×10^6)	732 (5.05×10^6)	730 (5.03×10^6)	720 (4.95×10^6)
Quad III	725 (5×10^6)	708 (4.88×10^6)	718 (4.95×10^6)	280 (1.93×10^6)
TVC injection duration, sec				
Quad I	20.1	20.0	20.1	20.1
Quad III	20.0	20.1	20.1	20.0
Motor duration, sec (action time)	24.2	24.8	24.7	24.6
Motor average pressure, psia (N/m^2) (action time)	603 (4.15×10^6)	608 (4.18×10^6)	604 (4.16×10^6)	606 (4.17×10^6)
Motor average flow rate, lb/sec (kg/sec)	37.50 (16.9)	37.82 (17.1)	37.57 (17.0)	37.70 (17.0)
Average flow rate ratio (W_s/W_a)				
Quad I	0.0447	0.0435	0.0435	0.0137
Quad III	0.0426	0.0449	0.0457	0.0137
Nozzle material	SP-8030-96	MXS-198	FM-5272	FM-5272
TVC on				
Quad I	1.1	1.1	1.1	1.1
Quad III	3.0	3.1	3.0	3.0
TVC off				
Quad I	21.2	21.1	21.2	21.2
Quad III	23.0	23.2	23.1	23.0
Throat diameter, in (m)				
Pre-test	3.508 (0.084)	3.508 (0.084)	3.508 (0.089)	3.508 (0.089)
Post-test	3.576 (0.091)	3.577 (0.091)	3.574 (0.091)	3.580 (0.912)
TVC injection orifice diameter, in (m)				
Quad I	0.055 (0.0014)	0.055 (0.0014)	0.055 (0.0014)	0.028(0.00071)
Quad III	0.055 (0.0014)	0.055 (0.0014)	0.055 (0.0014)	0.038(0.00097)

TABLE XI. - SUMMARY OF LITVC TESTS 6107, 6108, 6109, and 6110

Figure 26. - Nozzle Condition, Quad I, Test 6107

Figure 27. - Nozzle Condition, Quad III, Test 6107

Figure 28. - Nozzle Condition, Quad I, Test 6108

Figure 29. - Nozzle Condition, Quad III, Test 6108

Figure 30. - Nozzle Condition, Quad I, Test 6109

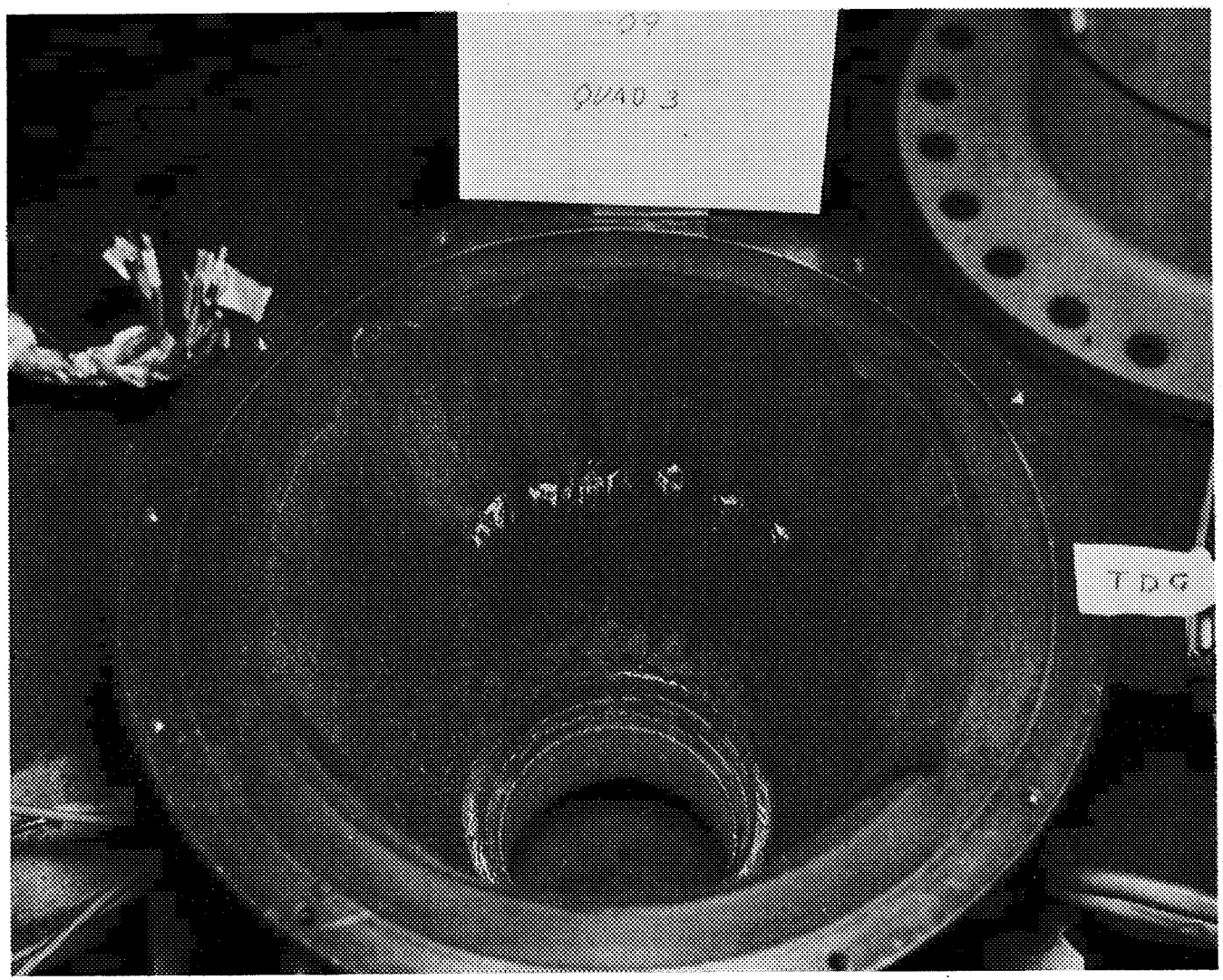

Figure 31. - Nozzle Condition, Quad III, Test 6109

Test 6110. - This test was conducted to evaluate the effect of injection pressure on ablation using the paper phenolic nozzle liner. N_2O_4 was injected in quadrants I and III at a flow rate ratio of 0.0137. The injection pressure in quadrant I was 720 psia (4.95×10^6 N/m^2), and in quadrant III the pressure was 280 psia (1.92×10^6 N/m^2). Conditions of the respective quadrants are shown in figures 32 and 33. Characteristic gouging of the paper is present, and a clear indication of injection pressure effect is shown. The grooves in quadrant I are deeper and extend to the exit, while those in quadrant III are shallower and blend into the TVC port ridges near the exit. Ablation was much higher for the high injection pressure which suggests a possible design consideration for low-cost materials with LITVC.

ABLATION DATA

Measurement of Ablation Depths

Prefire measurements of the length, ID, and OD were made at the forward and aft ends of the test material liner. Extensive postfire ablation depth measurements were taken in the nozzle exit cone at stations shown in figure 34, using the measurement tool shown in figure 35. This tool has a rod that is aligned with the nozzle centerline on which a dial gauge is mounted. The rod can be rotated and raised or lowered to any nozzle station. A positioning pin is used to establish axial station location.

Angular stations A and G are in the region not affected by LITVC. Angular stations B through F are not precisely fixed but are located to record the greatest depth between the injection ports. For the FM-5272 crepe paper phenolic, the wide extent of the TVC ablation pattern required additional measurements. The additional measurement locations are shown as dashed lines in figure 34. In each nozzle exit cone, sufficient measurements of radii from the nozzle centerline were taken to fully characterize the ablation pattern in that individual nozzle. Prefire radii were calculated from the prefire measurements of the diameters and length. The difference in radii were calculated to give the ablation depths. For each axial location, the maximum depth measured between injection ports were averaged and tabulated as presented in the appendix at the end of this report.

Ablation Results

The average ablation depths are plotted in figures 36 through 53 as a function of area ratio for all tests. Both the TVC effected and non-TVC ablation depths are plotted to illustrate the effect of TVC. The following general observations can be made from these figures:

A. FM-5504 high silica phenolic, SP-8030-96 high silica double-weight phenolic, and MXS-198 silica epoxy novalac show similar ablation characteristics in regions affected by liquid injection. With N_2O_4 as the injectant fluid, there is a distinct point of maximum ablation

Figure 32. - Nozzle Condition, Quad I, Test 6110

Figure 33. - Nozzle Condition, Quad III, Test 6110

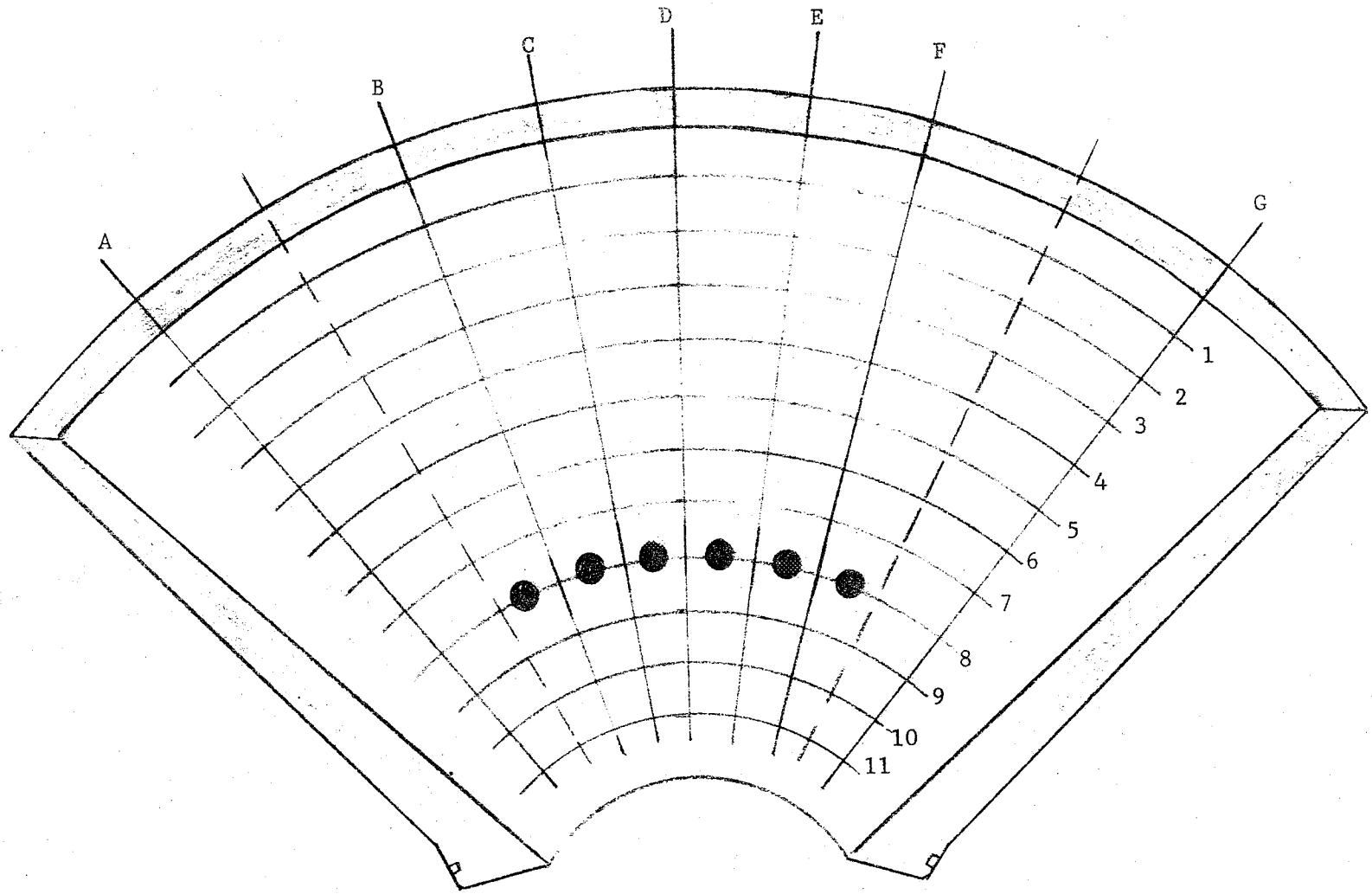

Figure 34. - Measurement Stations in LITVC Test Motor Exit Cone.

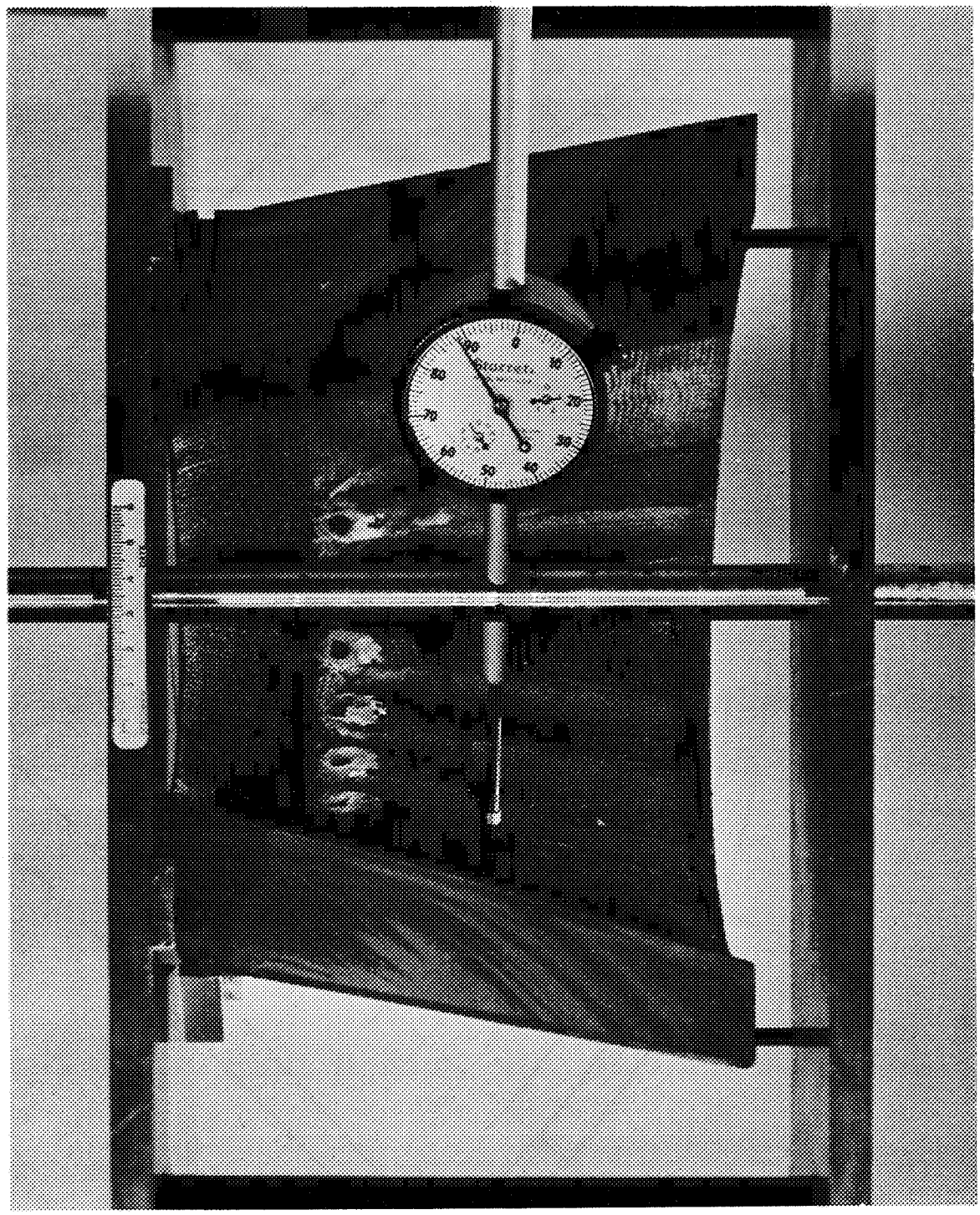

Figure 35. - Ablation Depth Measuring Apparatus

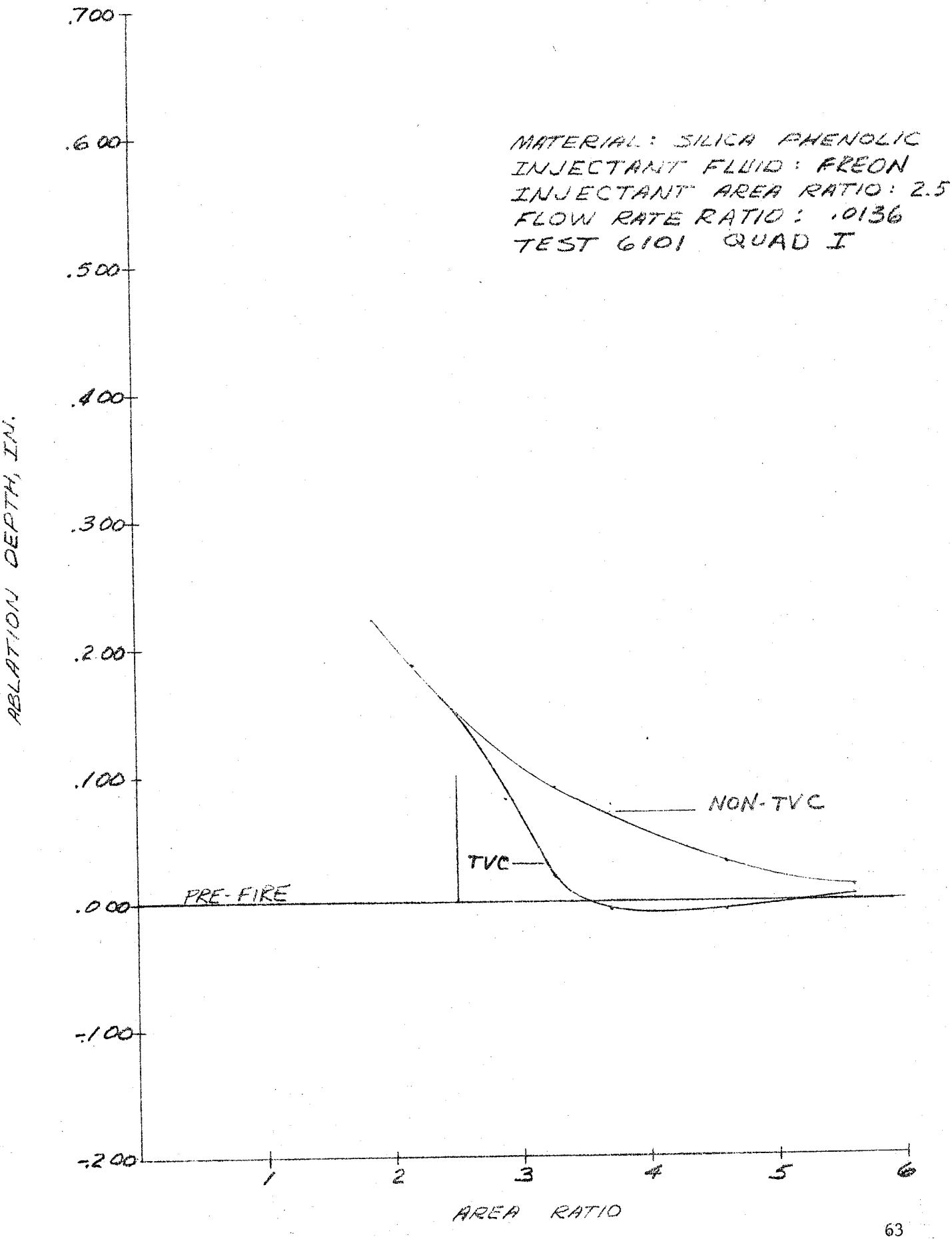

Figure 36. - Nozzle Ablation, Quad I, Test 6101.

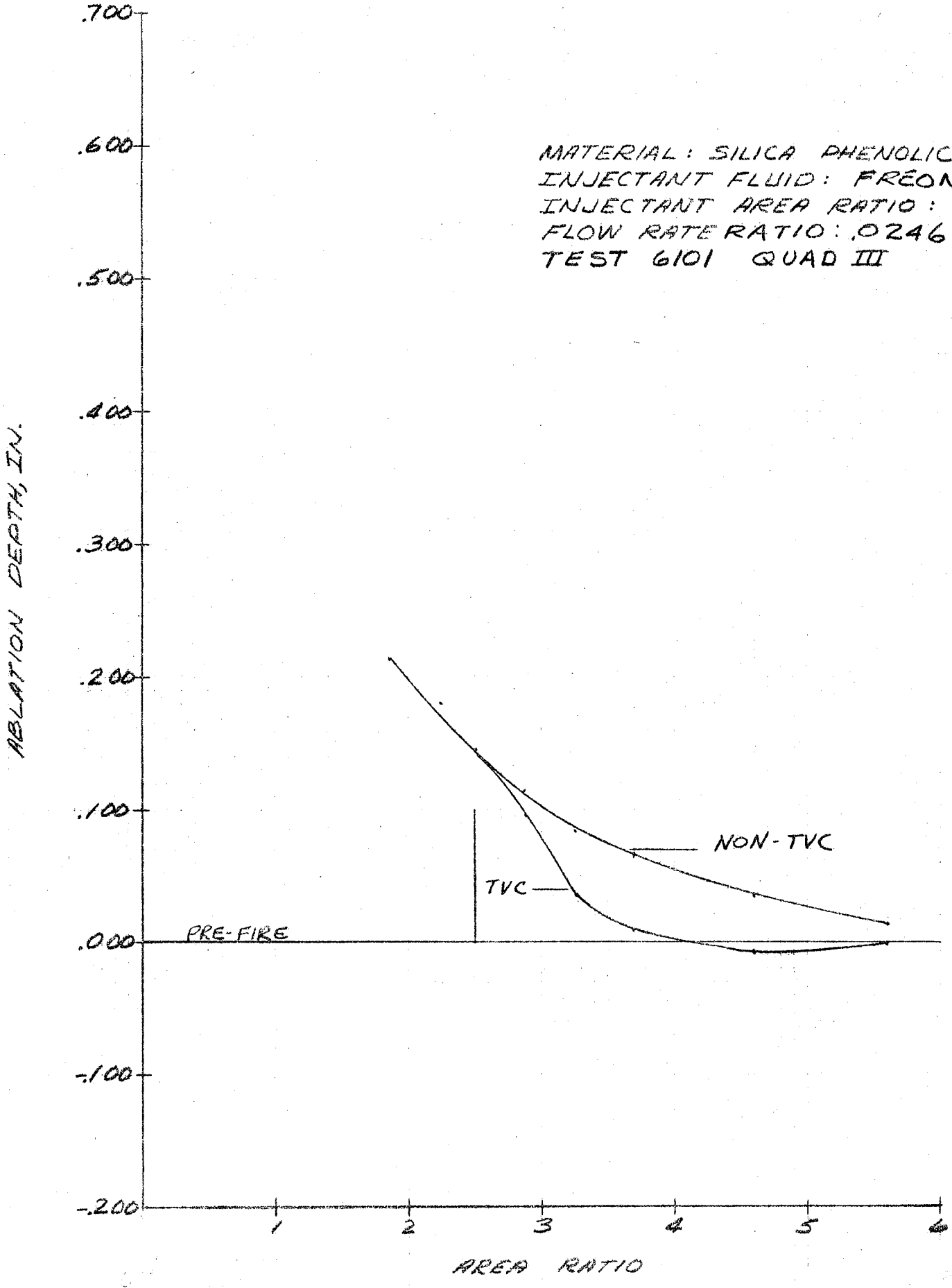

Figure 37. - Nozzle Ablation, Quad III, Test 6101.

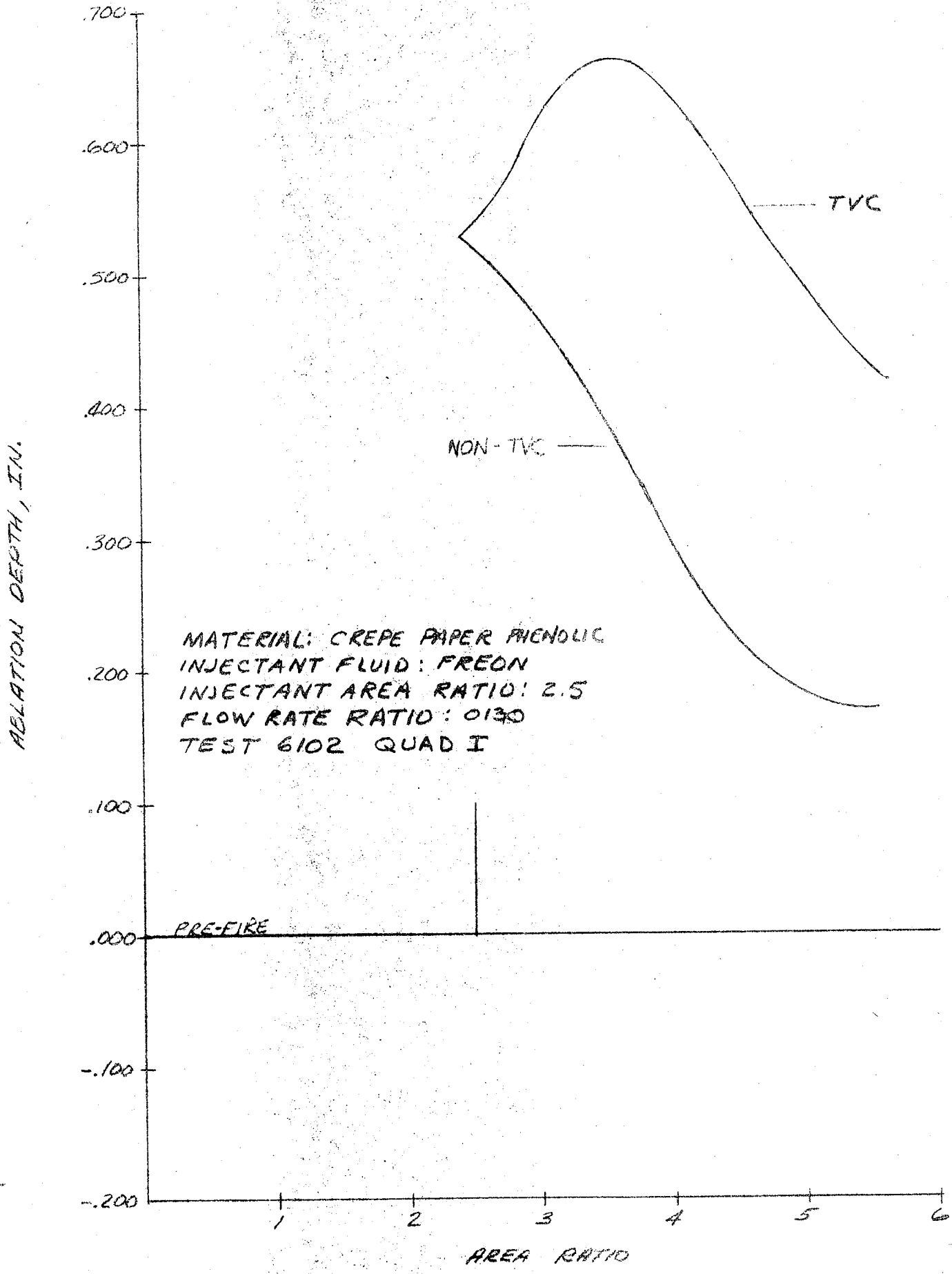

Figure 38. - Nozzle Ablation, Quad I, Test 6102.

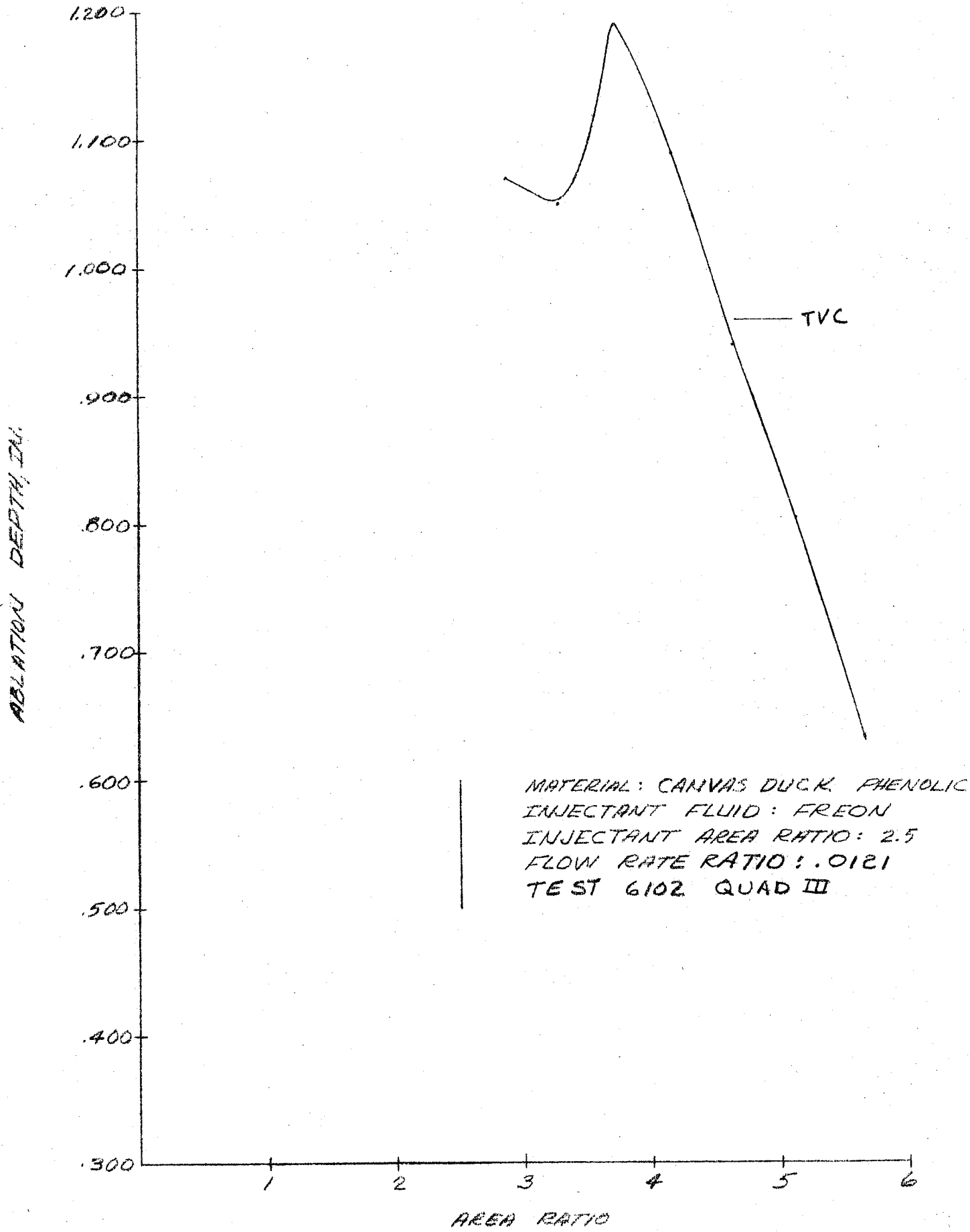

Figure 39. - Nozzle Ablation, Quad III, Test 6102.

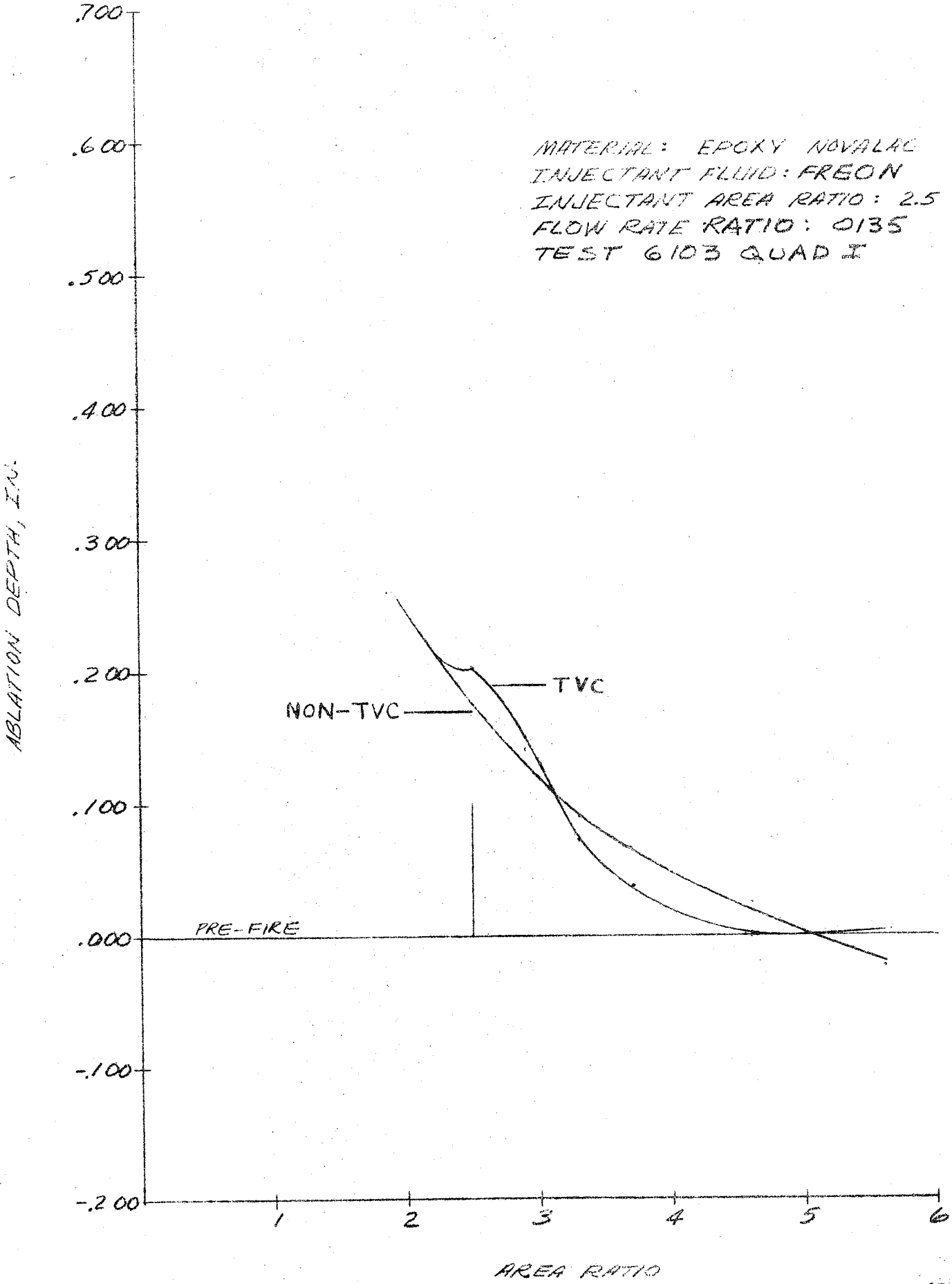

Figure 40. - Nozzle Ablation, Quad I, Test 6103.

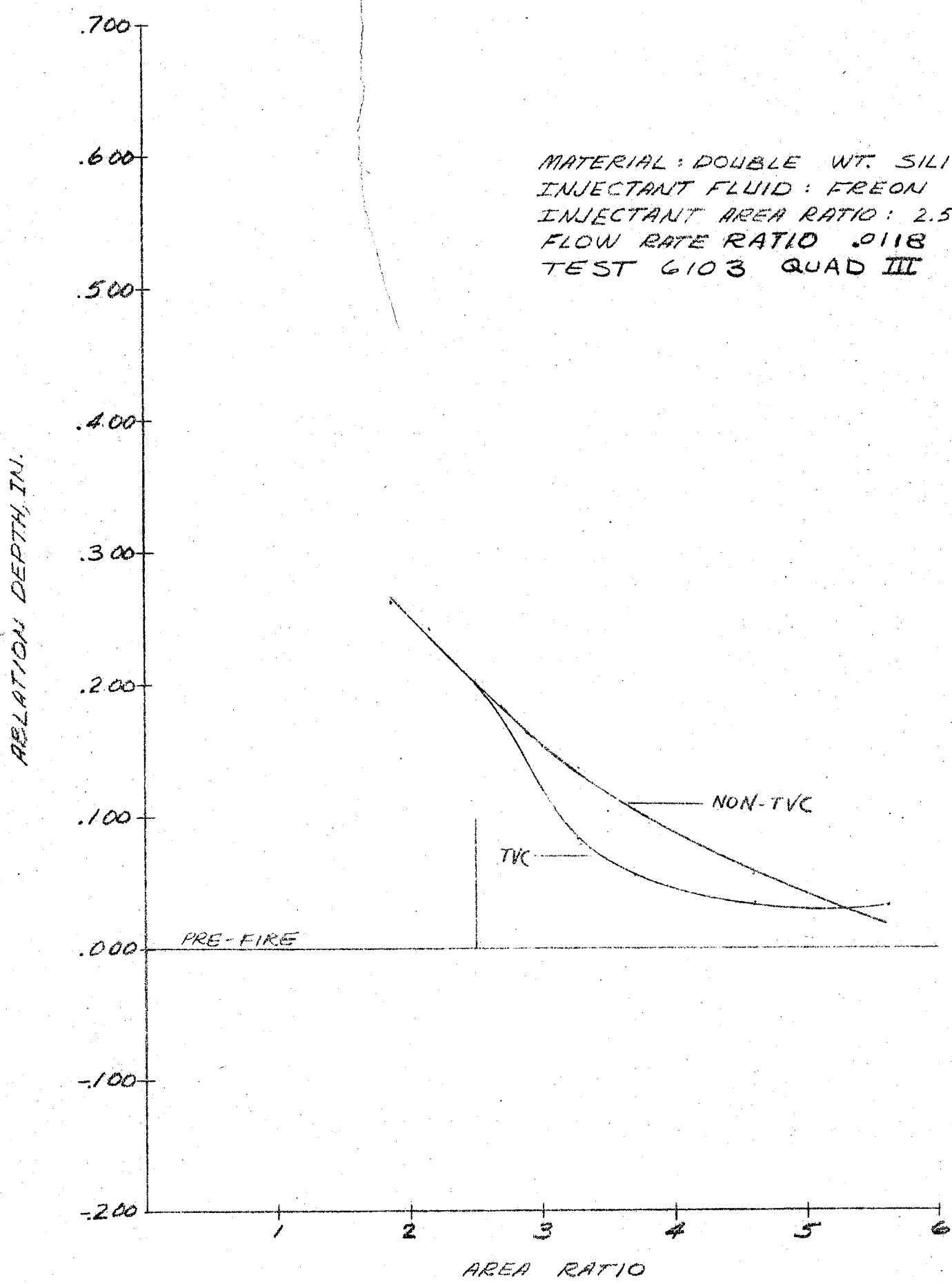

Figure 41. - Nozzle Ablation, Quad III, Test 6104.

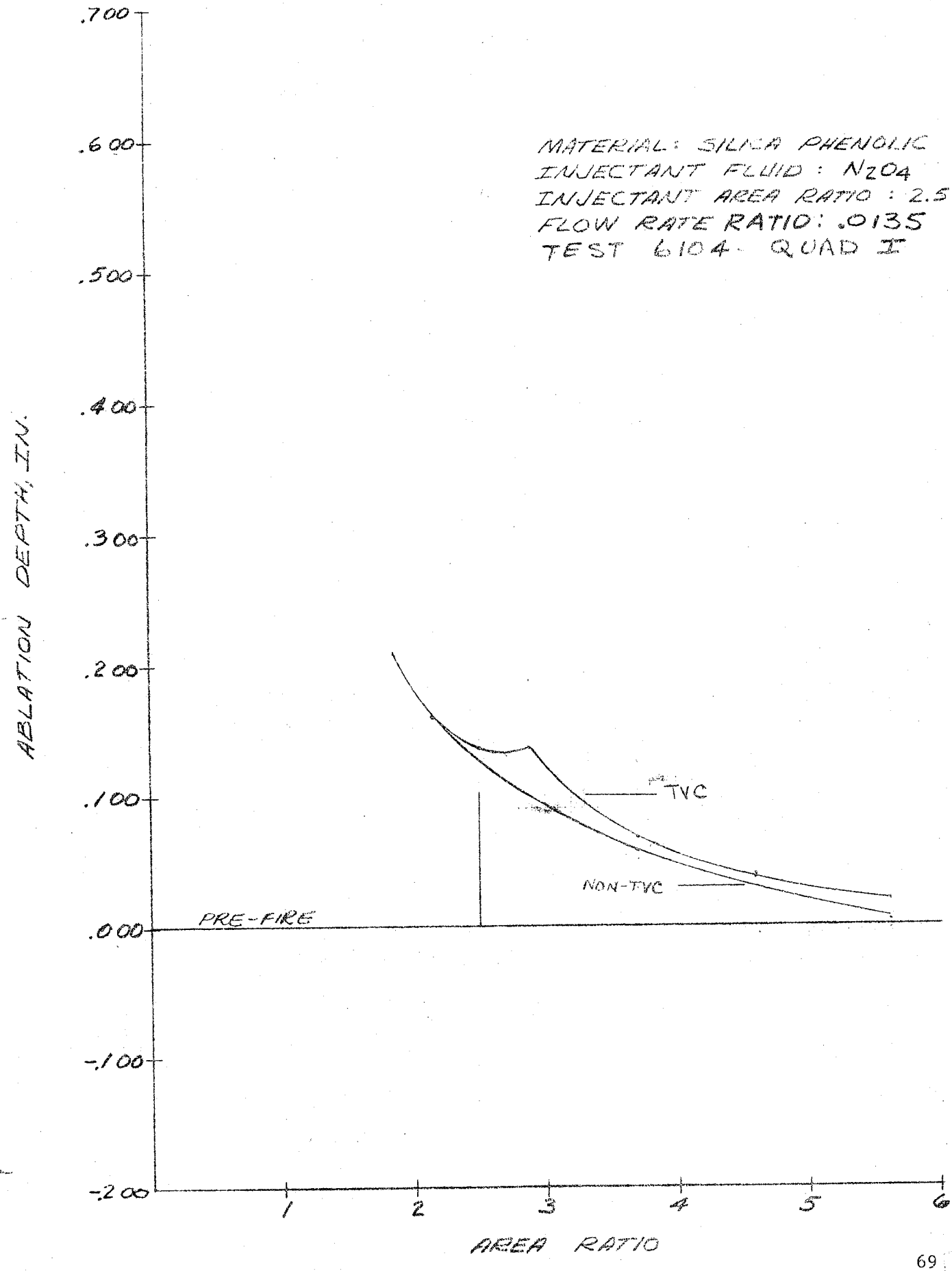

Figure 42. - Nozzle Ablation, Quad I, Test 6104.

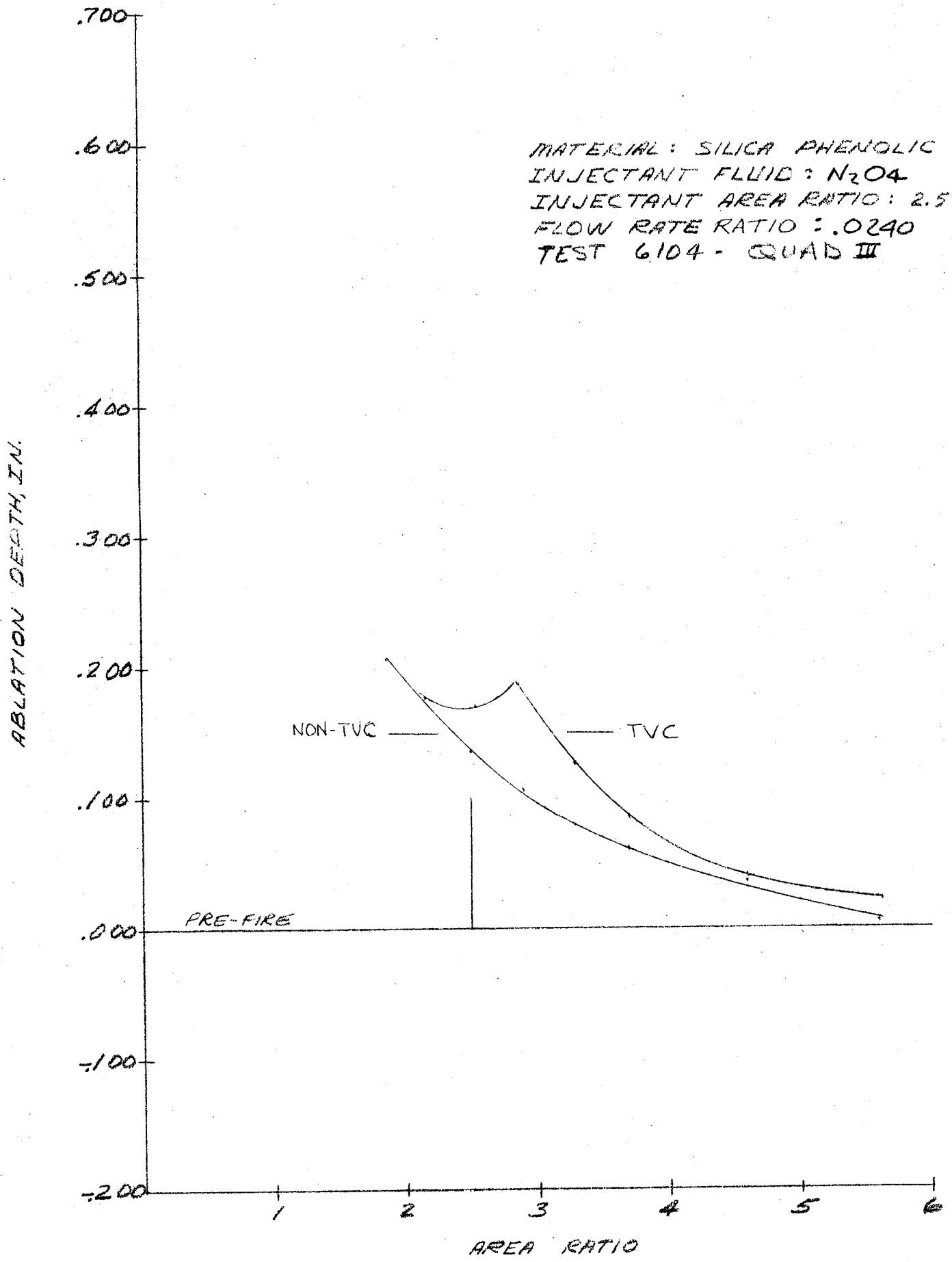

Figure 43. - Nozzle Ablation, Quad III, Test 6104.

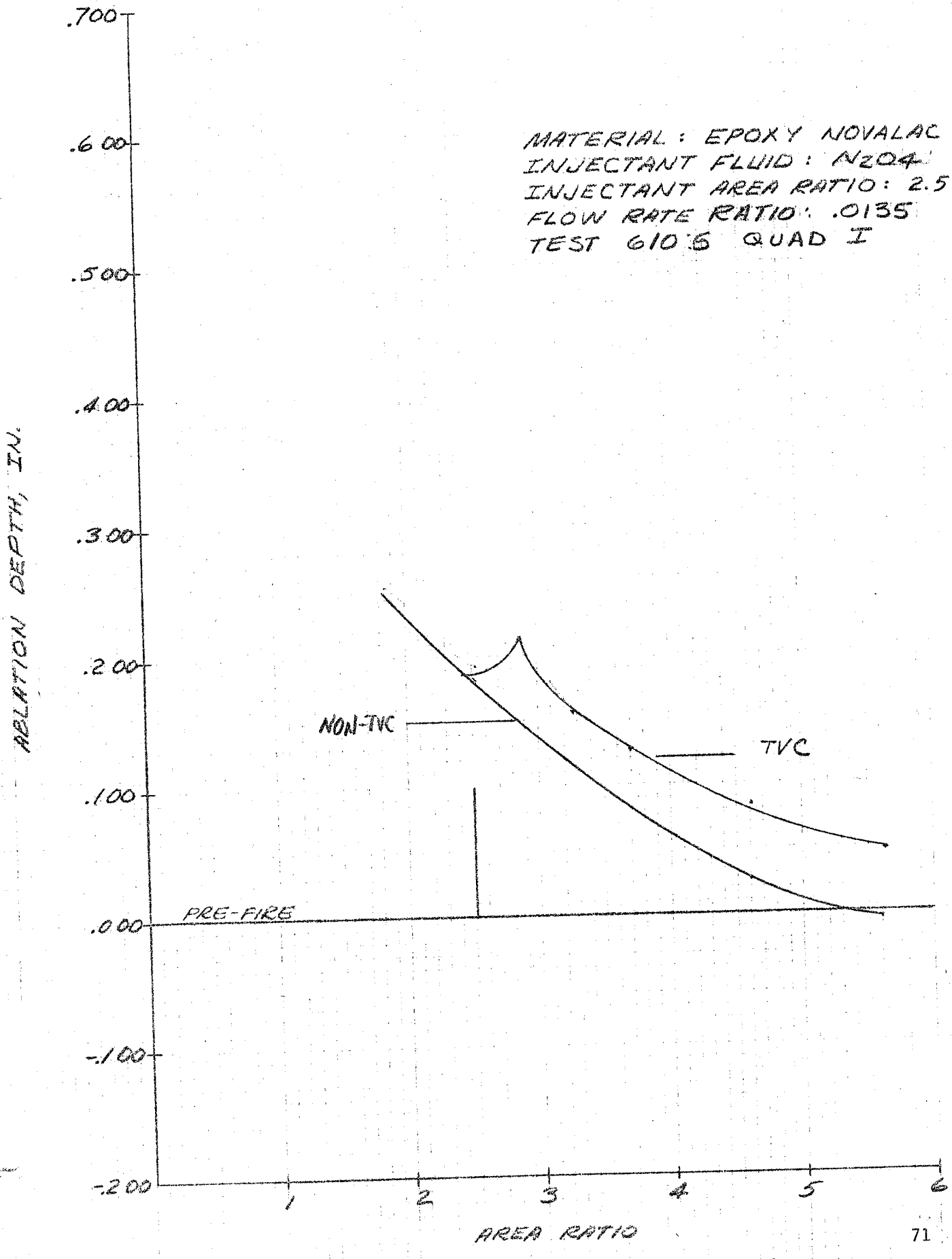

Figure 44. - Nozzle Ablation, Quad I, Test 6106.

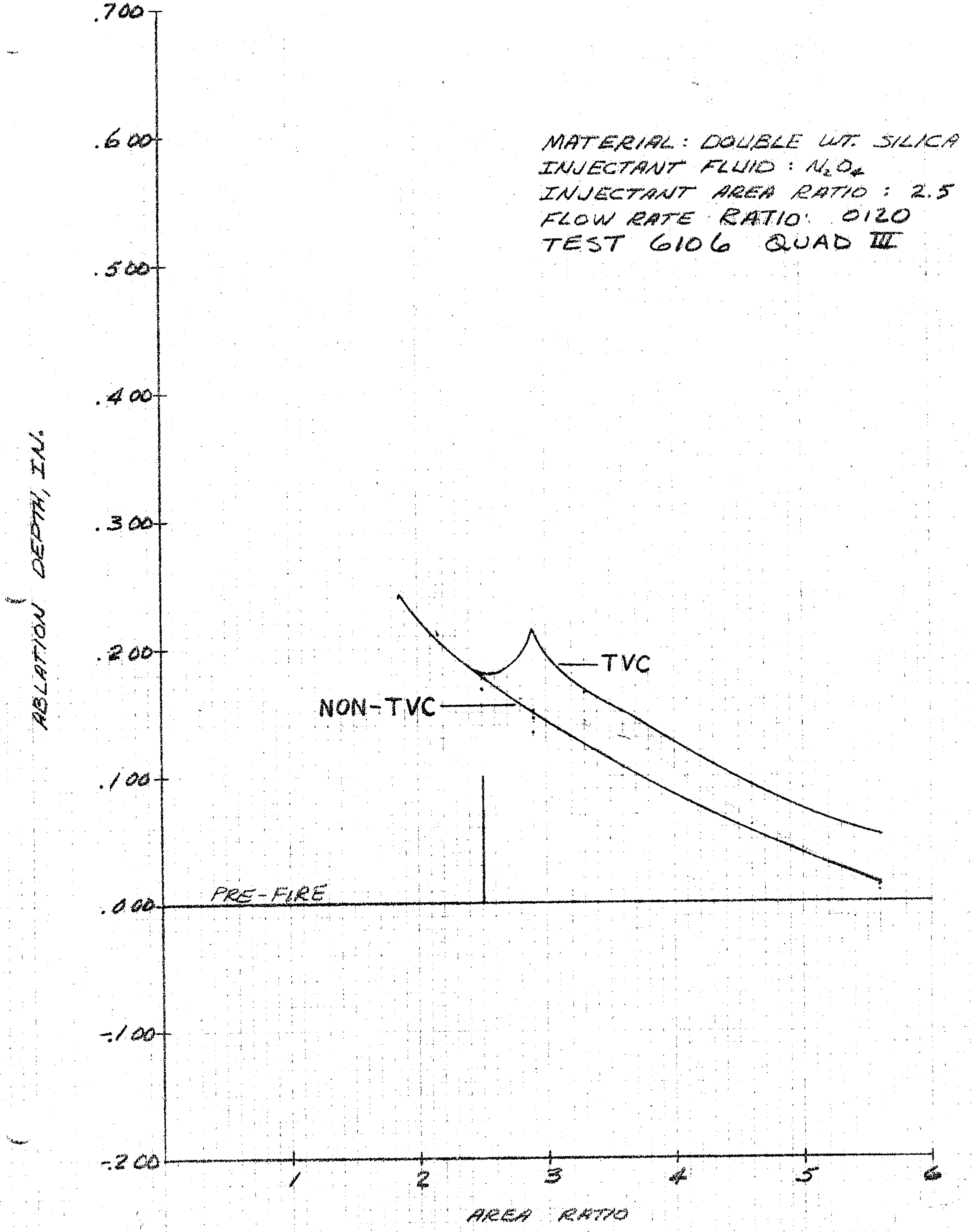

Figure 45. - Nozzle Ablation, Quad III, Test 6106.

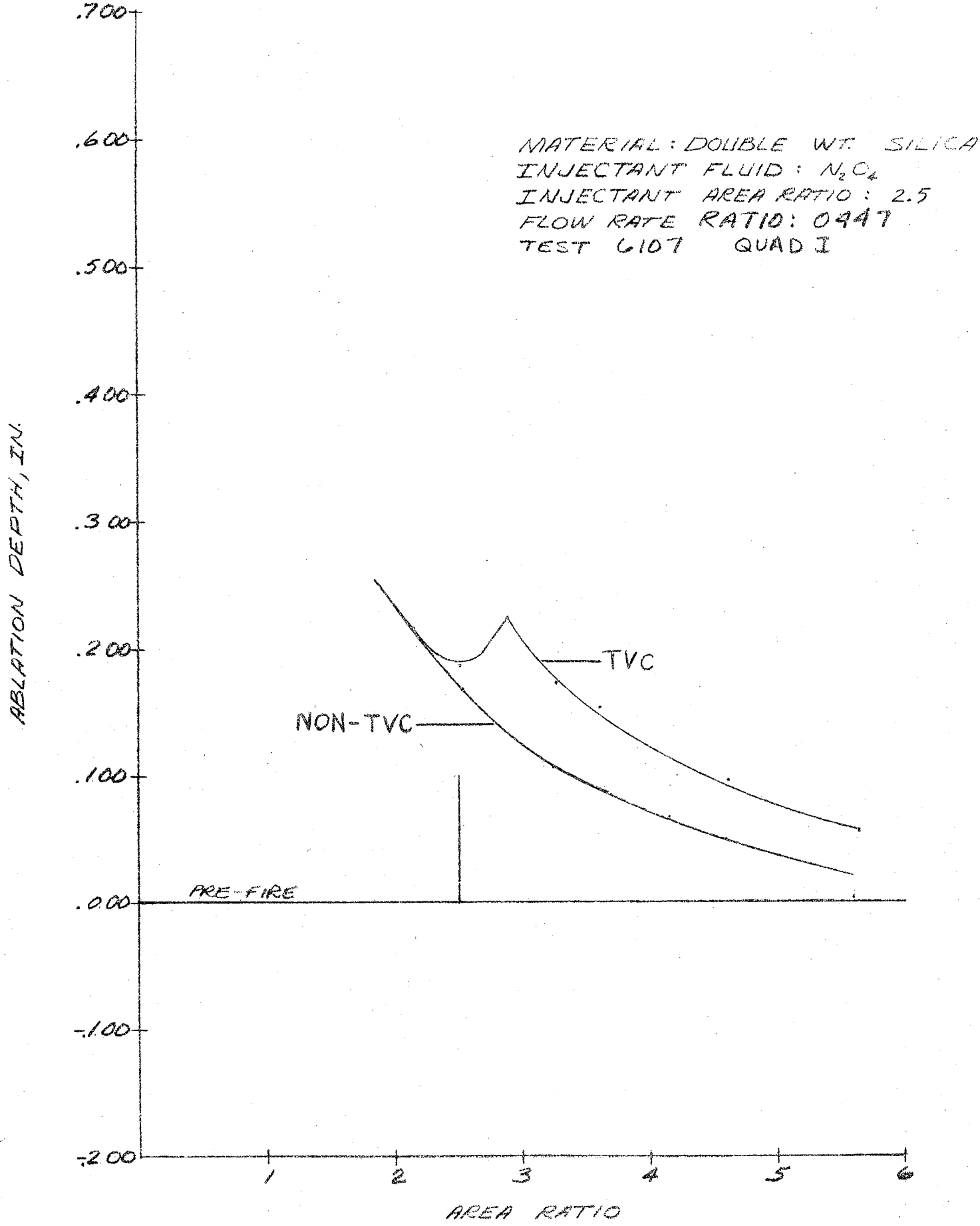

Figure 46. - Nozzle Ablation, Quad I, Test 6107.

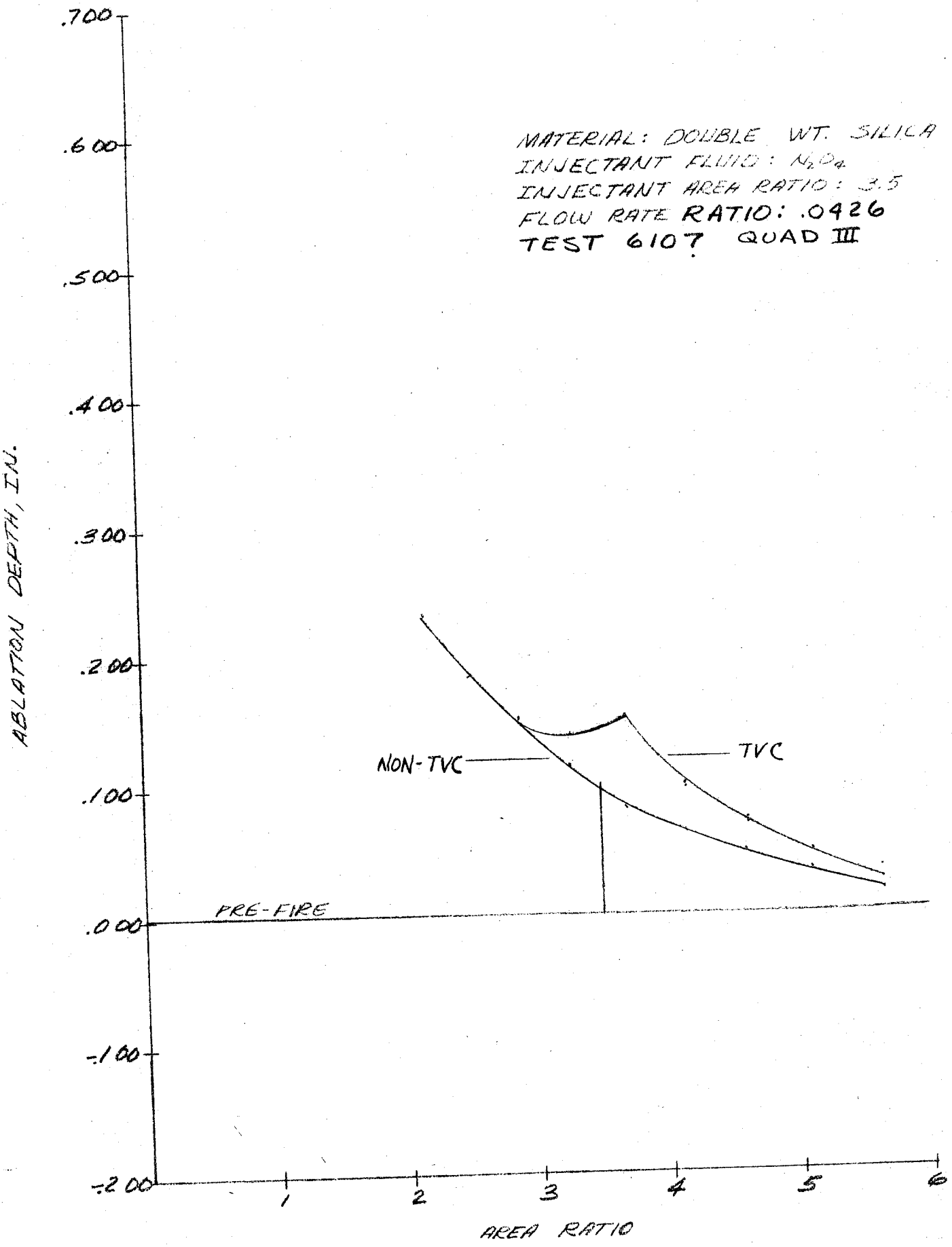

Figure 47. - Nozzle Ablation, Quad III, Test 6107.

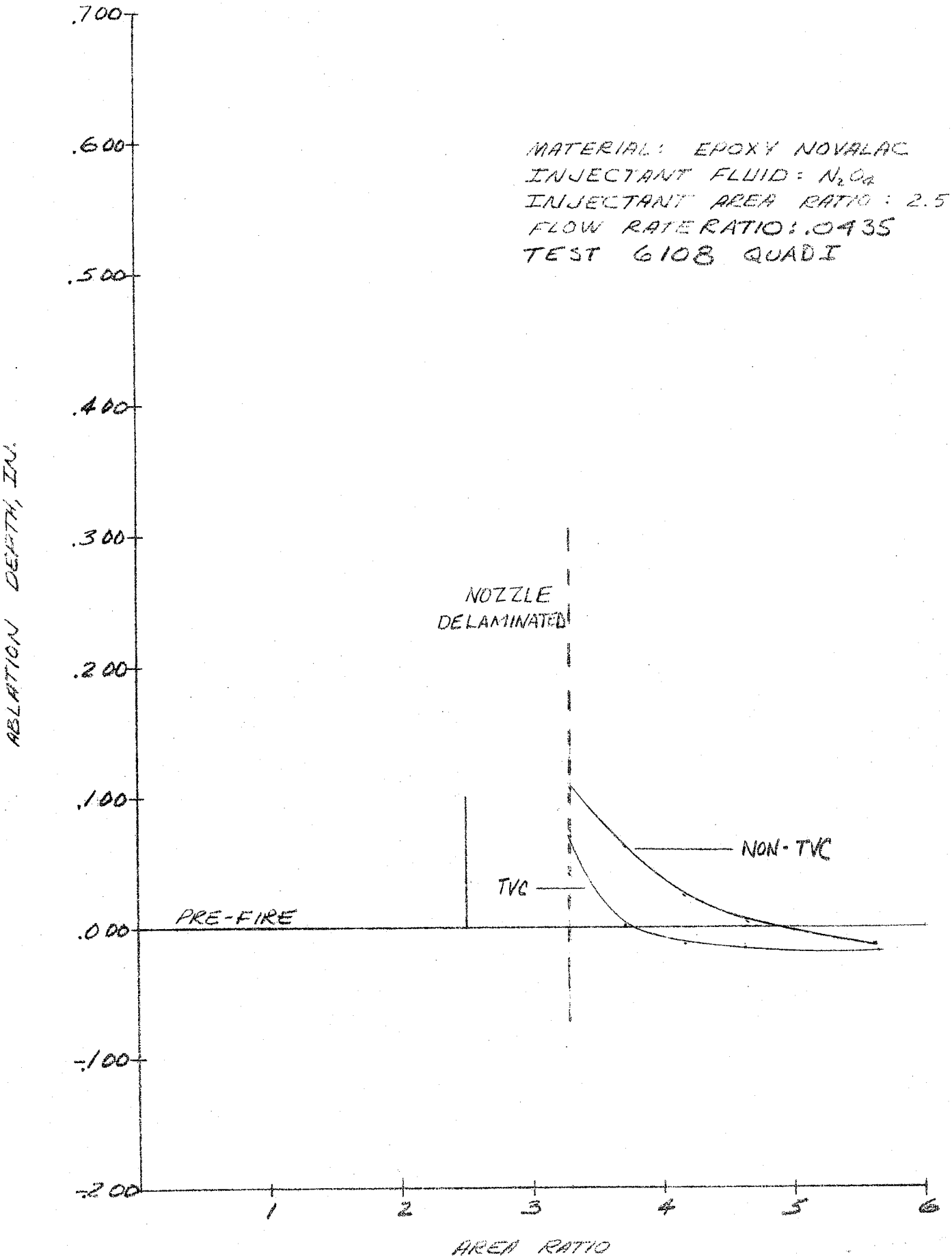

Figure 48. - Nozzle Ablation, Quad I, Test 6108.

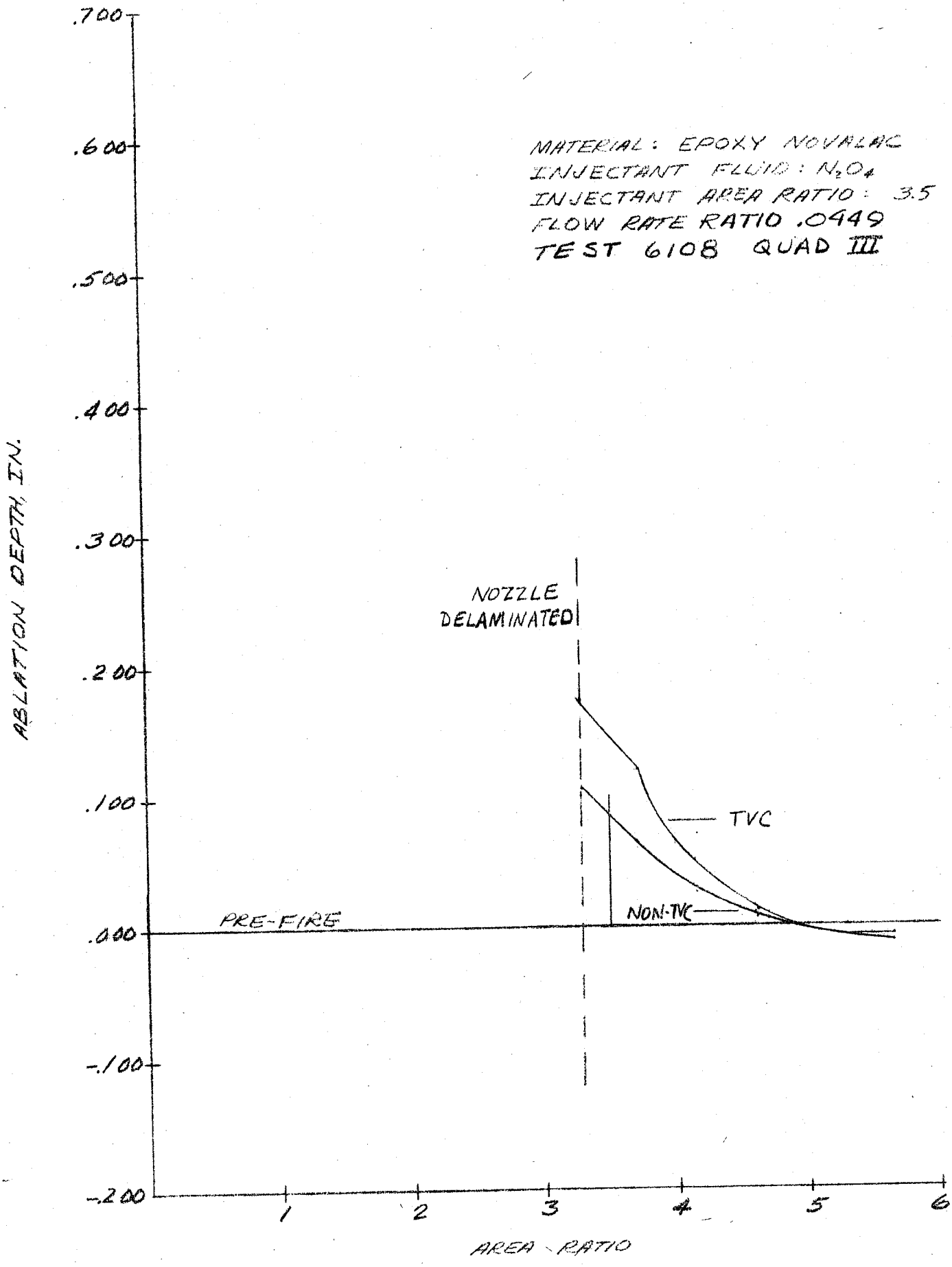

Figure 49. - Nozzle Ablation, Quad III, Test 6108.

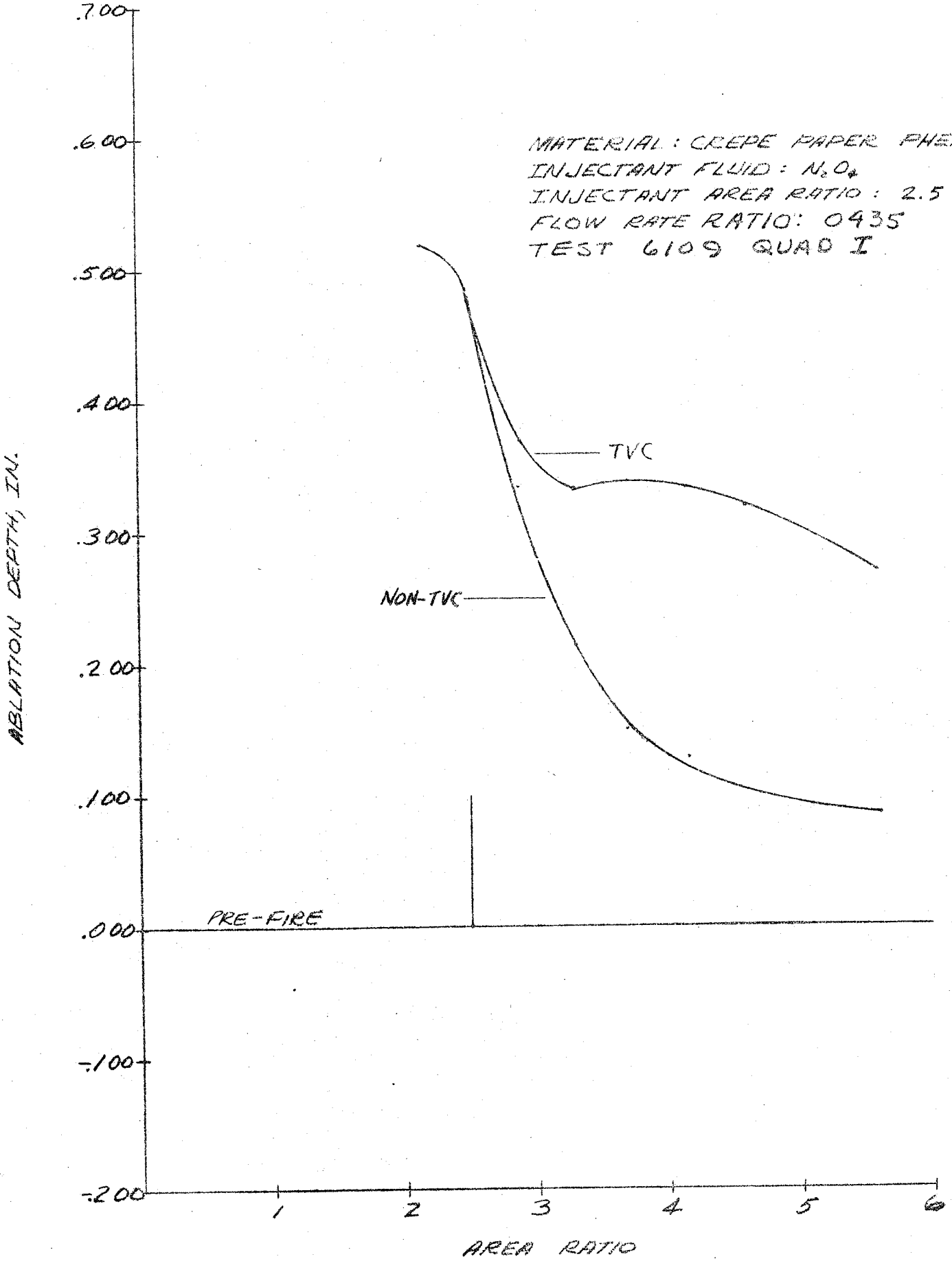

Figure 50. - Nozzle Ablation, Quad I, Test 6109.

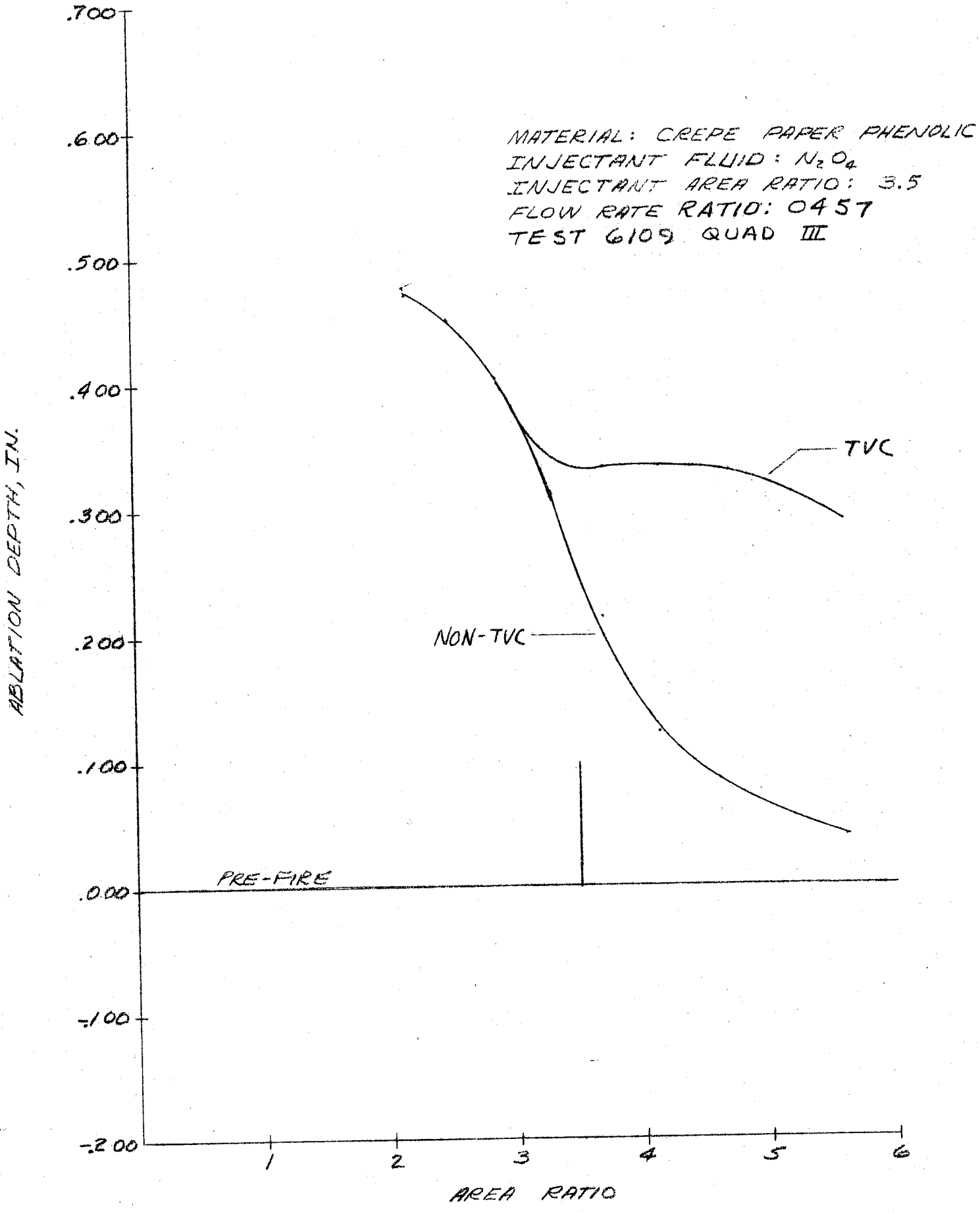

Figure 51. - Nozzle Ablation, Quad III, Test 6109.

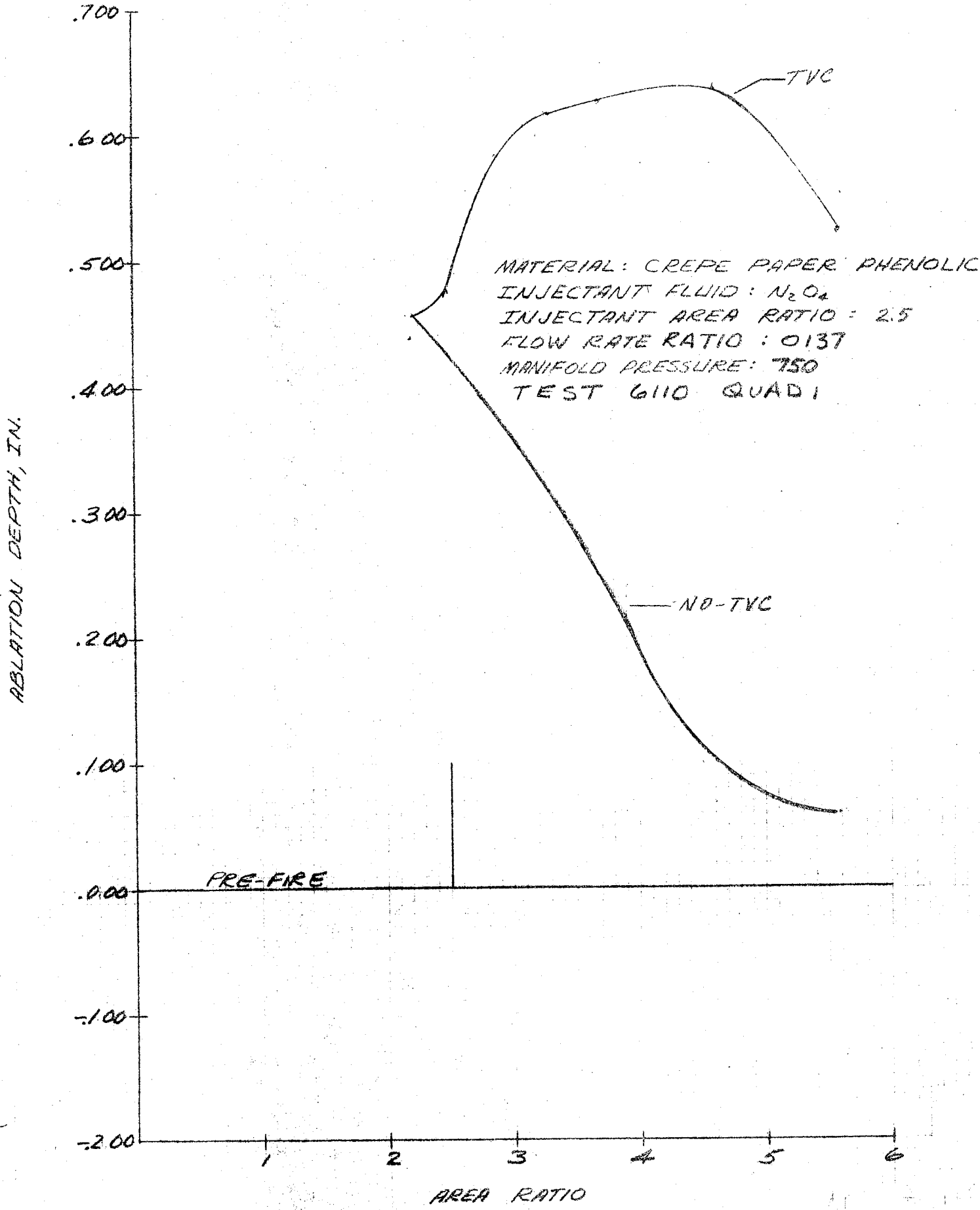

Figure 52. - Nozzle Ablation, Quad I, Test 6110.

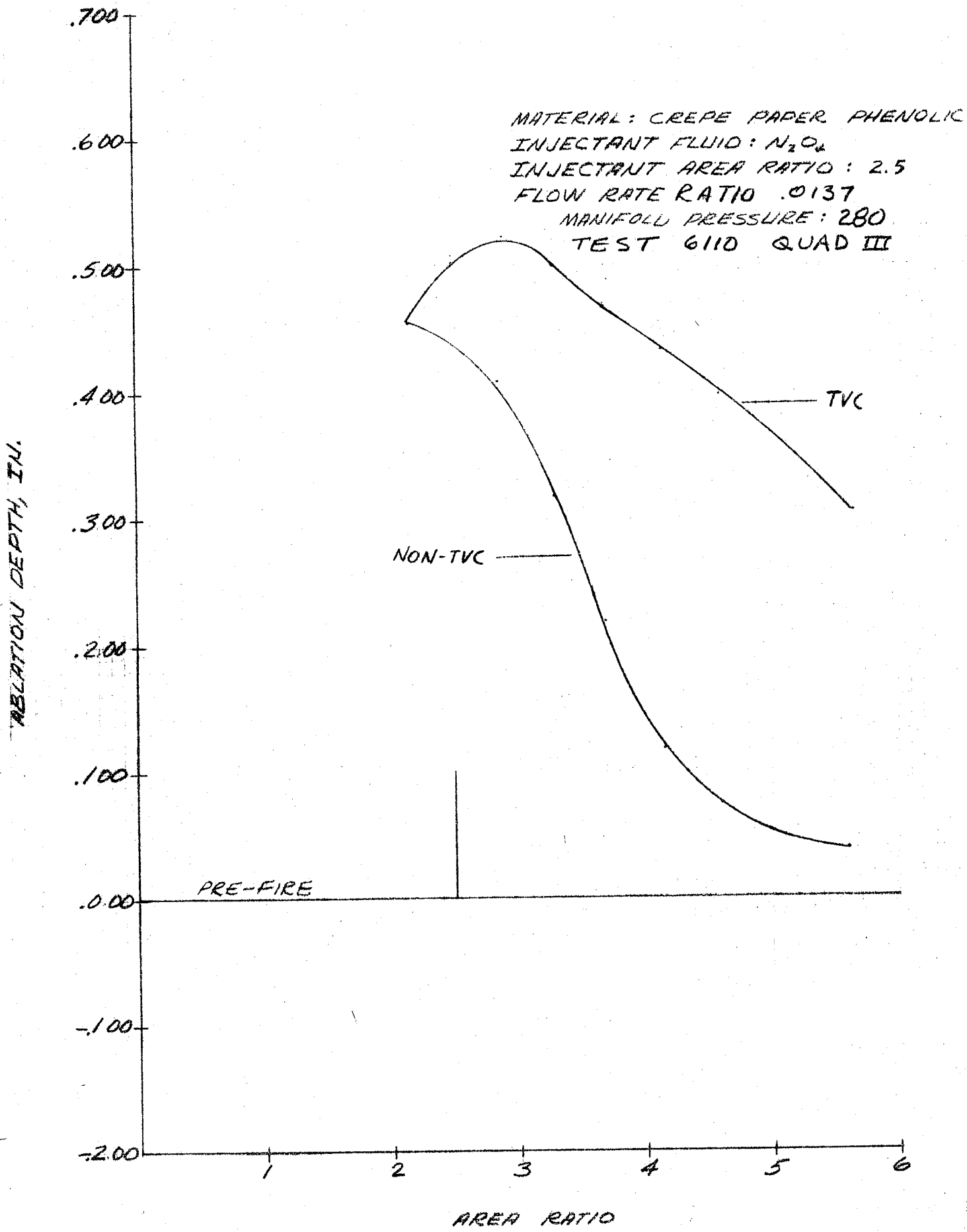

Figure 53. - Nozzle Ablation, Quad III, Test 6110.

depth located just aft of the injection port. This distinct point of maximum ablation is not evident with Freon injectant, at least for the flow rates covered in this set of tests.

B. Freon injectant causes less ablation than N_2O_4. This is the result of a stronger shock created by the injection of N_2O_4, the greater energy released in the reactions of exhaust gases and N_2O_4, chemical reaction between N_2O_4 and the material surface, or a combination of these effects. Both injectants actually cool the nozzle immediately downstream of the injection ports producing less ablation than in the non-TVC areas.

C. FM-5272 crepe paper phenolic ablates at a much higher rate than FM-5504, MXS-198, or SP-8030-96. The ablation distribution for FM-5272 crepe paper phenolic was quite different with the maximum depths occurring further downstream than for the other materials.

The data for KF-418 canvas duck phenolic are very limited because they were acquired only at one circumferential location for one firing with Freon. The ablation of this material was extreme and is presented in figure 39. The peak ablation from these data is twice that of FM-5272 and nearly 10 times that of FM-5504.

D. The ablation data from test 6108 is questionable because forward delaminations occurred which may have influenced the ablation during the test. Swelling of the nozzle in the delaminated areas also effected the accuracy of the measured ablation.

RESULTS/ANALYSIS

The results and analysis are presented in two categories, TVC performance and ablation performance. In addition, a prediction TVC ablation for the candidate material on a 260-in.-diameter nozzle is presented, using the results obtained during this program.

TVC Performance

Side force performance was determined for each injectant tested during the program. TVC injection was accomplished in two quadrants during all the tests. Injection was staggered to have one quadrant injection for 2 sec to obtain side force data. The results of all the tests are presented in table XII. In figure 54 the data are presented as a ratio of side force to axial force (F_s/F_a) versus the ratio of injectant flow rate to motor flow rate (W_s/W_a) for both N_2O_4 and Freon. At the minimum value of W_s/W_a, the N2O4 gives 45% more side force. At the highest value of W_s/W_a for both N_2O_4 and Freon, the N_2O_4 gives 37% more side force. This is approximately the performance difference predicted for these two fluids.

Test No.	Quad	In-jectant	E_i	P_c, psi (N/M^2)	F_a, lb_f (N)	F_s, lb_f (N)	W_s, lb/sec (Kg/sec)	W_a, lb/sec (Kg/sec)	PM, psi (N/M^2)	W_s/W_a	F_s/F_a	I_{sp_s}, sec
6101	I	Freon	2.5	736 (5.05×10^6)	10,600 (47,000)	97 (430)	0.577 (0.26)	45.7 (20.8)	765 (5.25×10^6)	0.0126	0.009	168
6101	III	Freon	2.5	642 (4.4×10^6)	9,400 (41,800)	165 (735)	1.043 (0.472)	39.9 (18.1)	730 (5.02×10^6)	0.026	0.0175	158
6102	I	Freon	2.5	749 (5.15×10^6)	10,900 (48,500)	95 (421)	0.560 (0.25)	46.6 (21.2)	765 (5.25×10^6)	0.0120	0.009	170
6103	I	Freon	2.5	734 (5.05×10^6)	10,450 (46,400)	100 (444)	0.581 (0.262)	45.7 (20.8)	780 (5.36×10^6)	0.0127	0.0095	172
6104	I	N_2O_4	2.5	735 (5.05×10^6)	10,450 (46,400)	145 (645)	0.577 (0.260)	45.7 (20.8)	830 (5.7×10^6)	0.0126	0.0139	252
6104	III	N_2O_4	2.5	660 (4.54×10^6)	9,500 (42,200)	251 (1110)	1.021 (0.464)	40.7 (18.5)	810 (5.57×10^6)	0.025	0.024	223
6105	I	N_2O_4	2.5	737 (5.06×10^6)	10,100 (44,800)	170 (755)	0.579 (0.261)	45.7 (20.8)	828 (5.7×10^6)	0.0126	0.0168	293
6106	I	N_2O_4	2.5	739 (5.06×10^6)	10,500 (46,700)	150 (667)	0.581 (0.262)	45.7 (20.8)	820 (5.64×10^6)	0.0127	0.0138	258
6107	I	N_2O_4	2.5	660 (4.54×10^6)	9,500 (42,200)	255 (1,105)	1.636 (0.744)	41.2 (18.7)	735 (5.05×10^6)	0.039	0.0268	155
6107	III	N_2O_4	3.5	545 (3.82×10^6)	7,000 (31,000)	155 (690)	1.596 (0.729)	33.9 (15.4)	725 (5×10^6)	0.047	0.0221	97
6108	I	N_2O_4	2.5	663 (4.55×10^6)	9,510 (42,300)	245 (1,080)	1.646 (0.749)	41.0 (18.6)	732 (5.04×10^6)	0.040	0.0257	149
6108	III	N_2O_4	3.5	530 (3.65×10^6)	6,700 (29,700)	160 (712)	1.699 (0.770)	32.0 (14.5)	708 (4.9×10^6)	0.053	0.0238	94
6109	I	N_2O_4	2.5	660 (4.54×10^6)	9,490 (42,200)	248 (1,100)	1.675 (0.763)	40.7 (18.5)	730 (5.02×10^6)	0.041	0.0261	148
6110	I	N_2O_4	2.5	655 (4.5×10^6)	9,450 (42,000)	126 (560)	0.515 (0.232)	41.0 (18.6)	720 (4.95×10^6)	0.0126	0.0133	244

TABLE XII. - TVC PERFORMANCE SUMMARY

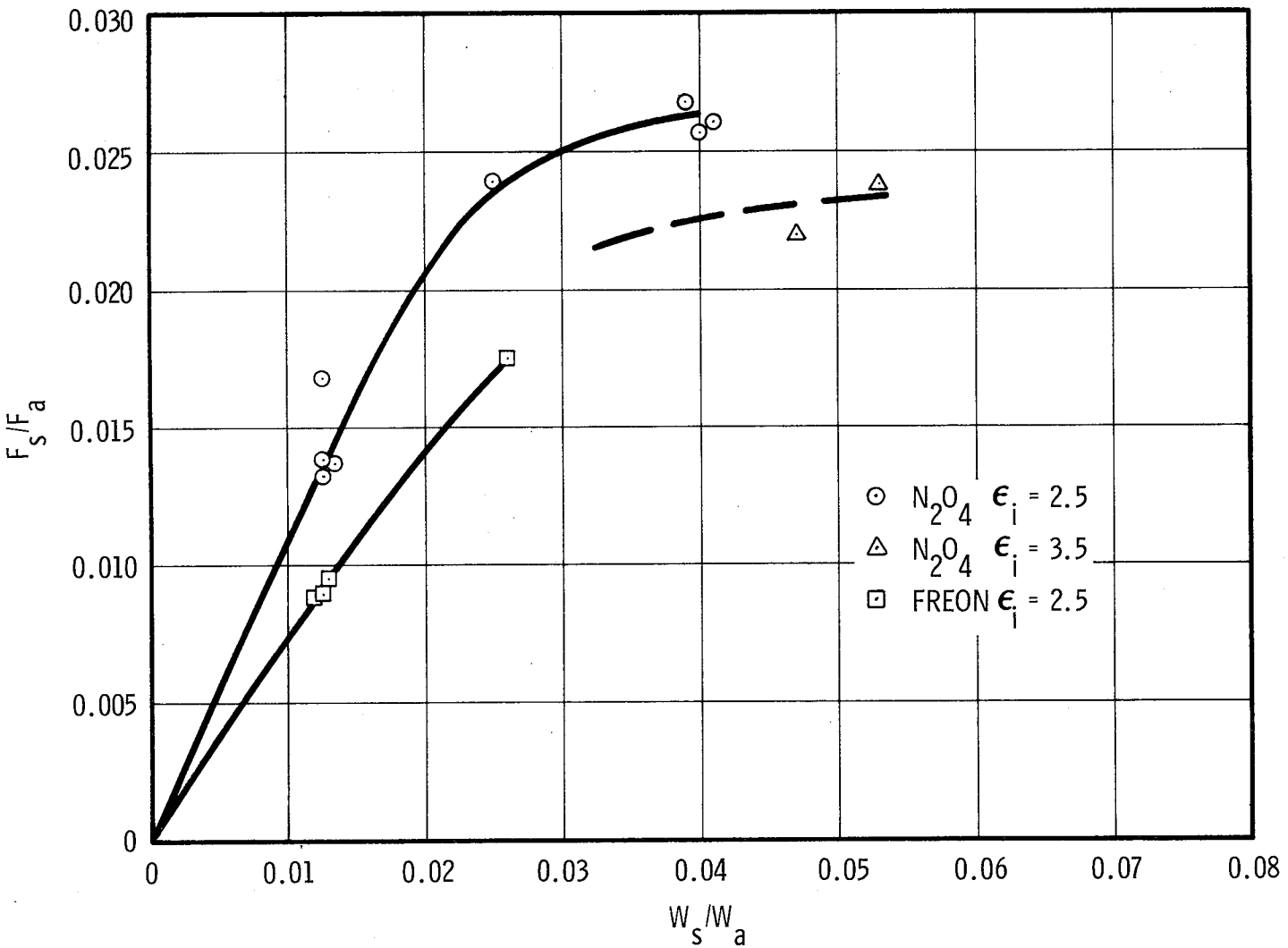

Figure 54. - Performance Summary

A better indication of TVC performance is obtained by comparing these data with similar data from the UTC 120-in.-diameter motors, as shown in figure 55. The N_2O_4 data from the Titan program is for both subscale (6.0-in. throat) and full scale (37.7-in. throat). The Freon data were obtained during initial TVC development tests at UTC with a similar TVC configuration. These data represent available industry data for Freon.

As shown in figure 55, there is a decrease in subscale LITVC N_2O_4 ablation rates as the W_s/W_a value increases. At a W_s/W_a of 0.04, the subscale LITVC N_2O_4 data fall on the curve for Freon 113, well below 120-in.-diameter motor data for N_2O_4. This phenomenon is explained by the physical limitations encountered in scaling LITVC systems. The use of a reactive injectant, such as N_2O_4, requires a system that allows sufficient reaction time of the N_2O_4, to obtain improved performance. The LITVC nozzle, which uses a 3.5-in. (0.089 m) throat, has a mixing length of only 4.82 in. in the nozzle from the point of injection to the exit. By comparison, the smallest subscale Titan nozzle had a mixing length of 10.8 in. (0.27 m). The effect of this mixing length has been observed on the Titan program between different size subscale motors and the full-scale motor. Figure 56 presents the results of several different size motor LITVC programs and the scale effect on side force for each motor. The mixing length is the controlling parameters, and at high flow ratios – greater than required for the 260-in.-diameter motor nozzle – even the 120-in.-diameter motor does not get complete reaction of the N_2O_4.

Based on this length limitation of the LITVC nozzle, the side force data predicated for the 260-in.-diameter motor nozzle in a later section will be based on the 120-in.-diameter motor performance with N_2O_4 for flow rate ratios in excess of 0.015.

Analysis of Ablation Data

A primary objective of this program was to develop a technique for the prediction of ablation performance in the presence of TVC for several candidate materials being considered for the 260-in.-diameter solid rocket motor exit cone liner. This was to be accomplished by using measured data from a series of subscale tests combined with extensive ablation data from 120-in. motor tests in areas affected by LITVC. The test motor nozzles were approximately 1/20 to 1/30 the size of the 260-in. motor nozzle.

Scaling ablation data are very complex because many parameters are needed to fully describe the process commonly called ablation. Addressing only the problems associated with phenolics, the following list of parameters should be incorporated into an ablation model:

A. Material susceptibility to chemical reactions

B. Material strength as a function of temperature

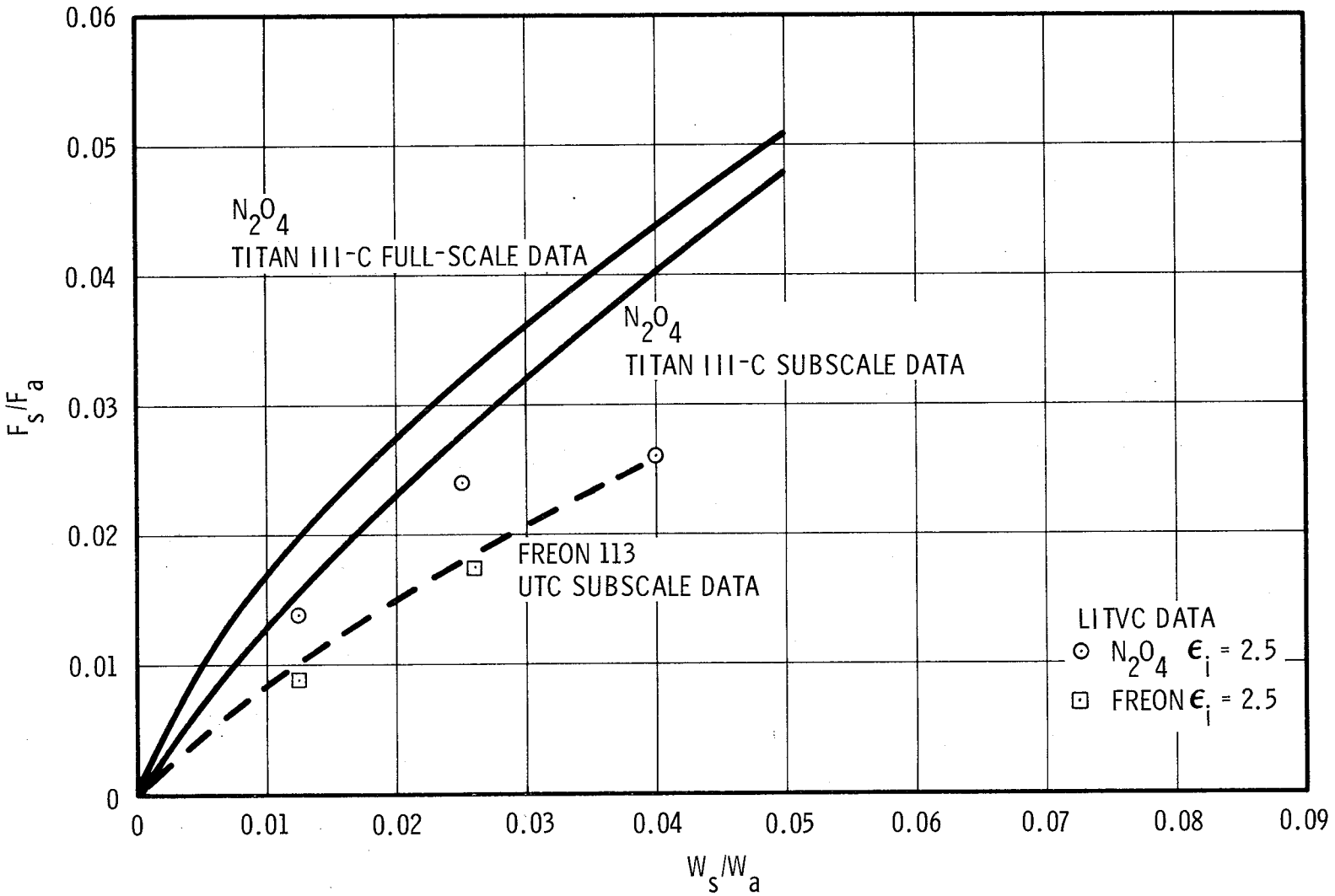

Figure 55. - Performance Comparison

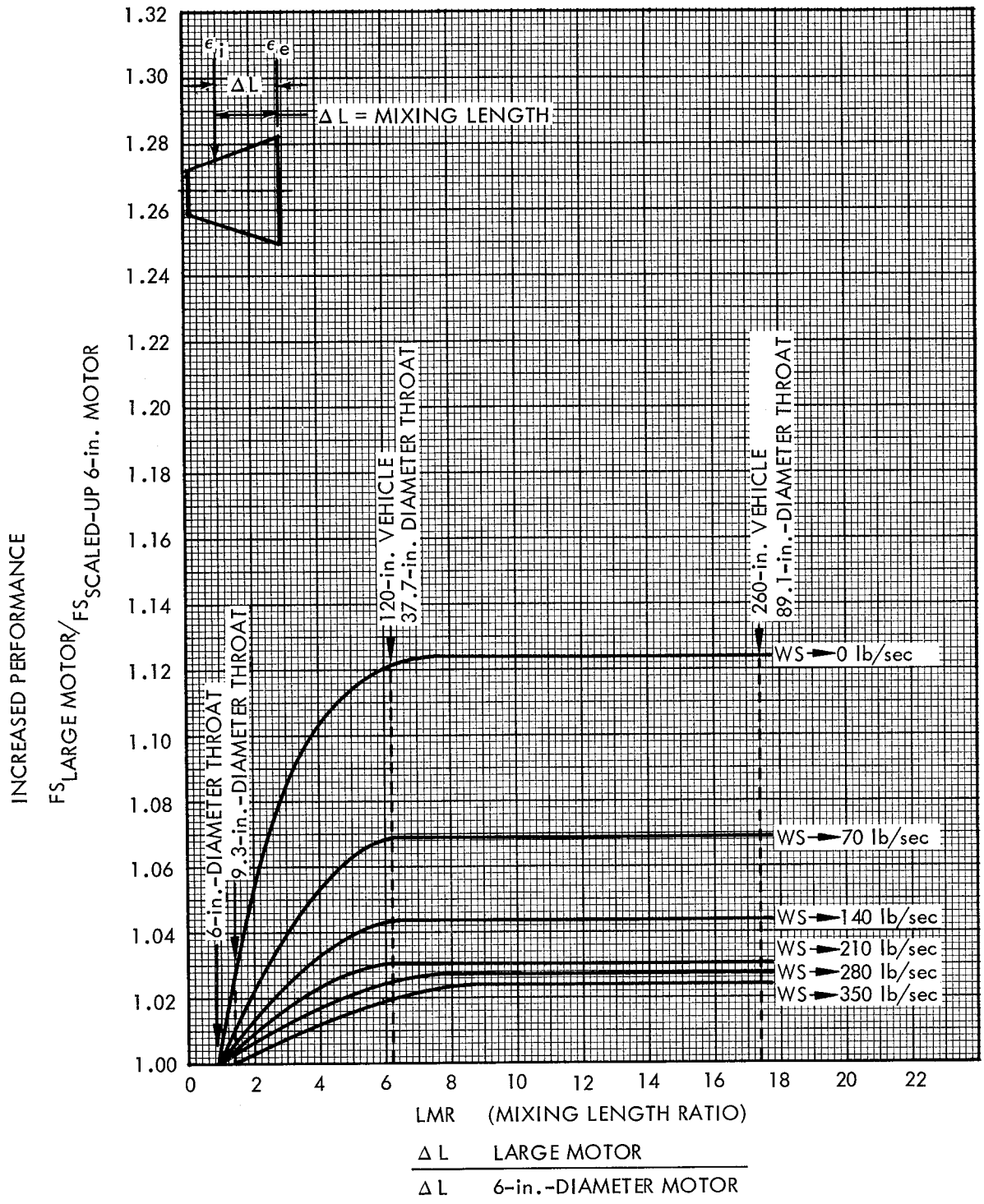

Figure 56. - Performance Increase in Large Motors and Subscale Prediction Resulting from Increased Mixing

C. Material thermal properties (thermal conductivity, specific heat, and density)

D. Corrosivity of the motor exhaust

E. Local heat transport properties (recovery temperature, heat transfer coefficient).

The above are some of the major areas of interest in determining ablation. Each can be related to more basic parameters which are mostly interrelated as shown here:

A. Chemical attack is governed by

1. Wall temperature
2. Chemical composition of ablative material
3. Surface gas composition
4. Surface gas recovery temperature.

B. Material strength and thermal properties are functions of wall temperature.

C. Motor exhaust corrosivity and its effect on ablation is a function of

1. Surface composition
2. Surface recovery temperature.

D. Heat transport mechanisms are a function of

1. Surface recovery temperature
2. Wall temperature
3. Heat transfer coefficient.

In examining the above, it can be seen that given wall temperature, recovery temperature, heat transfer coefficient, material chemical composition, and surface gas composition, one could construct a model of the ablation process. Furthermore, if a separate model is prepared for each combination of propellant gas and ablative material composition with the assumption of frozen flow, the number of parameters can be reduced by two (material chemical composition and surface gas composition). This leaves wall temperature, heat transfer coefficient, and recovery temperature.

Two approaches are possible in the determination of the relationship between ablation rate and the parameters affecting it. One is the theoretical approach in which some model of the process is derived from fundamental considerations. Because of the complexity of the phenomenon, this has generally only been mildly successful for non-graphite based materials. The second approach is to determine the relationship on a semi-empirical basis. This generally consists of making relatively inexpensive subscale motor tests and using the data to predict the ablation in the full-scale motor under consideration. When this is done, one

or two parameters are generally singled out as independent variables with which to form a correlation with measured ablation rate. Parameters which have been used in areas not affected by LITVC include area ratio, Mach number, heat transfer coefficient and wall heat flux.

The development of an accurate and usable model for predicting ablation in regions affected by LITVC is significantly more difficult than for regions not affected by LITVC. The difficulty arises from several causes:

A. The necessity to include the effect of different LITVC flow rates

B. The more complex flow field produced by injection

C. More complex chemical reactions which may take place between the injectant and the ablative material.

Before one can hope to develop a TVC ablation model which works for subscale and full-scale motors, it is necessary to sufficiently understand the ablation process so that ablation in regions not affected by LITVC can be accurately predicted. For example, to isolate the ablation depth occurring during injection, a predicted depth during times without injection must be subtracted from the total measured depth. Because of this need for an accurate prediction model for areas not affected by LITVC, considerable effort has been expended to refine present methods.

Ablation Prediction in Regions not Affected by LITVC

For some time, UTC and other companies have used heat flux as the correlating parameter because it contains the parameters that are most likely to affect ablation rate. Data from different size motors generally have not been consistent, requiring the determination of a multiplier to be used when going from subscale to full-scale motors. The need for such a multiplier implies one of two possibilities:

A. Wall heat flux is not a satisfactory parameter with which to correlate ablation rate, and a more complex relationship exists between ablation rate and the three parameters, recovery temperature, surface temperature, and heat transfer coefficient.

B. Calculation of the heat flux is incorrect; if it were correctly calculated, a good correlation would result and be valid for all conditions without the need of scale-up multipliers.

Silica phenolic ablation data taken from 120-in. static motor firings had been correlated with heat flux in the past at UTC. Such a correlation was attempted for the silica phenolic in this series of tests using data from quadrants II and IV where liquid injection had no effect. The attempted correlation is shown in figure 57 along with the 120-in. correlation. Not only is there poor agreement between small-scale and large-scale data, but there is wide scatter in the small-scale data. If heat flux is an appropriate correlation parameter, the data in figure 57 indicate that the heat flux calculated for the

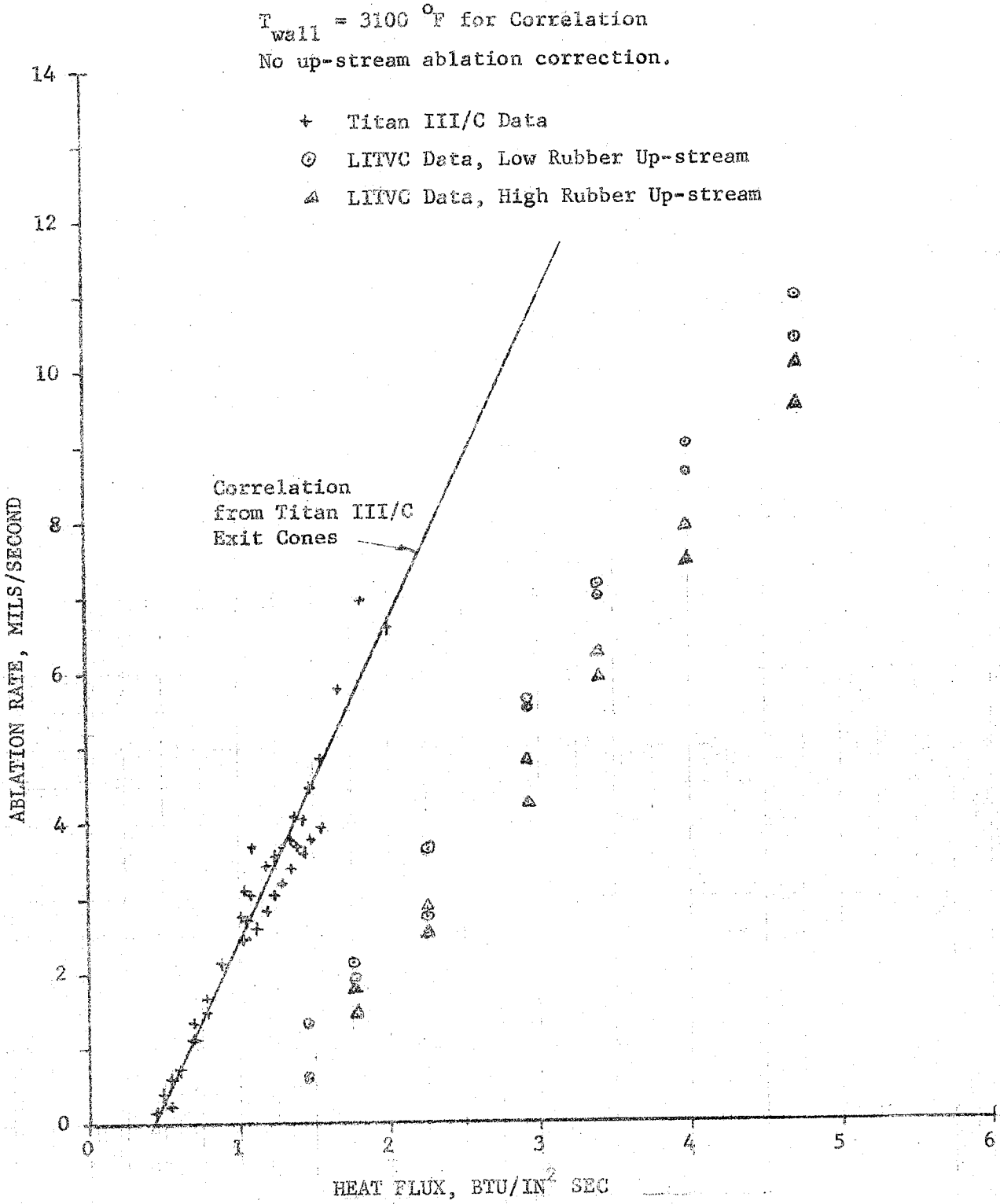

Figure 57. - Silica Phenolic Ablation Rate vs Heat Flux for Titan III-C Exit Cones and LITVC Subscale Exit Cones (TM-3 Tests).

120-in. motor is too low or that the heat flux calculated for the subscale is too high. Furthermore, a similar error appears between quadrant II and IV in the subscale data.

A careful examination was made of the method of heat flux calculations used to create figure 57. The following points were considered:

A. Calculation of the heat transfer coefficient had been done using the simplified Bartz equation. This technique failed to account for nozzle geometry other than local diameter. Instead, a boundary layer analysis technique developed by Aerotherm Corp. (formerly Vidya) was used. The entire nozzle geometry is input to the computer program BOUND/LAYER which solves the integral boundary layer equations at incremental distances along the nozzle surface.

B. An arbitrary constant wall temperature had been used in the past. The reasoning had been that the use of the same temperature (called the correlation temperature) in developing a correlation and in using it for predictions would yield consistent results. That is, if a different correlation temperature was chosen, a different correlation curve would result along with correspondingly different fluxes calculated when making predictions. The end result would be the same ablation rate predicted using either correlation temperature.

   A problem arises in motors which may have significantly different heat transfer coefficients. Using the arbitrary correlation temperature method, the flux calculated is proportional to heat transfer coefficient (holding recovery temperature constant). The actual heat flux, on the other hand, is not proportional to heat transfer coefficient because a higher flux raises the wall temperature lowering the driving potential.

   The improved method of selecting a wall temperature is to use a one-dimensional transient heat conduction computer program to establish the steady state wall temperature, based upon the local heat transfer coefficient and measured or preliminary ablation rate estimate. This, of course, implies an iteration might be necessary when using the model for predictions.

C. Most significantly, the method of calculating recovery temperature was changed to account for film cooling caused by the addition of upstream ablation products to the boundary layer gases. It had been assumed that the recovery temperature was not affected by upstream ablation and could be calculated in the usual way:

$$T_R = (1 + P_r^{1/3} \frac{\gamma - 1}{2} M^2) T_S$$

where:

P_r = Prandtl Number

γ = Ratio of specific heats

M = Mach number

T_s = Static temperature corresponding to M.

Most solid rocket motors have aft closures insulated with rubber which ablate at high rates and at low temperatures. When the products of this ablation enter the boundary layer, they lower the effective stagnation and recovery temperatures seen by the nozzle walls downstream of the rubber insulation.

It is assumed that the upstream ablation products remain in a narrow region near the nozzle wall (similar in concept to a boundary layer) and mix with a fraction of the free stream gases. This fraction is the ratio of the annular flow area near the wall, $2\pi R\Delta$, to the total nozzle area, πR^2. The mass flow in this annular area is, therefore, given by:

$$\dot{m}_g = \dot{M}_g \frac{2\pi R\Delta}{\pi R^2} = \dot{M}_g \frac{2\Delta}{R}$$

where $\dot{M}_g$ = total motor mass flow rate

$\dot{m}_g$ = mass flow in annular area

R = local radius of nozzle

Δ = a thickness such that if the gas with which upstream ablation products mix were at free stream conditions, this gas would occupy a flow area along the wall of thickness Δ.

To determine the effective stagnation temperature, T_o', an energy balance is made with the upstream ablation products and the mass flux $\dot{m}_g$. To account for the growth in the boundary layer and the mixing of free stream gases with the cooled boundary layer, the thickness Δ is assumed to be proportional to the boundary layer energy thickness,

$$\Delta = A\delta$$

The energy thickness, δ, is calculated by the same boundary layer analysis computer program used to calculate heat transfer coefficient. Thus, T_o' is given by

$$T_o' = \frac{\dot{m}_g C_{P_G} T_o + \dot{m}_R C_{P_R} T_{o_R}}{\dot{m}_g C_{P_G} + \dot{m}_R C_{P_R}}$$

where T_o = free stream stagnation temperature

T_{o_R} = stangation temperature of upstream ablation products

C_{P_G} = specific heat of free stream gas

C_{P_R} = specific heat of upstream ablation products

$\dot{m}_R$ = mass flow of upstream ablation products

and $\dot{m}_g$ is given by

$$\dot{m}_g = \dot{M}_g \frac{2\Delta}{R} = \dot{M}_g \frac{2A\delta}{R}$$

Recovery temperature is calculated as

$$T_R' = T_o' \frac{(1 + P_r^{1/3} \frac{\gamma-1}{2} M^2)}{(1 + \frac{\gamma-1}{2} M^2)}$$

The constant, A, can be determined empirically by using ablation data from at least two tests which have different values of $\dot{m}_R$ the mass flow of upstream ablation products. Fortunately, three such tests with silica phenolic ablation data are available for this determination:

A. LITVC test 6101 quadrant IV where $\dot{m}_R$ from upstream rubber ablation is 0.1928 lb/sec (0.869 kg/sec)

B. LITVC test 6101 quadrant II where $\dot{m}_R$ from upstream rubber ablation including an additional test strip is 0.2718 lb/sec (0.123 kg/sec)

C. 120-in. motor data where $\dot{m}_R$ from aft closure rubber ablation is 5 lb/sec (2.26 kg/sec).

Calculations of heat flux at each ablation measurement station were made for several values of A using wall temperatures calculated with a one-dimensional heat condition computer program, heat transfer coefficients calculated with the boundary layer analysis program, and a recovery temperature which accounts for upstream rubber ablation. A least squares fit line was determined for each test and each value of A. The correct value of A is that which makes all three lines coincide for that single value of A. It was found that the value of A = 1.2 brought the three tests into closest agreement. Figure 58 shows the data from all three tests using a value of A = 1.2. There is less than 0.5 mil/sec rms deviation from the least squares best fit line drawn through the data, and the resulting statistical correlation coefficient was 0.9834 for the correlated data. The tremendous improvement over the previous correlation technique can be seen by comparing figures 57 and 58.

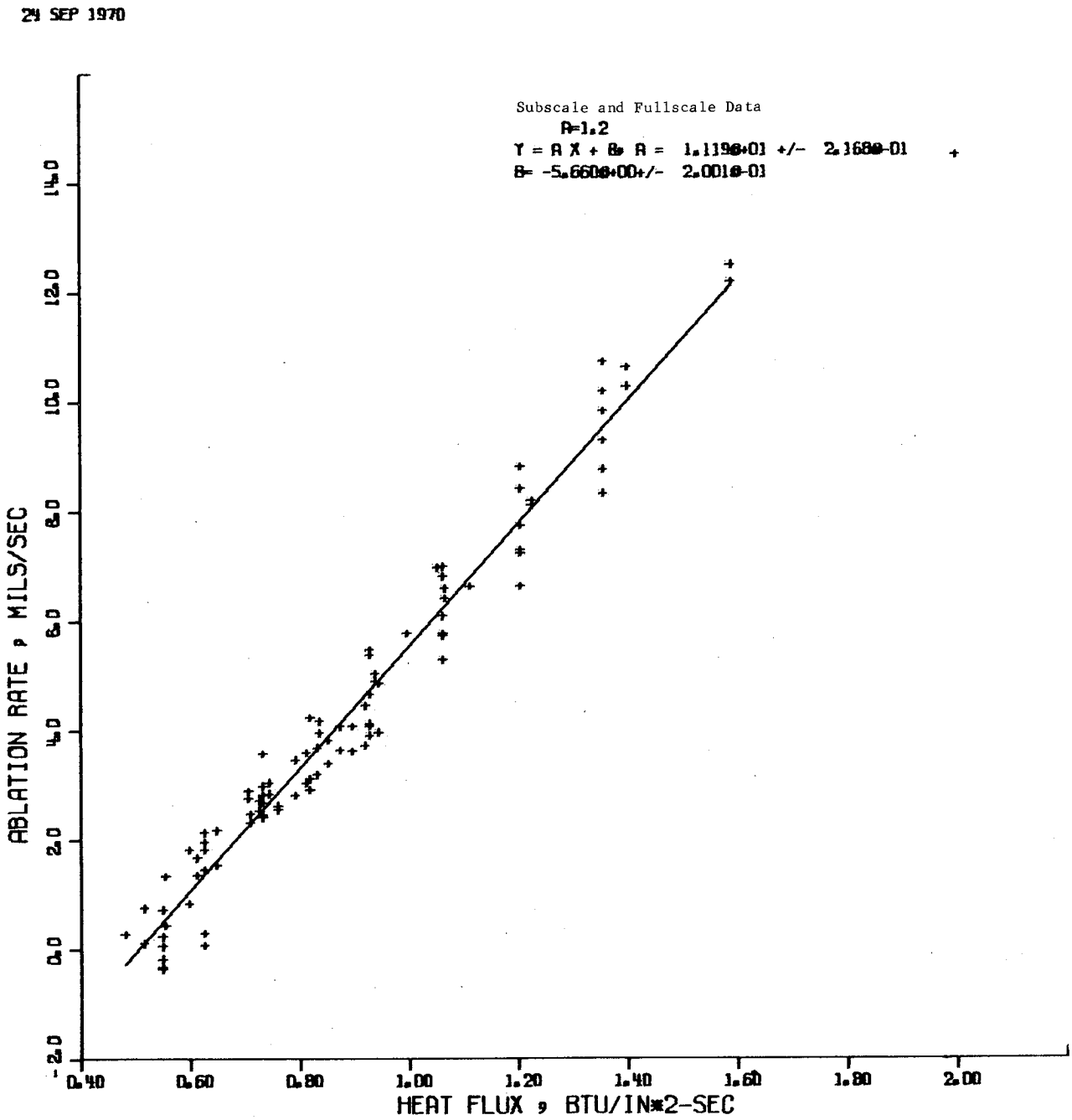

Figure 58. - Correlation of Ablation Rate versus Heat Flux for FM-5504.

Figure 59 presents a correlation for a value of A equal to 1 million which is equivalent to neglecting the effect of upstream ablation products. The effect of failing to consider this effect in the calculation of the heat flux can be seen by comparing figure 59 with figure 58. The scatter of data about the best fit line is much greater. Furthermore, use of this correlation in a region where very little upstream ablation occurs would result in large errors in ablation prediction.

Graphs of energy thickness, heat transfer coefficient, and wall temperature as functions of Mach number that were used in these calculations are shown in figures 60, 61 and 62.

Ablation Prediction in LITVC Regions

UTC has developed a TVC ablation prediction model that accurately models ablation in 120-in. motors with injection at an area ratio of 3.5. In developing the model, the approach was to consider which parameters are important and then to find their functional dependence from the test data available. Ideally, these parameters will sufficiently represent the important pecularities of any motor so that the ablation depth can be predicted for an arbitrary motor with characteristics different from the 120-in. motors upon which the original investigation was based.

The following considerations were taken into account in arriving at the appropriate correlation parameters:

A. Ablation rate of silica cloth phenolic in the absence of TVC fluid has been successfully correlated with combined convective and radiative heat flux. It is assumed that this correlation is also valid in regions affected by LITVC, provided the correct heat flux at the wall can be calculated. Thus, what is needed is an empirical correlation with which to calculate heat flux in areas influenced by liquid injection. Such a correlation also makes it possible to predict ablation rates for any material once the correlation of ablation rate and heat flux has been obtained for that material.

B. The mechanism by which liquid injection produces the desired side force is through the creation of a protuberance in the gas stream, causing a higher static pressure behind the resulting shock wave. The protuberance also disturbs the flow pattern in its vicinity, resulting in increased local flow velocity which increases heat transfer coefficients. Extensive tests have been made to determine the increase in heat transfer around solid protuberances in supersonic flow. The results indicate that for protuberances of a given shape the increase in heat transfer coefficients is primarily a function of the size of the protuberance. This suggests that an appropriate parameter with which to relate heat flux in LITVC-affected regions to injectant flow rate is the height of the resulting protuberance.

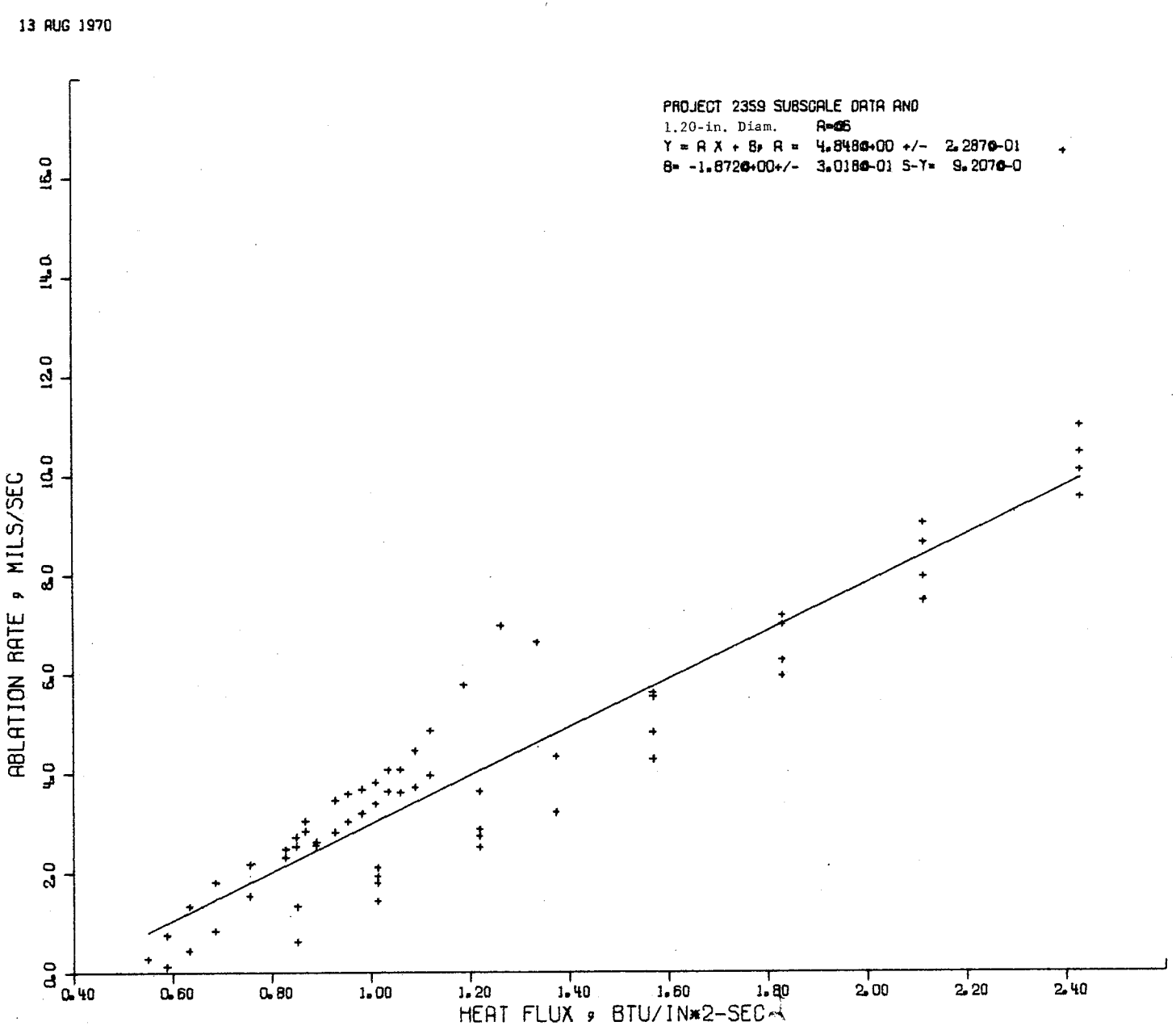

Figure 59. - Silica Phenolic Ablation Correlation
Based on Previous Heat Flux Correlation Techniques

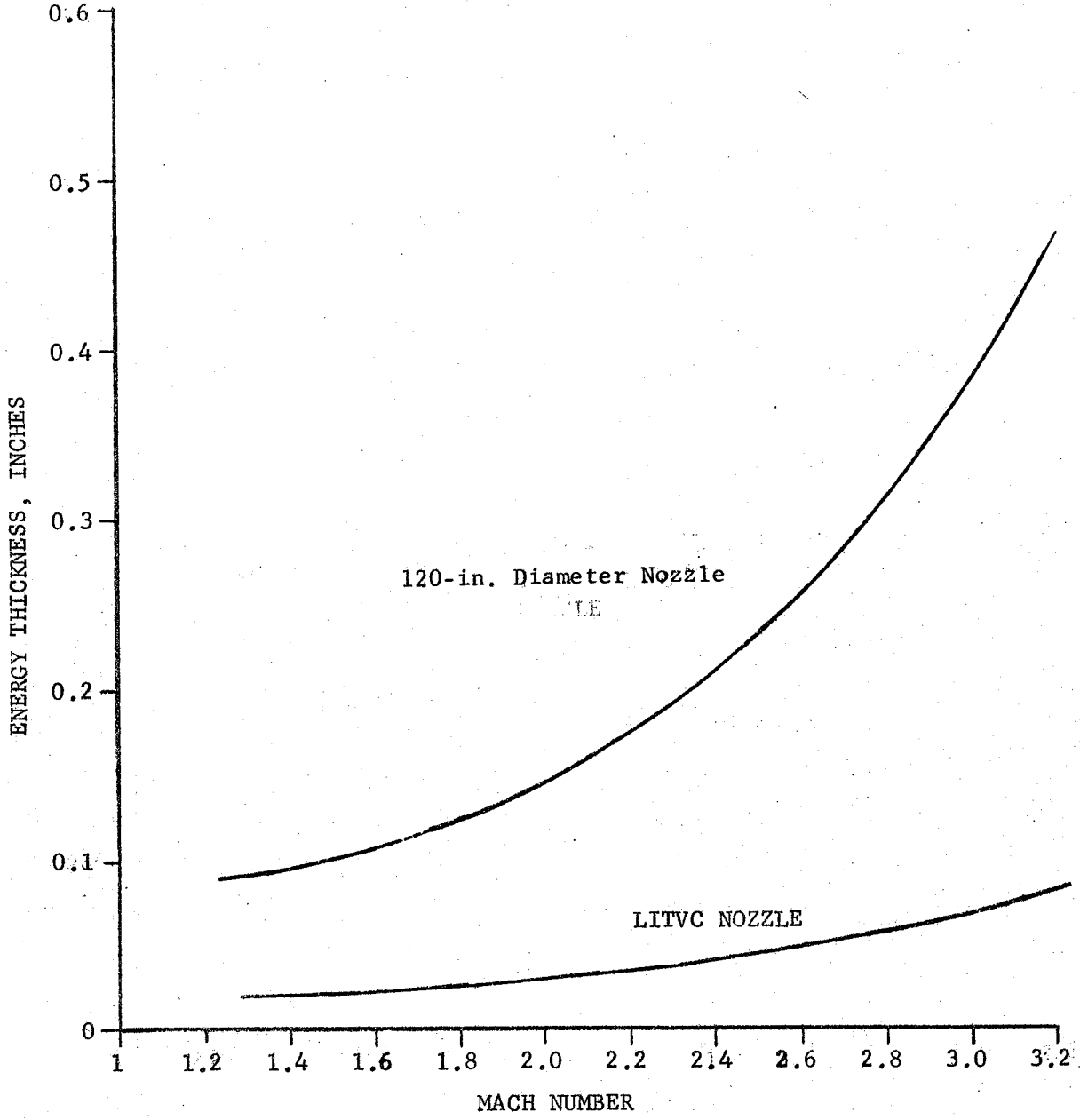

Figure 60. - LITVC Nozzle and Titan III-C Nozzle Energy Thickness vs Mach Number.

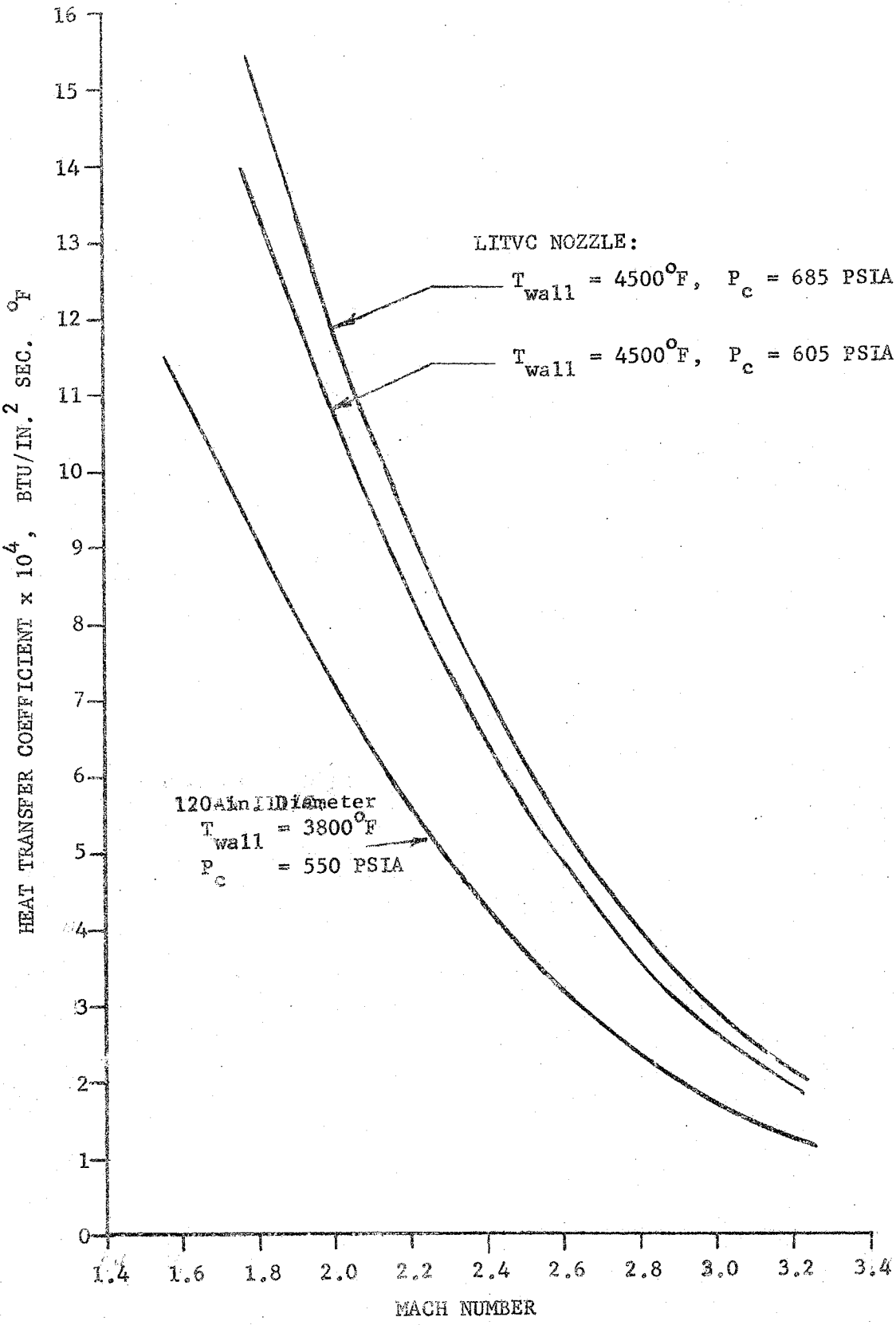

Figure 61. - Exit Cone Heat Transfer Coefficients vs Mach Number from Boundary Layer Analysis.

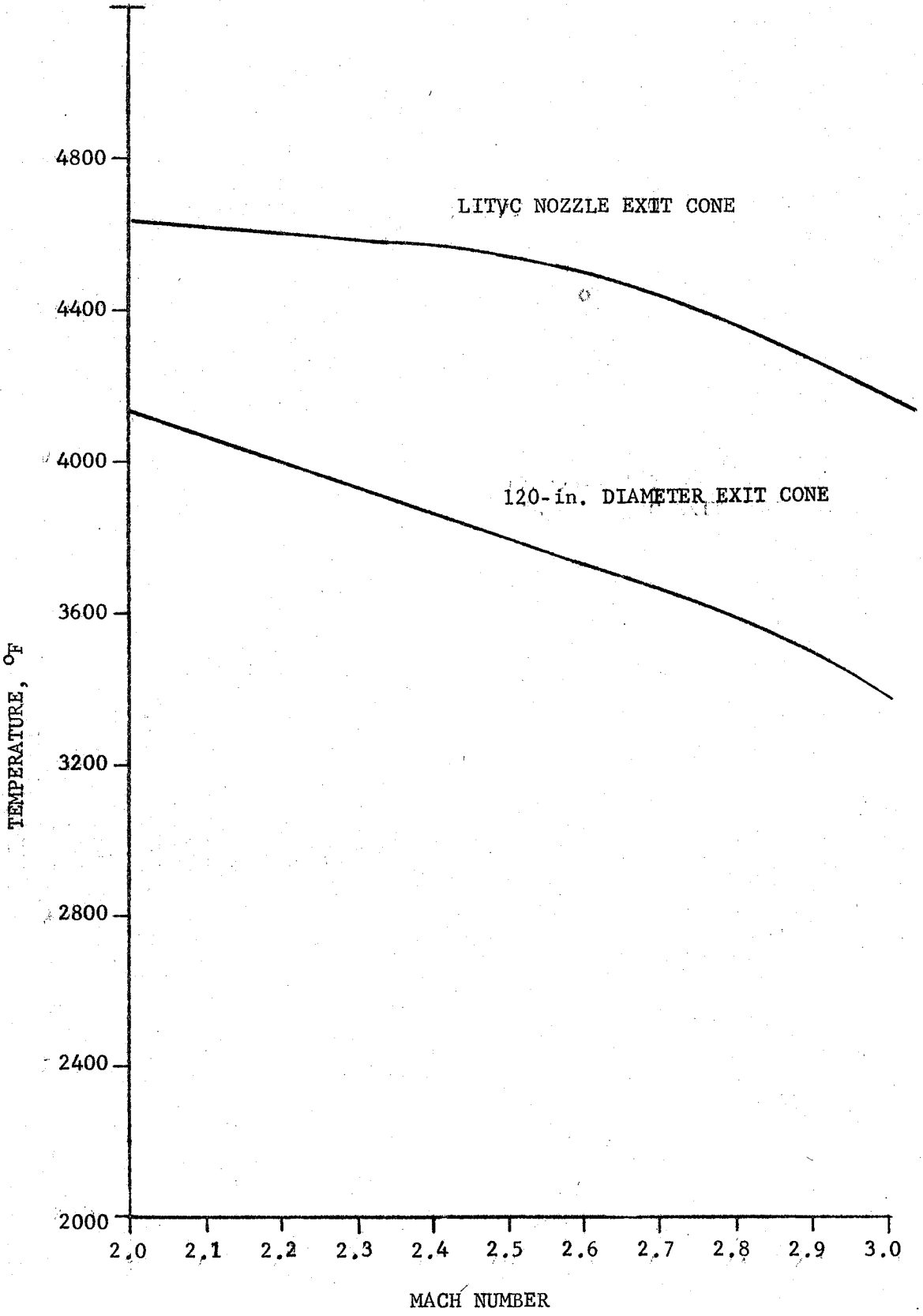

Figure 62. - Exit Cone Steady State Wall Temperatures vs Mach Number for Silica Phenolic.

Kolpin, Horn, and Reichenbach[b] have developed a correlation of maximum injection penetration height as a function of mainstream gas flow and injectant parameters. The correlation they present is

$$\frac{hM}{d_e} = 6.77 \left[\left(\frac{P_i}{P_s} \right) \left(\frac{P_2}{P_v} \right)^n \right]^{0.51}$$

where h = protuberance height

M = free stream Mach number

P_i = injectant back pressure

P_s = free stream static pressure

P_2 = static pressure behind a normal shock

P_v = vapor pressure of injectant

n = 0.25 for $P_v > P_2$; = 0 for $P_v < P_2$

d_e = injectant equivalent diameter

$$d_e = (4 \dot{m}_i / \pi V_i \rho_i)^{1/2}$$

where $\dot{m}_i$ = injectant mass flow rate

V_i = injectant velocity

ρ_i = injectant density.

The effective protuberance body height is assumed to be proportional to h. Since the effective height is to be used only as a correlating parameter, the proportionality constant does not have to be known and the constant 6.77 in the above equation may be eliminated. For the purposes of this study, P_2 is always greater than P_v so that $n = 0$. This leaves

$$H = d_e (A_e P_i / M^2 P_s)^{0.51}$$

as an appropriate correlation parameter with which to relate increased wall heat flux in the vicinity of injection to injectant flow rate.

C. The size of the area affected by liquid injection is a function only of the protuberance height and is independent of the nozzle size. For example, if the injection hardware and injectant mass flow rates used in this program were used to inject into a very large nozzle, the ablation pattern would not be expected to change. The location of the ablation pattern is clearly tied to the location of the injection ports. Thus, an appropriate parameter relating increased heat flux to axial location in the nozzle is the distance, L, along the surface from the injection port.

[b]Kolpin, M. A., K. P. Horn, and R. E. Reichenbach, "Study of Penetration of a Liquid Injectant Into a Supersonic Flow," AIAA Journal: 853-858, May 1968.

D. By using the ratio of heat flux due to injection to the heat flux without injection as the dependent variable, the correlation becomes independent of the many parameters affecting heat flux. It can be used in conjunction with a standard non-TVC heat flux calculation technique to predict increased heat flux due to injection and ablation rates in any motor.

One further assumption was made before forming a relationship of ablation depth and these parameters; namely, ablation rate was assumed not to depend on previous ablation. This is not strictly valid because the irregular grooves produced around the TVC ports probably influence further ablation. However, until more data are available, this assumption is a reasonable first approximation.

To calculate the ratio of heat flux due to liquid injection to normal heat flux, called the heat flux multiplier, ablation rates during injection must be determined first. From these measured rates and from the correlation of ablation rate and heat flux, the heat flux required to produce the ablation can be calculated. Dividing this flux by the value calculated without injection yields the heat flux multiplier. Using data from 120-in. motor firings, a correlation of ablation rate as a function of L and H was first developed. Then, heat flux multipliers were calculated in the manner described.

According to the considerations and assumptions made, the ablation depth, a, at an axial distance from injection is given by:

$$a = \int_{t_N} \dot{a}_N (L,t)dt + \int_{t_T} \dot{a}_T (L,t)dt$$

where $\dot{a}_n(L,t)$ = the non-TVC ablation rate at time, t, and distance, L

$\dot{a}_T(L,t)$ = the TVC induced ablation rate at time, t, and distance, L

t_N = the time during which no TVC fluid flows

t_T = the time during which TVC fluid flows.

The term, $\dot{a}_N(L,t)$, is related to L and t through the correlation of ablation rate and heat flux as shown in figure 58. The heat flux is calculated using the method outlined in a previous section.

Employing the considerations previously mentioned, the term $\dot{a}_T(L,t)$ can be written in the following functional form:

$$\dot{a}_T (L,t) = E \quad (L, H)$$

where E is the function relating ablation rate to the parameter L and H.

From the above equation, ablation depth can be predicted once E(L,H) is known.

Empirical Determination of the Function E(L,H)

To determine the dependence of ablation rate on L and H, empirical data that give ablation rates for a variety of TVC flow conditions and area ratios are needed. Such data are available from 120-in. motor static tests 1205-8, 1205-9, 1205-10, 1205-12, 1205-13, and 1205-14. These data were first reduced to a set of ablation depths, each corresponding to a unique arrangement of area ratio and TVC flow conditions. A further reduction was made by separating these depths into two components: (1) the depth ablated during TVC flow and (2) the depth in absence of TVC flow. This was done by using the standard heat flux correlation from the 120-in. motors to predict ablation depth in absence of TVC flow. The difference between the measured depth and this non-TVC depth is the ablation depth induced by TVC flow.

Since the ablation data consisted of measurements at discrete area ratios, the function relating ablation rate and H was determined for each area ratio for which measurements were available. The function E (L,H) is represented by the entire set of these discrete functions as shown in figure 63.

Ablation Data in Areas Not Affected by LITVC

Based upon measured data a separate correlation of ablation rate and heat flux was made for each of the test materials using the technique previously described. These correlations are presented in figure 58 and figures 64, 65, and 66 with a least squares best fit line. The correlation for FM-5504 and SP-8030 is very consistent and represents data from both subscale and 120-in.-diameter motor firings. In addition, these graphs contain data from firings with different amounts of rubber coming from the aft closure. The correlations for MXS-198 shown in figure 65 exhibit much higher scatter in the data. This is probably due to posttest swelling caused by internal delaminations which occur due to the low pressure cure. Figure 66 presents the correlation for crepe paper phenolic. These data exhibit a definite curvature, possibly because the high heat flux ablation reduces the downstream ablation. This is the same trend that was exhibited in previous programs using this material. Figure 67 shows the relationship between these best fit lines including the line for the standard silica phenolic, also shown in figure 58. Double-weight silica and epoxy novalac ablated roughly 12 to 25% faster than the standard silica, whereas, crepe paper phenolic ablated more than three times as fast as the standard material.

Ablation in LITVC Affected Regions

Figures 68 through 74 present comparisons of ablation depths in regions affected by injection. Figure 68 compares each of the materials for injection of N_2O_4 at an area ratio of 2.5 and for the highest injectant flow rate for each material. Except for the epoxy novalac data which seems affected by the loss of a large portion of the upstream liner, the depth trends are consistent with non-TVC data. That is, the standard silica is lowest, the double-weight slightly higher and the paper phenolic much higher. This consistency

H = Protuberance Height Parameter

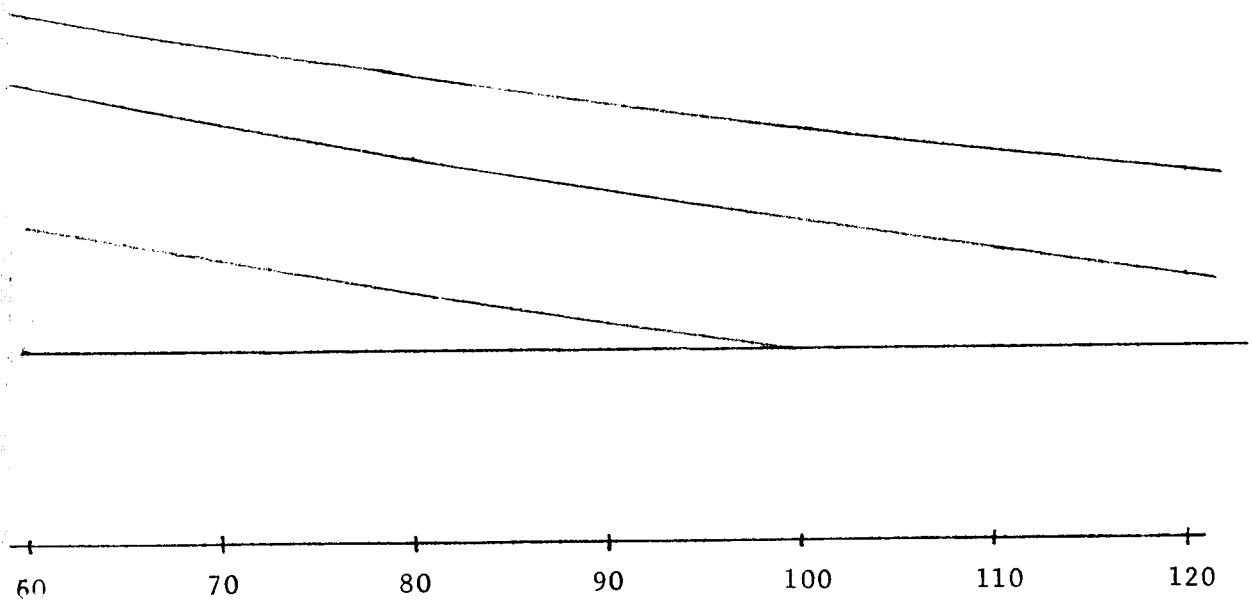

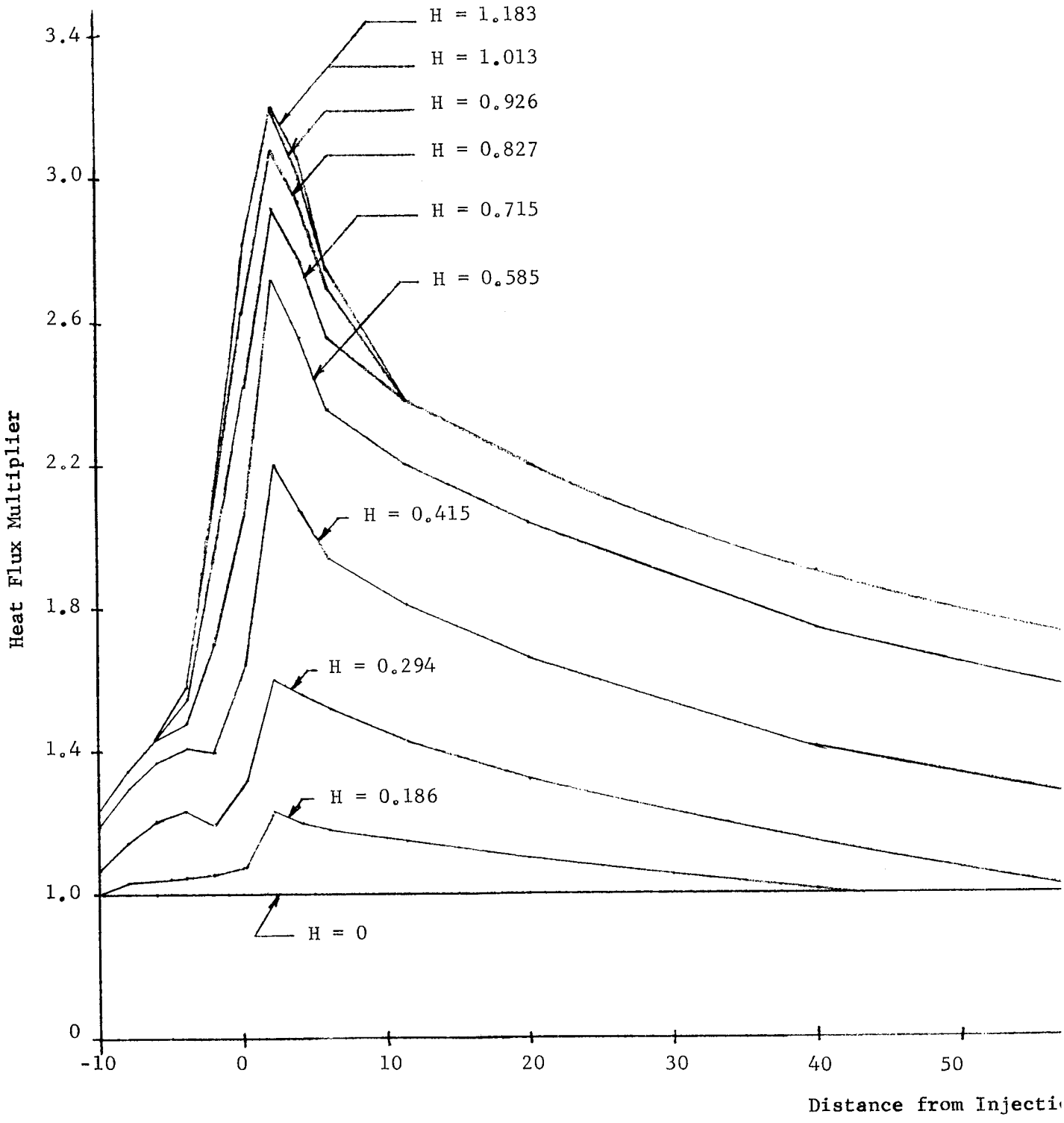

Figure 63. - Correlation of Heat Flux Multiplier as a Function of Distance from Injection Port and Protuberance Height Parameter.

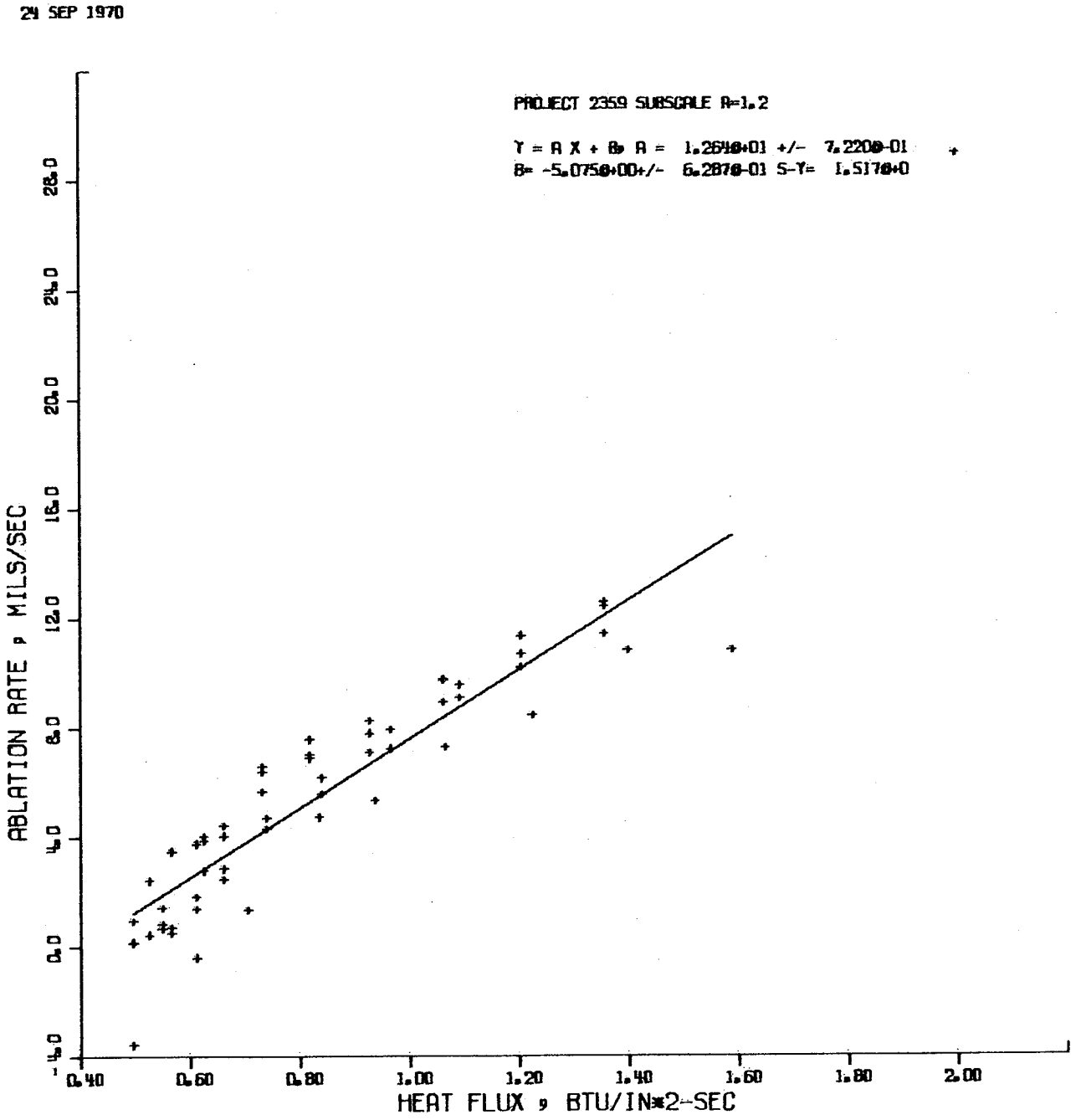

Figure 64. - SP-8030 Ablation Correlation.

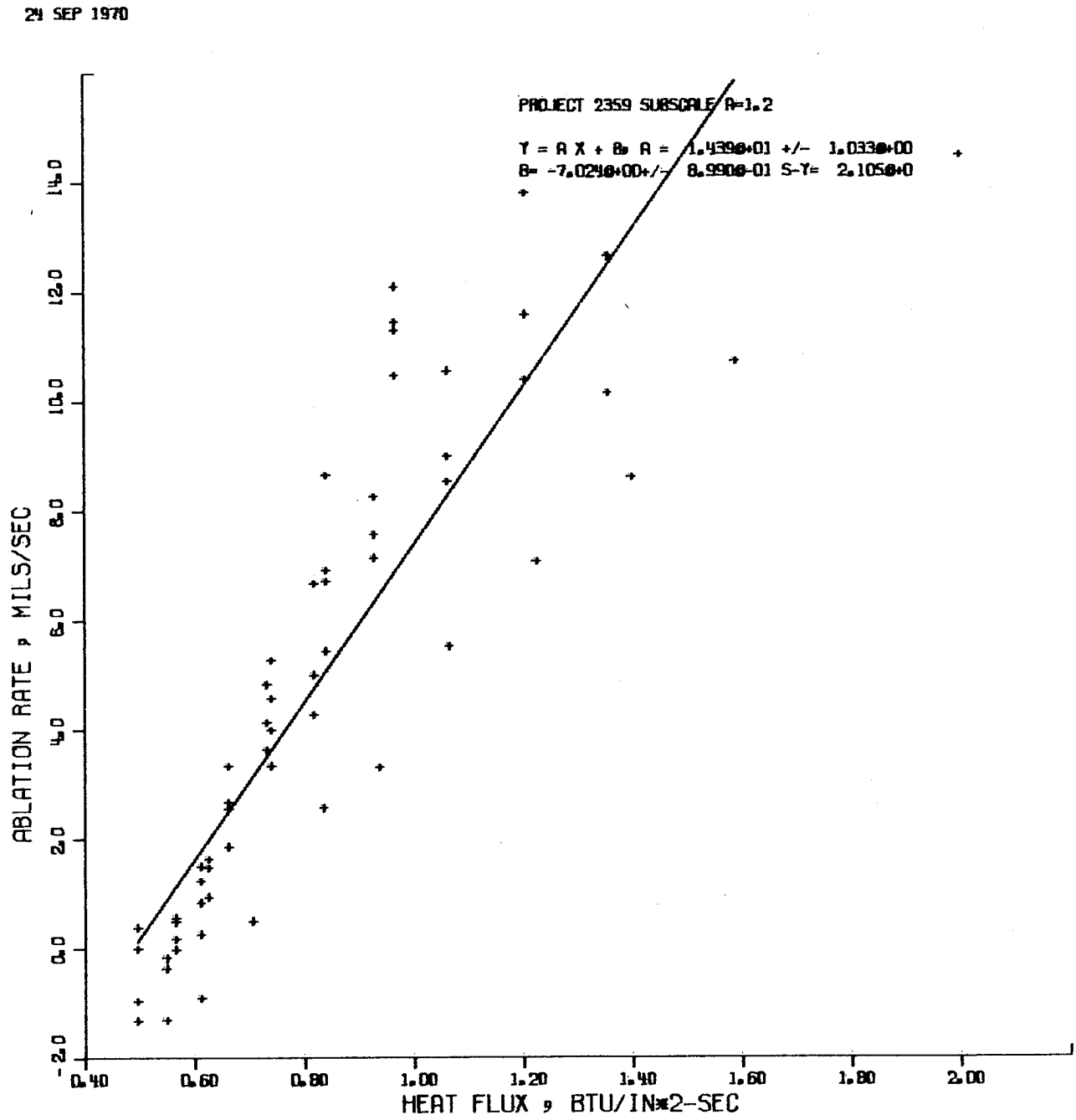

Figure 65. - MXS-198 Ablation Correlation.

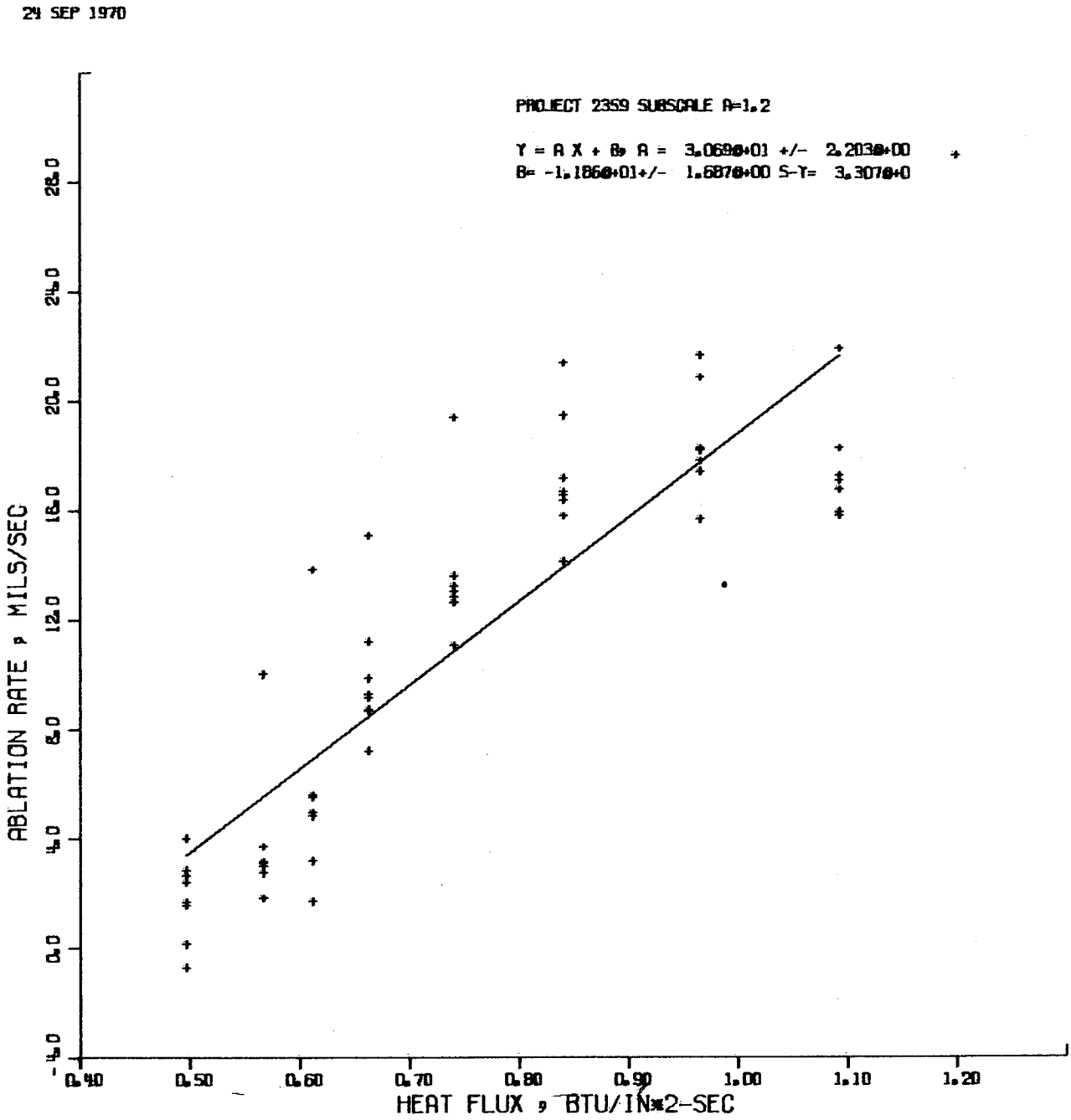

Figure 66. - FM-5272 Ablation Correlation.

Figure 67

COMPARISON OF NON-TVC ABLATION RATE

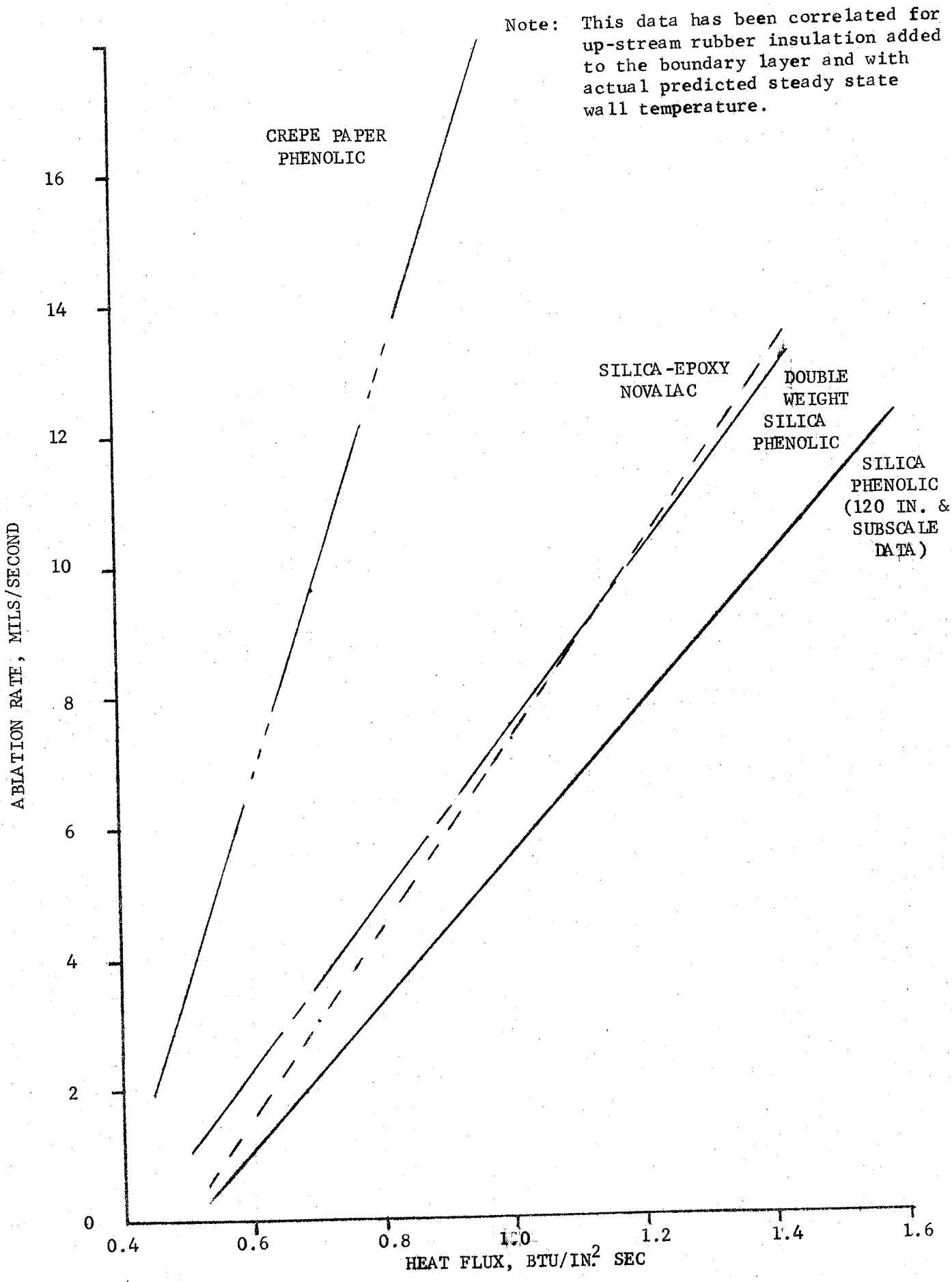

Figure 67. - Comparison of Non-TVC Ablation Rate.

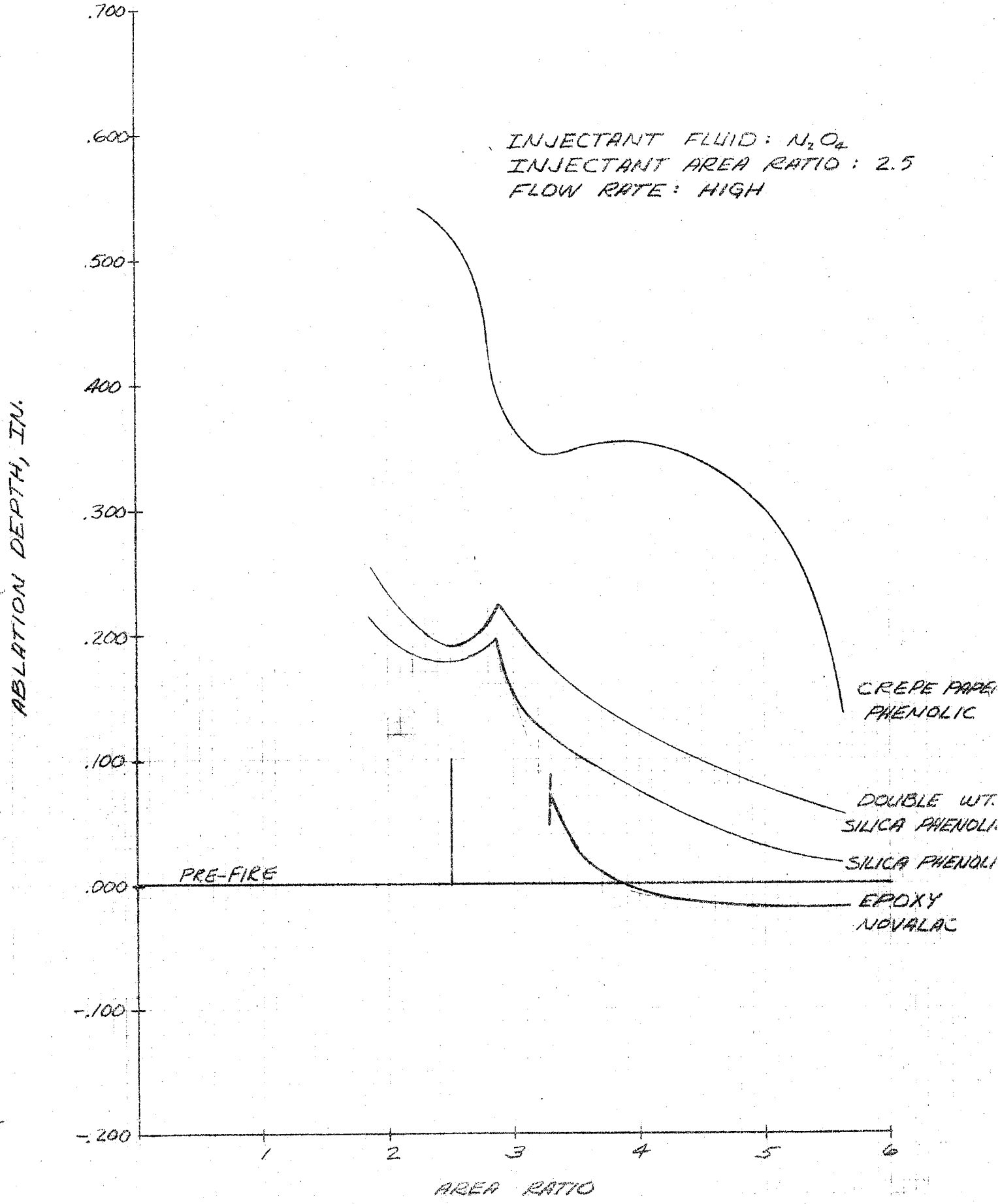

Figure 68. - Nozzle Ablation Comparison N_2O_4, E_i 2.5, High Flow.

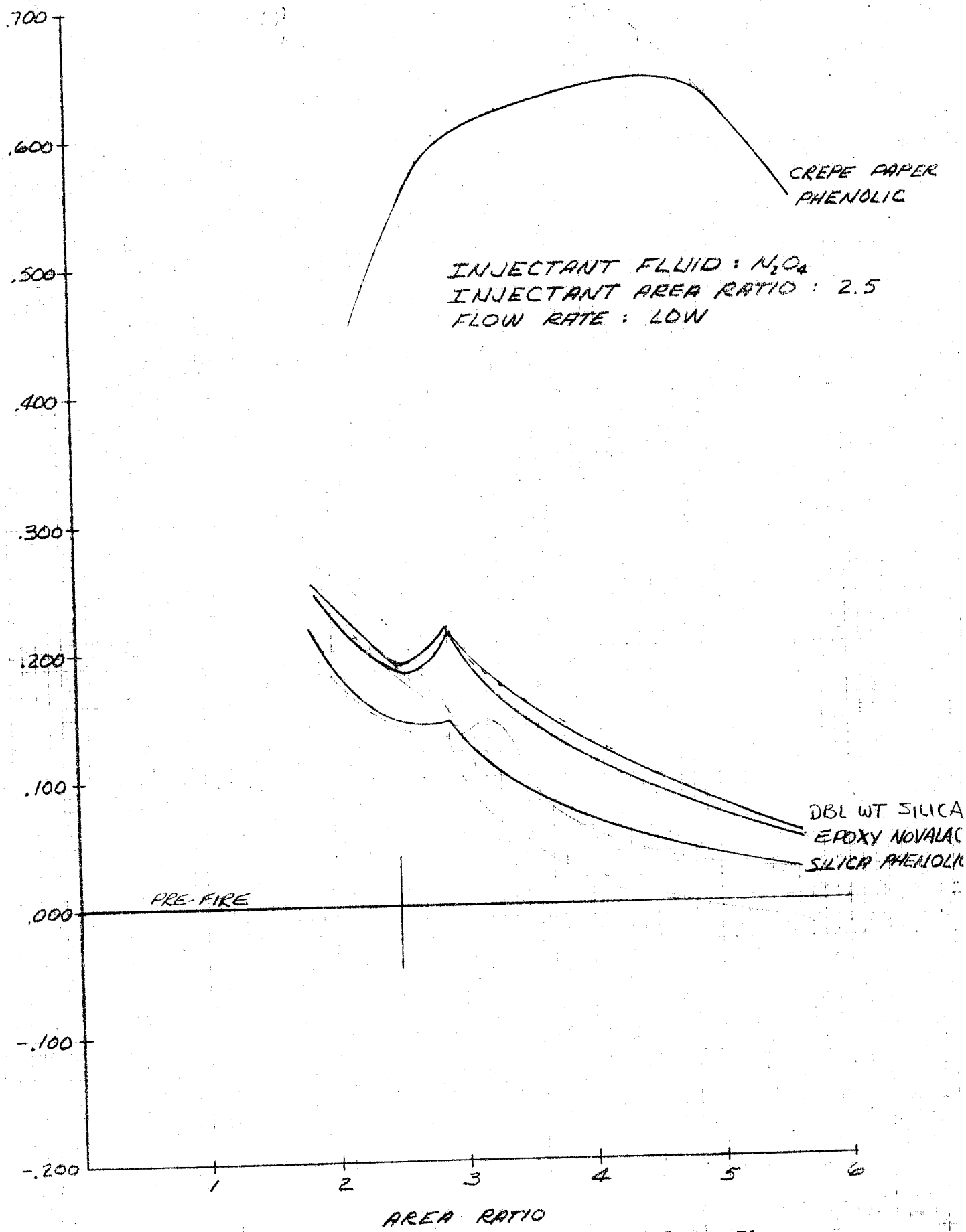

Figure 69. - Nozzle Ablation Comparison N_2O_4, E_i 2.5, Low Flow.

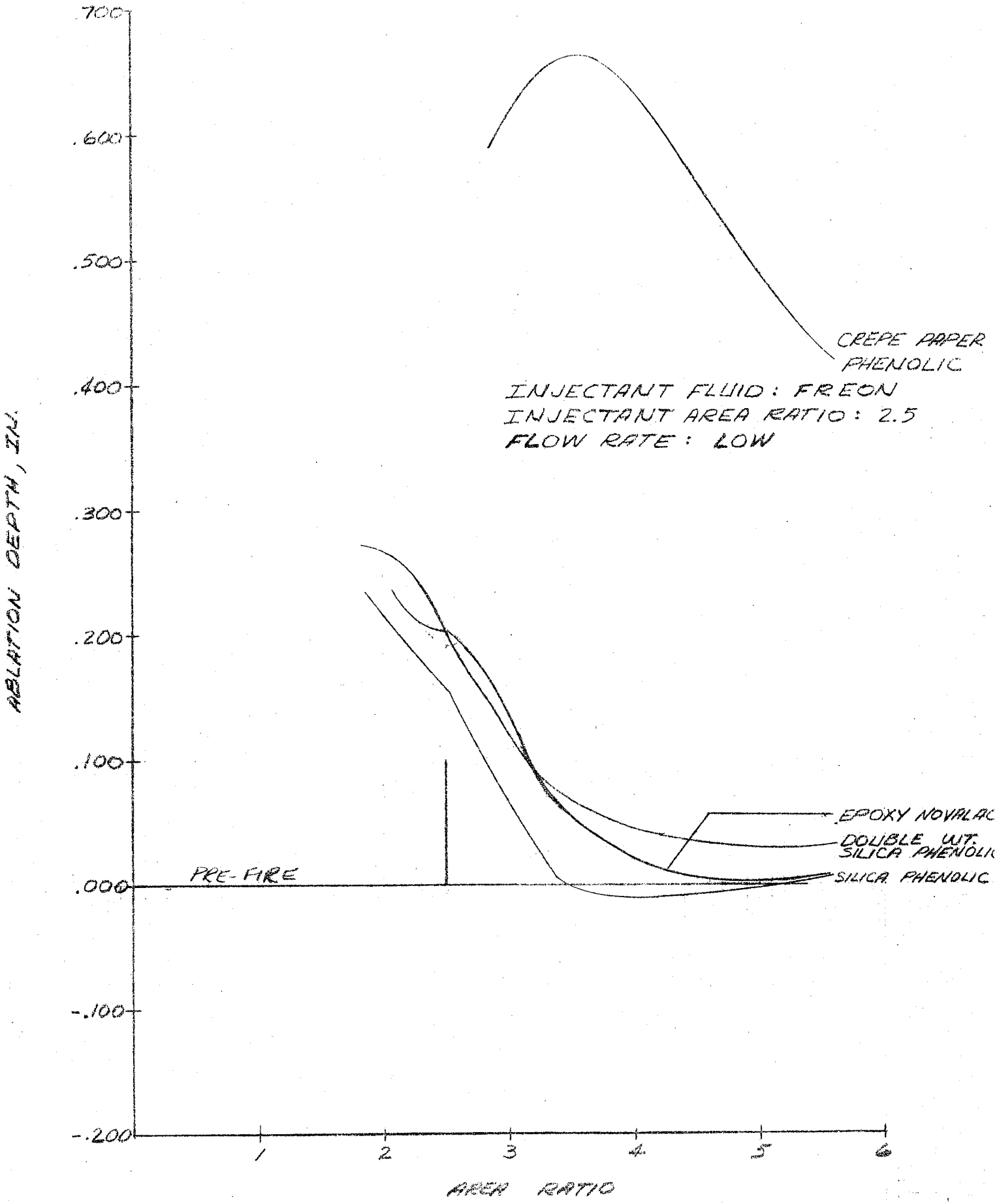

Figure 70. - Nozzle Ablation Comparison Freon, E_i 2.5, Low Flow.

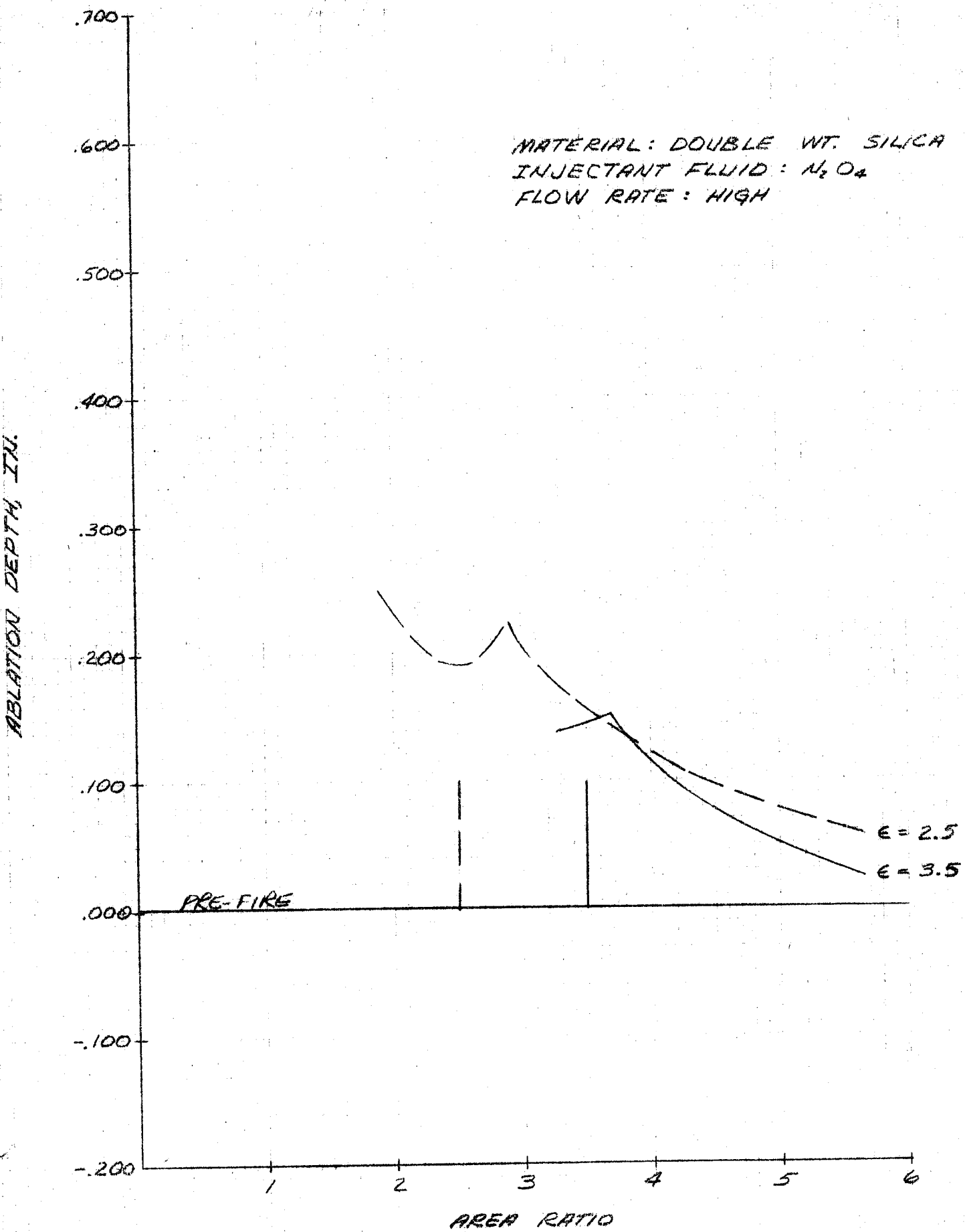

Figure 71. - Nozzle Ablation Comparison SP-8030-96.

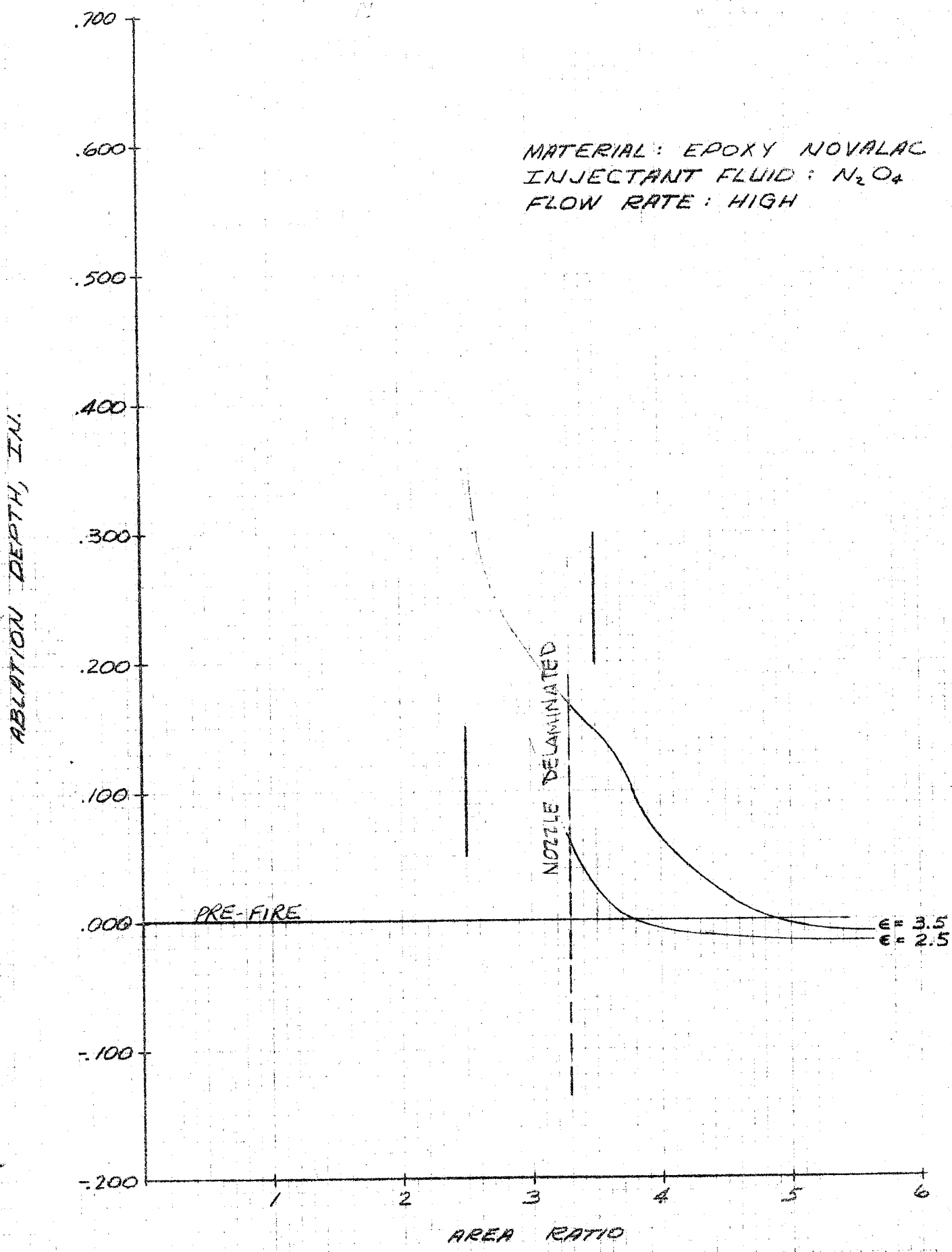

Figure 72. - Nozzle Ablation Comparison MXS 198.

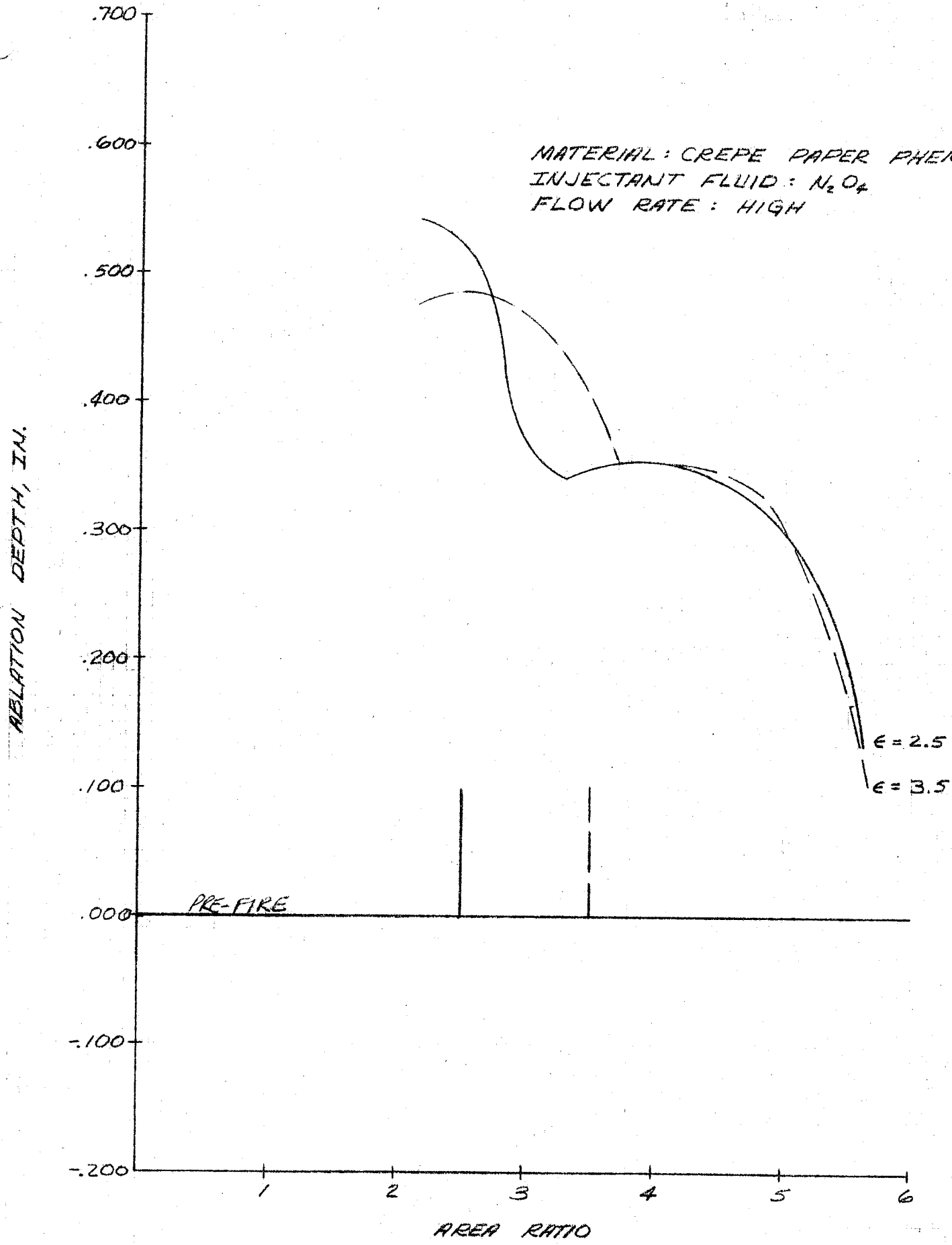

Figure 73. - Nozzle Ablation Comparison FM-5272.

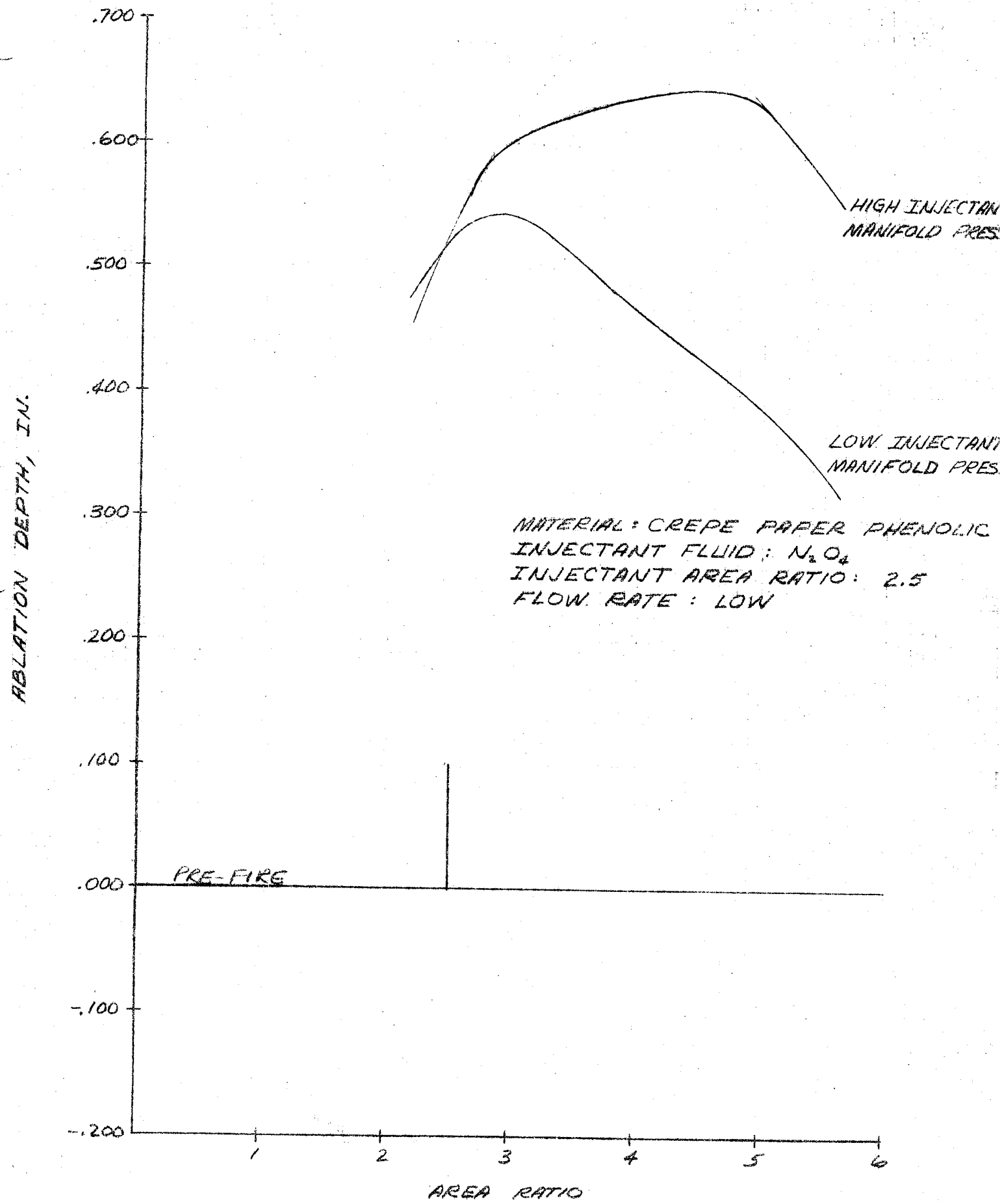

Figure 74. - Nozzle Ablation Comparison, FM-5272, Injectant Pressure Effects.

is continued in figure 70 which shows the same comparison for low injectant flow rates. In this case, the epoxy data is valid and shows the close agreement with double-weight that was found in the non-TVC data.

Figure 71 shows the comparison of the same materials with Freon injected at an area ratio of 2.5. The ablation depths are related to each other in the same way as with N_2O_4 injectant and as for no injection. Except for the paper phenolic, however, the depths are significantly less. All three silica phenolics are without the local maximum depth characteristically found with N_2O_4 at an area ratio of about 2.9. The reduced ablation rates in the silica phenolics are probably a result of cooling of the boundary layer by the non-reacting injectant.

The performance of paper phenolic requires special consideration. Ablation consists of both chemical reaction of free stream and wall species and char removal by shear forces. Because the ablation rate of paper phenolic is so high, the concentration of ablation products in the boundary layer is also high and the diffusion of oxidizing species to the wall is significantly reduced. This difficulty in diffusing of oxidizing species and the low shear strength of the paper phenolic char layer indicate that ablation of paper phenolic is primarily governed by the rate of char removal by shear forces and the rate of char production by heat flux. Thus, the paper phenolic ablation should be nearly independent of injectant fluid type but can be expected to increase with injection due to increased heat flux behind the shock wave.

The ablation data for TVC affected regions must be used with caution. Some of the data, particularly with Freon injectant, indicate that ablation rates can be lowered below that of non-TVC areas by the use of liquid injection. Yet quite the opposite has been demonstrated in large motor firings. This difference can be explained by examining several injection processes which affect the ablation rate.

A. A shock wave is produced which tends to increase the heat flux and, therefore, the ablation rate.

B. The flow is distributed by the presence of the protuberance. This effect is strongest when the penetration height is large so that the stream stays somewhat collimated for a significant distance above the surface.

C. The injectant may react with the free stream gases tending to add heat flux to the wall. The injectant may also react with the wall directly.

D. If the penetration distance is very low, part of the injectant stream may remain sufficiently close to the wall to provide significant film cooling.

The protuberance height for the small scale motors tested was of necessity very small compared to large scale motors. Because of this, the relative importance of the above phenomena may be different from large protuberances found in full scale motors. The first three effects are probably all present

for the conditions of the 120-in.-diameter motors from which the heat flux multiplier correlation was developed. The cooling effect probably was not present on the 120-in.-diameter motors as the penetration is sufficient to prevent return to the surface until it has been heated by the free stream.

The reaction of N_2O_4 with the exhaust should increase the gas temperature more than injection with Freon. Hence, greater ablation with N_2O_4 would be expected on a full scale nozzle, but not to the degree exhibited in our subscale test.

It is significant that the subscale LITVC data confirm that the basic correlation of ablation rate and heat flux is still valid with injection. This is clearly demonstrated in the relative ablation rates of the various materials. For example, in the case of N_2O_4 injection as shown in figure 69, and at an area ratio of 2.89, the heat flux multipliers calculated for each of the materials are as follows:

Paper phenolic	1.25
Double-weight	1.30
Epoxy novalac	1.28
Standard silica	1.16

This demonstrates that for the same flow conditions, the resulting heat flux is consistent and that the non-TVC correlation will predict the ablation rate if the heat flux were correctly calculated.

In addition to material comparisons, tests were conducted to show the effect of injectant area ratio. In figures 71, 72, and 73 are presented comparisons of injection at area ratios of 2.5 and 3.5. The materials presented are double-weight silica, epoxy novalac and crepe paper phenolic, respectively. The results here are not unusual in that in each case the ablation pattern remained about the same and shifted towards the injectant port.

The final comparison made was the evaluation of injectant pressure. This has the effect of changing the stream momentum per unit flow area. This data is presented in figure 74 and shows that the higher the momentum the higher the ablation. The flow rate in these two tests were the same. This result is what one would expect in that the momentum should be a measure of how far the injectant will penetrate into the exhaust stream which governs the strength and size of the shock.

260-in.-Diameter TVC Performance Prediction

The TVC performance for the 260-in.-diameter motor is predicted based on the design criteria as shown below and in figure 75:

Injectant	N_2O_4
Injection area ratio	2.71
Nozzle area ratio	8.515
Defection range	0.42° (0.0073 rad) to 1.2° (0.021 rad)
X/L	0.35
Injectors/quadrant	4

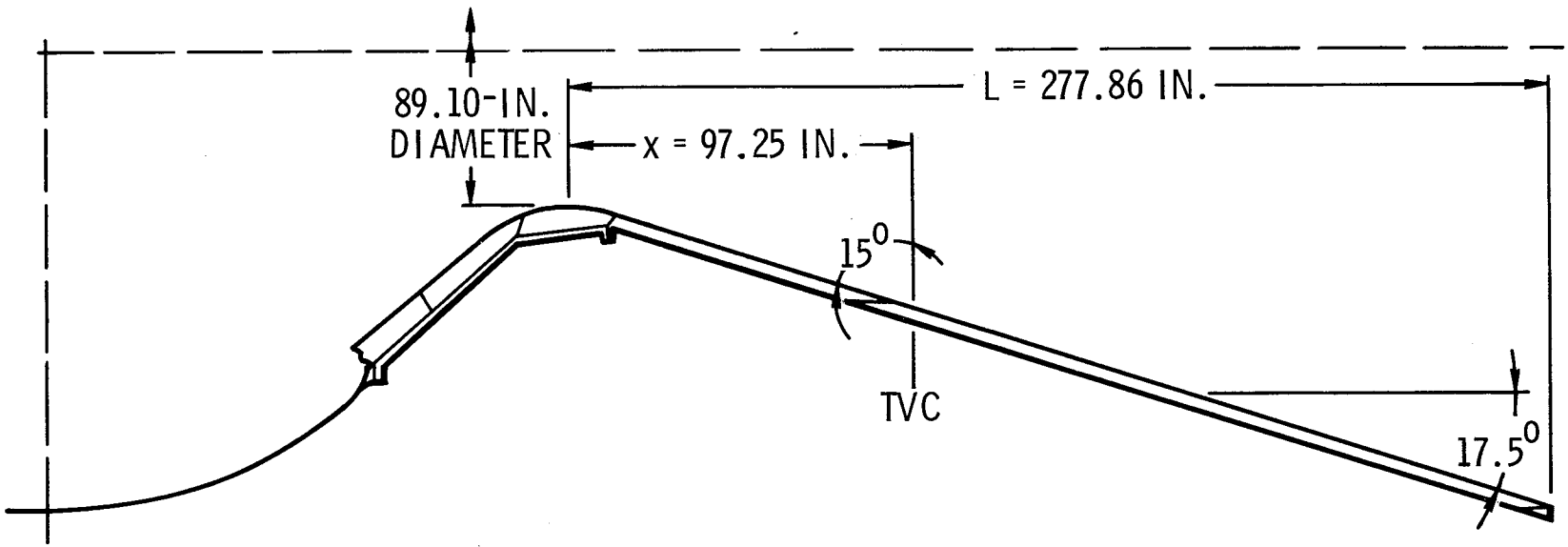

Figure 75. - 260-in.-Diameter Nozzle LITVC Configuration

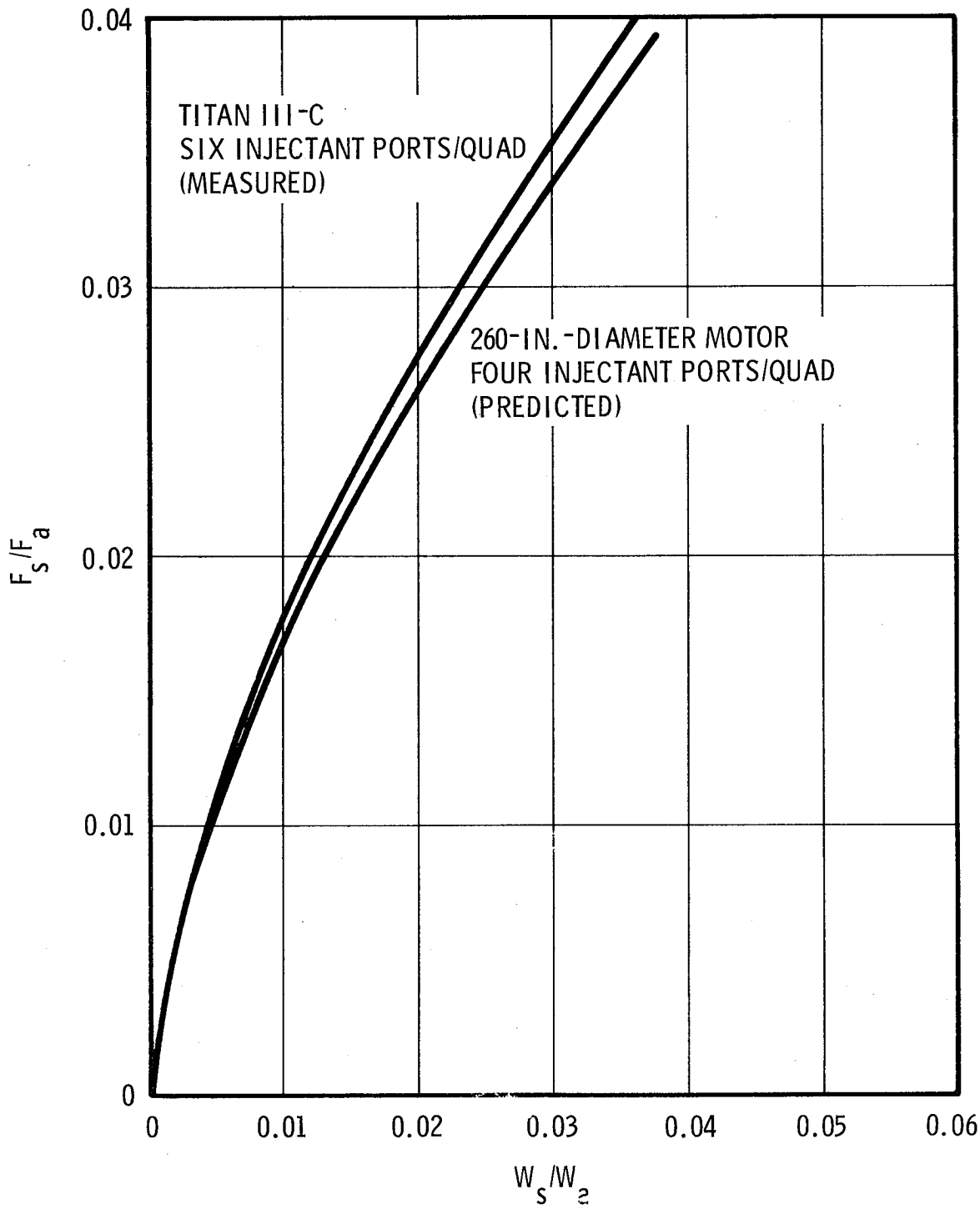

Figure 76. - Predicted Side Force Performance for 260-in.-Diameter Nozzle

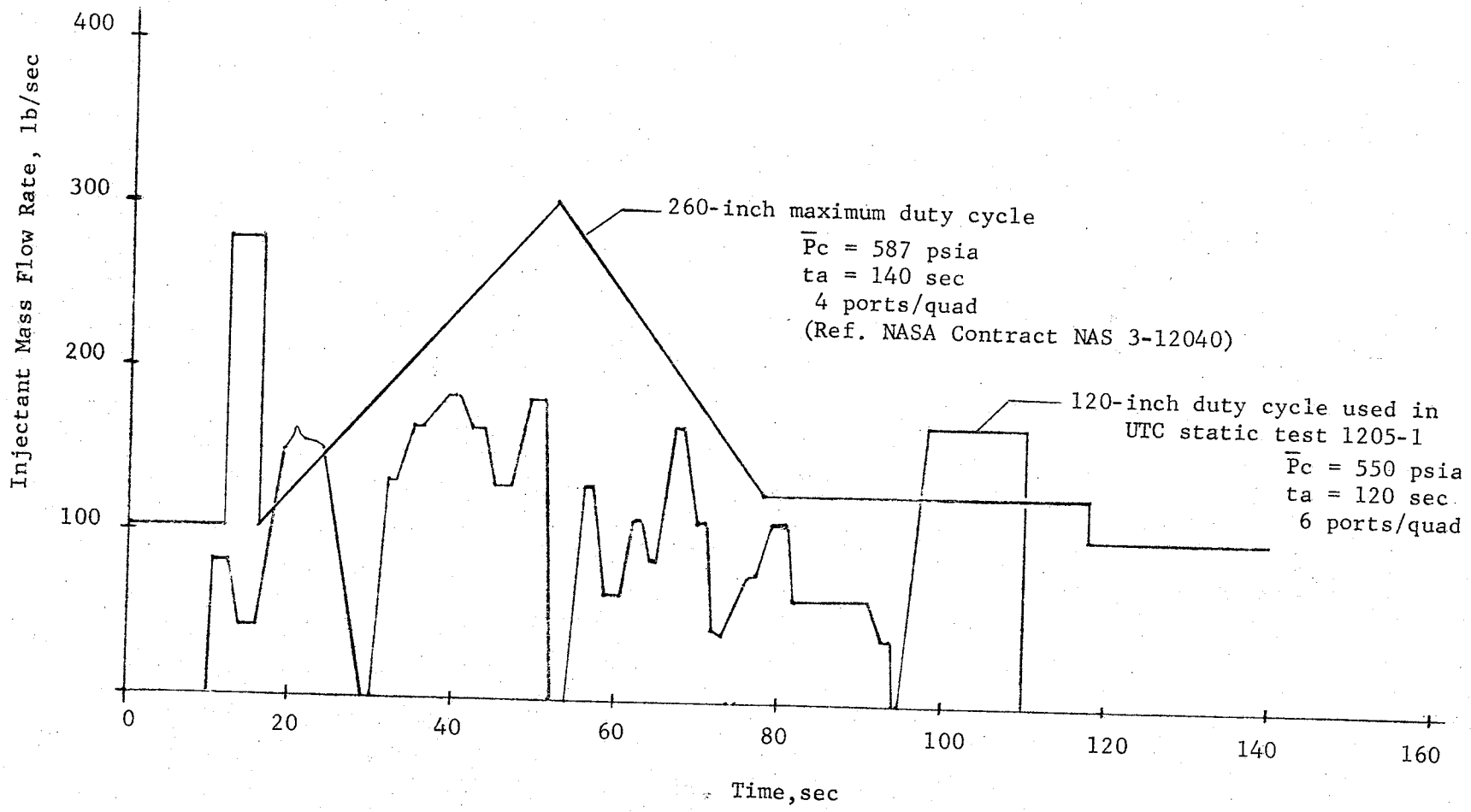

Figure 77. - Comparison of 260-Inch and 120-Inch TVC Injection Duty Cycles.

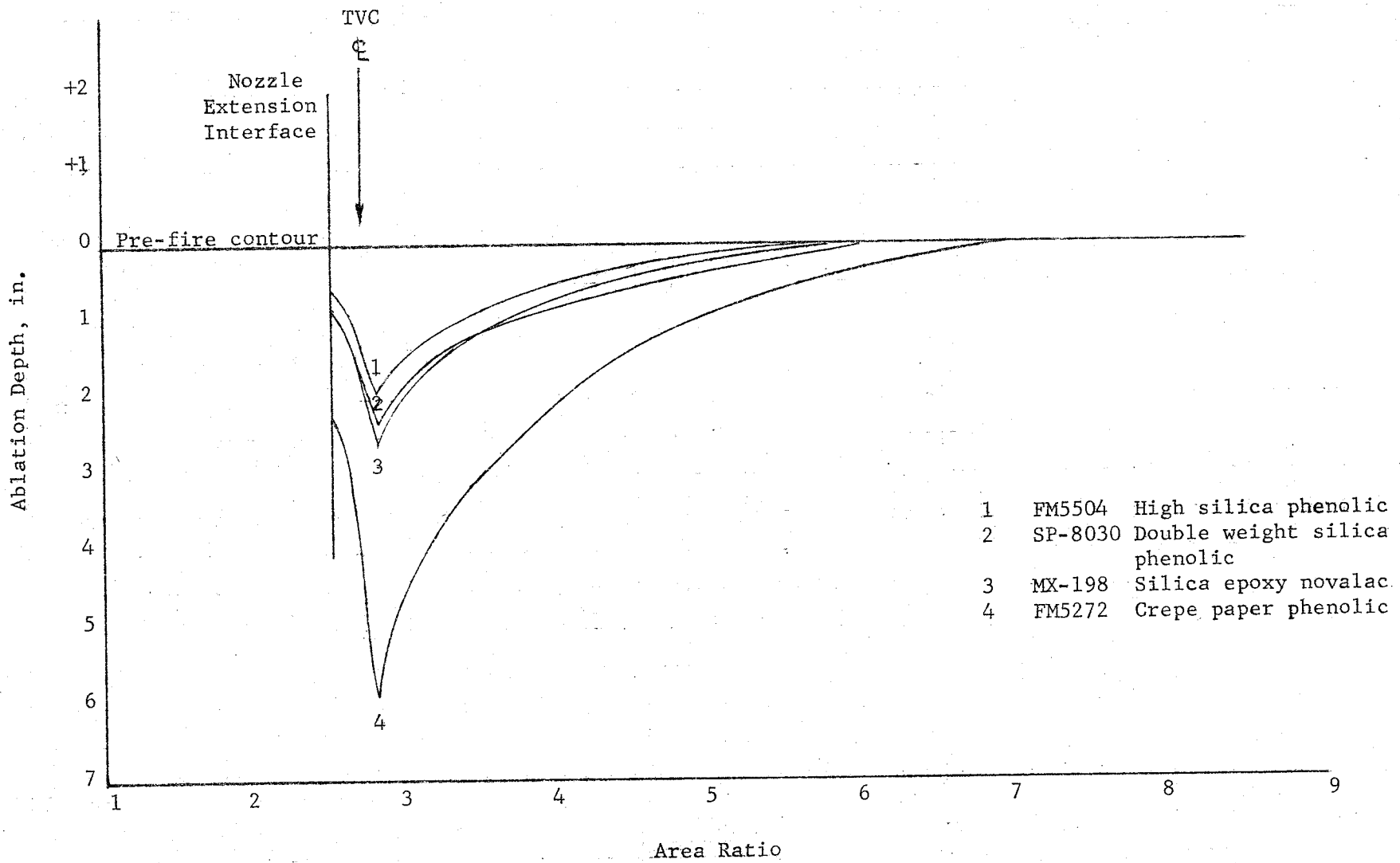

Figure 78. - 260-Inch Nozzle Ablation Prediction for Maximum Duty Cycle.

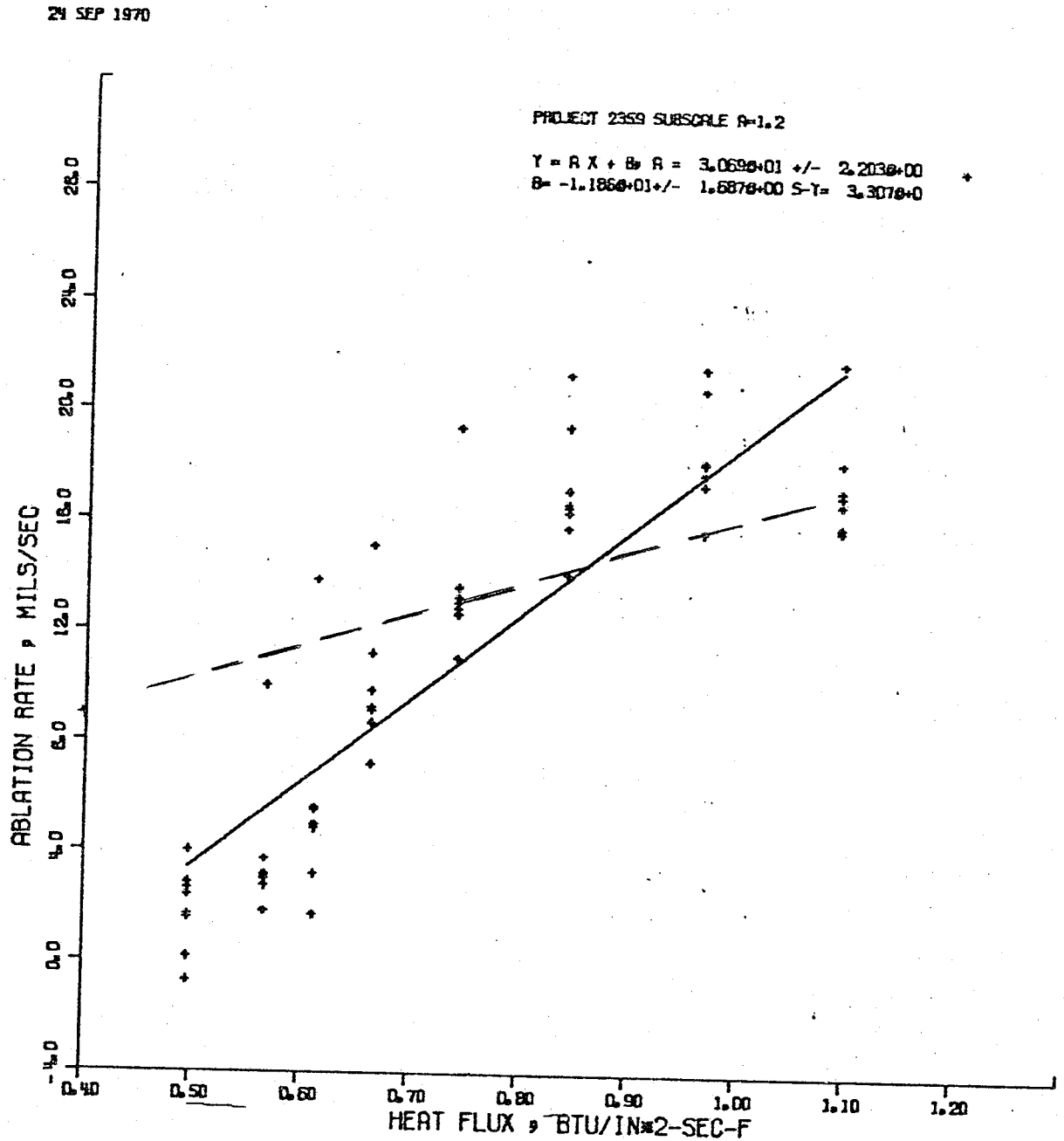

Figure 79. - FM-5272 Ablation Correlation Corrected for Upstream Ablation.

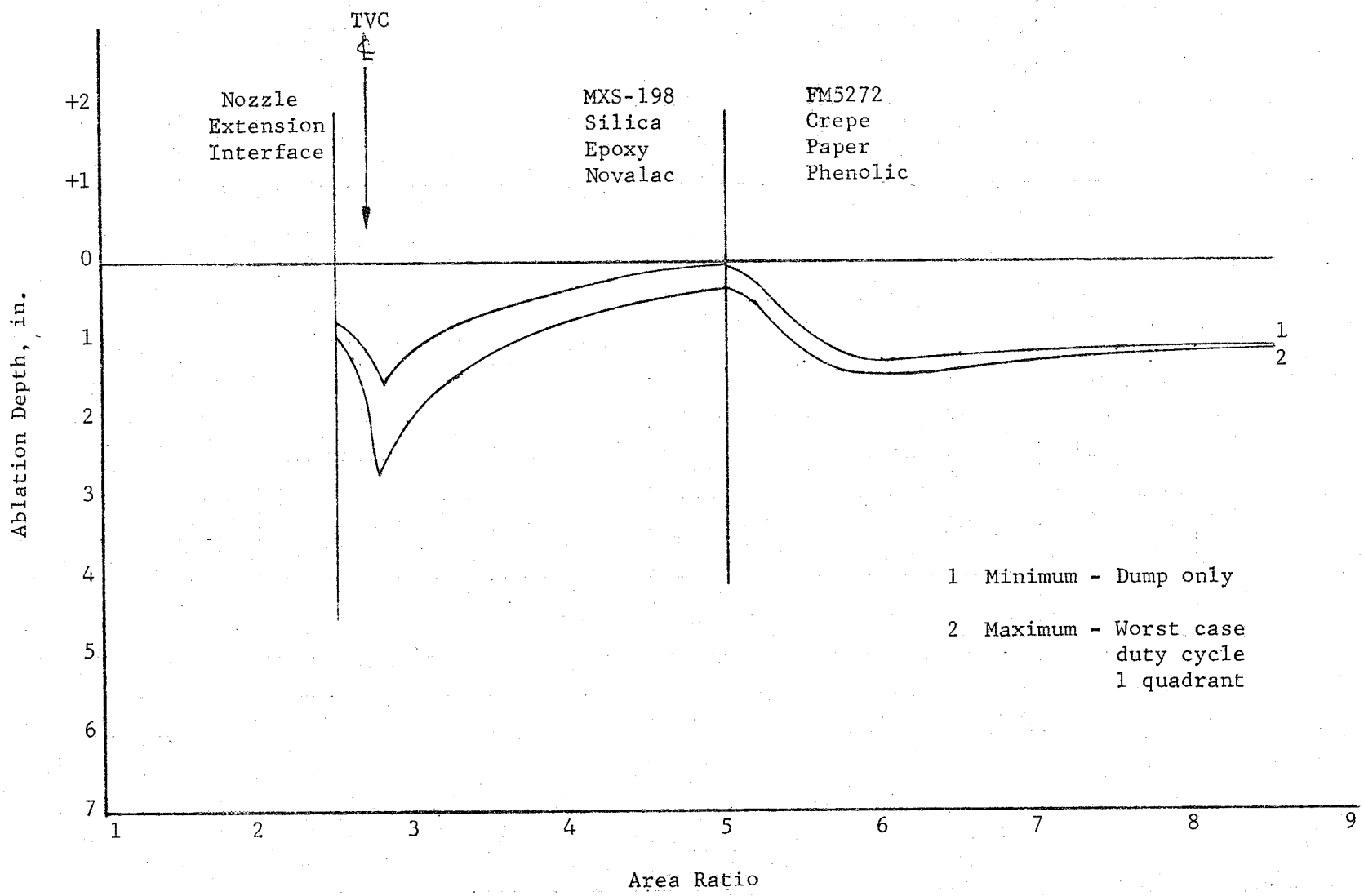

Figure 80. - 260-Inch Optimum Nozzle Ablation Prediction.

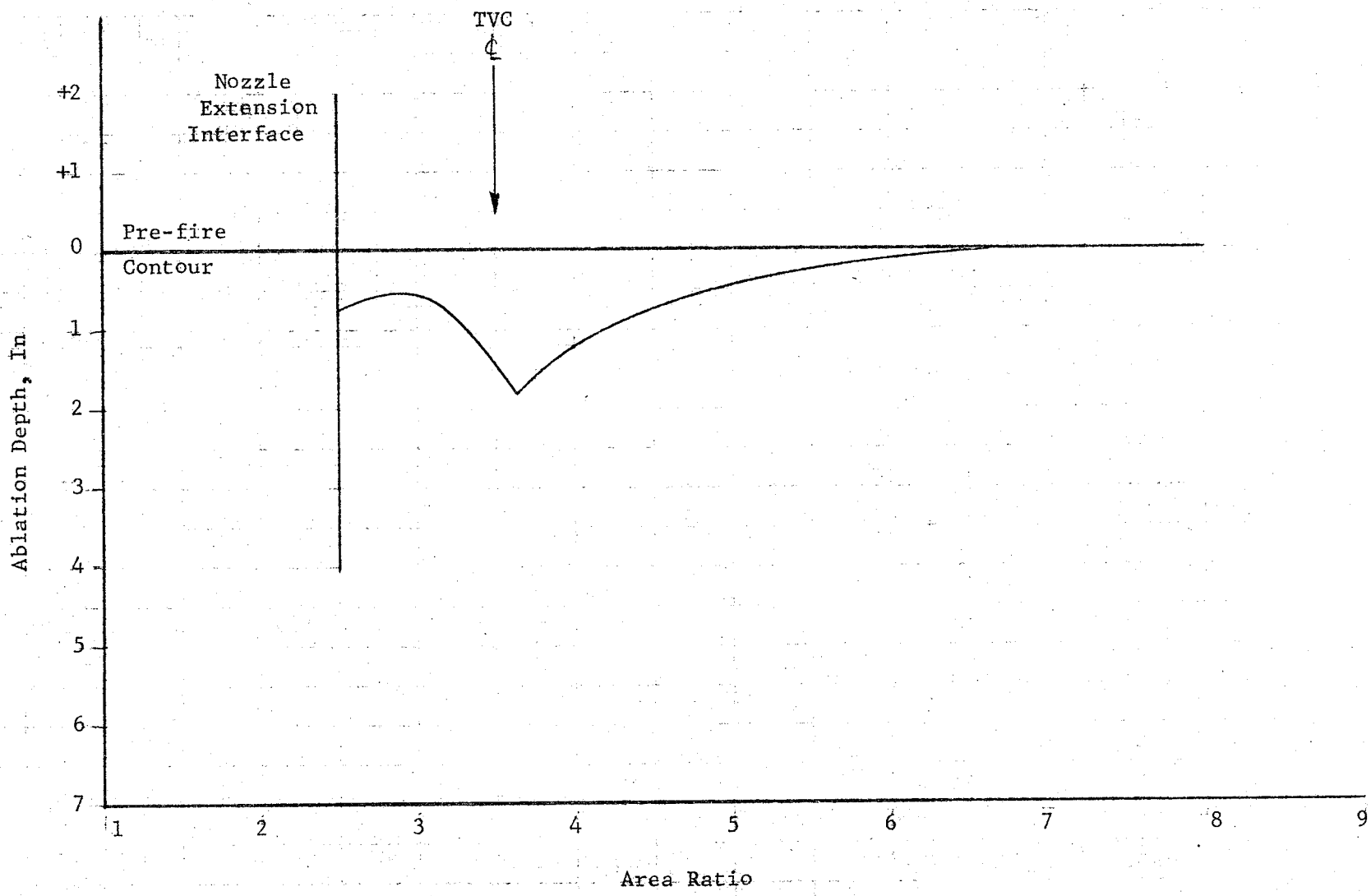

Figure 81. - 120-Inch Nozzle LITVC Ablation.

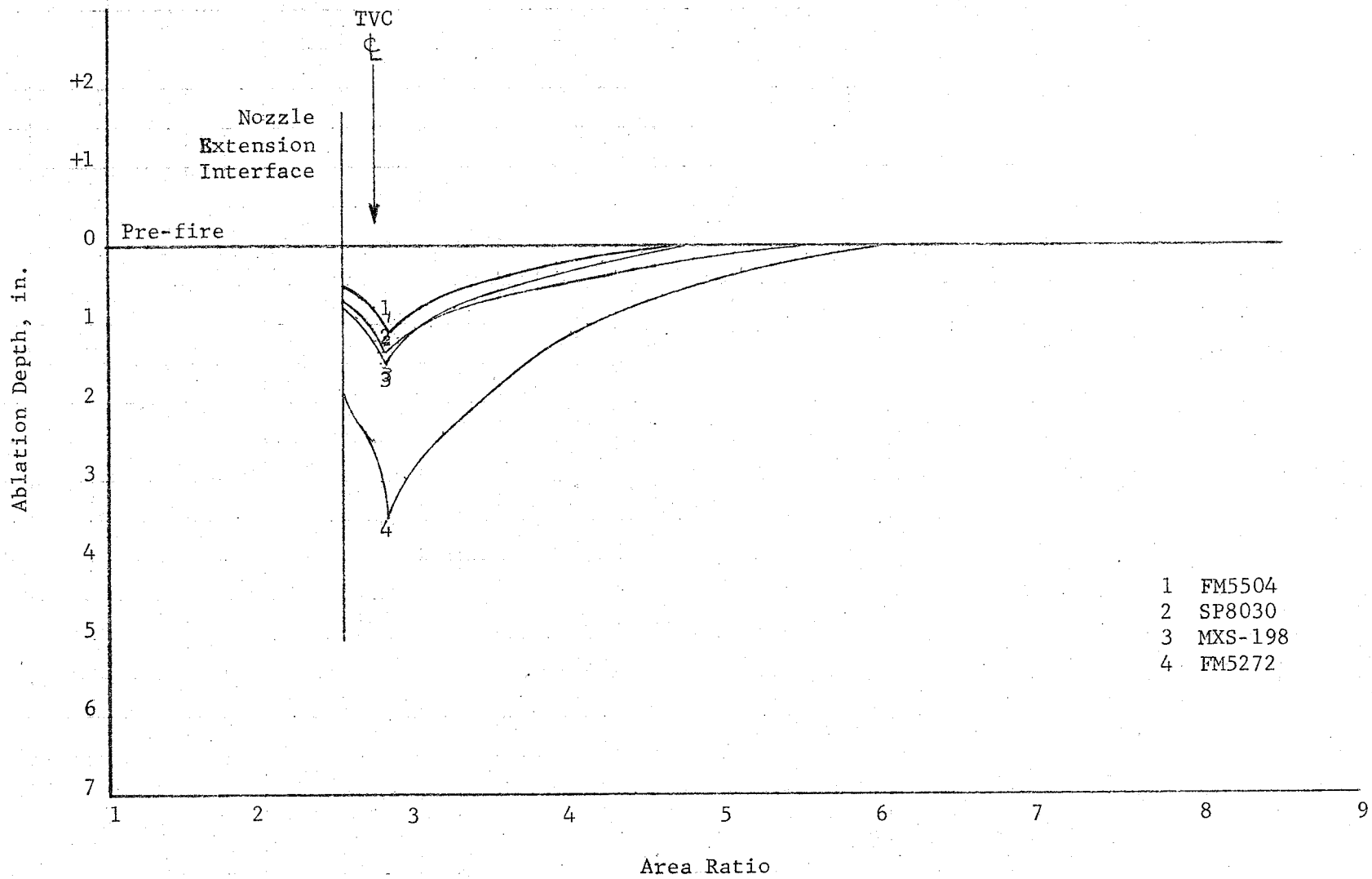

Figure 82. - 260-Inch Nozzle Ablation Prediction for Minimum Duty Cycle. (All Dump)

The predicted performance of the 260-in. diameter nozzle with N_2O_4 injectant is presented in figure 76. The low deflection requirements of the 260-in.-diameter motor are in the maximum LITVC performance range for N_2O_4. The resultant F_s/F_a for the maximum side force is only 0.0209. Using four injector ports/quadrant, this requires a W_s/W_a of 0.014. Data from the 120-in.-diameter motor program, utilizing six valves/quadrant would require a W_s/W_a of 0.0134, or only a 4% decrease in performance for four injectors instead of six.

TVC Ablation Prediction for the 260-in.-Diameter Motor

The maximum ablation in the TVC affected region of the 260-in.-diameter motor was found to range from 1.98 in. (0.05 m) to 6.0 in. (0.15 m) depending on the material used as exit cone liner. The TVC duty cycle used in the prediction is shown in figure 77 and was developed under Contract No. NAS 3-12040. This duty cycle represents the maximum steering correction expected for a 260-in. diameter motor flight. This duty cycle assumes all of the fluid to be dumped into one quadrant. This, of course, is a very conservative assumption. It has been found from Titan III-C launch experience that typically only 30% is injected into any one quadrant. The results of these predictions are shown in figure 78. Due to the predicted large ablation, the use of crepe paper phenolic in the injectant area would be impractical. There is a possibility, however, that using the crepe paper phenolic at some area ratio downstream could produce an acceptable design.

Examination of the paper phenolic non-TVC ablation indicates that ablation of paper phenolic is affected by the large amount of upstream ablation taking place tending to further lower heat fluxes in the higher area ratio regions. Use of figure 78 to find the area ratio at which paper phenolic could be used would be incorrect because the correlation on which it is based assumes paper phenolic ablation upstream. Therefore, an additional analysis was conducted using the higher correlation shown in figure 79. These results are plotted in figure 80 and show that using the crepe paper phenolic at area ratios in excess of 5 produce acceptable erosion pattern for the present TVC duty cycle. The other three low cost materials shown in figure 81 all exhibit reasonable ablation rates and the choice of best material must be made based upon manufacturing cost and weight tradeoffs. Similar trends exist between predicted 260-in.-diameter and measured 120-in.-diameter motor data. For comparison purposes, ablation data from a high TVC flow rate static firing of the 120-in.-diameter motor is also plotted in figure 81 using the duty cycle which is included in figure 77.

Additionally, a prediction under minimum control requirements has been made in figure 82. This assumes uniform dump of all fluid through the injection port to achieve maximum useful payload. These results represent the minimum ablation that can be expected in the TVC affected region.

Predictions of the 260-in. nozzle extension show that the three silica materials, FM-5504, high silica, SP-8030, double weight silica, and MXS-198, expoxy novalac silica, can be used in the baseline nozzle presented in figure 75. This nozzle has a 3.1-in. (.0787 m)-thick nozzle liner, which is larger

than the worst-case LITVC ablation predicted. The crepe paper phenolic, FM-5272, was found to be unacceptable for use in the 260-in. nozzle at area ratios below 5. It does look favorable at area ratios above this value, and an optimum low-cost nozzle would employ the MXS-198 silica from an area ratio of 2.5 to 5, and the FM-5272 from 5 to 8.515.

Comparison of the nozzle liner weights from an area ratio of 2.5 to the exit, for LITVC, is presented in Table XIII for each of the silicas, plus the optimum combination. The combination shows a weight savings of 3,960-lb. (1,797 kg) over the FM-5504 and SP-8030 materials, and a weight savings of 1,430 lb. (650 kg) over the MXS-198 material. The combination MXS-198/FM-5272 would also have a substantial cost savings with the lower cost crepe paper.

TABLE XIII. - 260-IN. NOZZLE LINER WEIGHT SUMMARY
(Liner used from ϵ = 2.5 to ϵ = 8.515)

Material	Liner Weight	
	lb	kg
FM-5504 (High Silica)	23,030	10,455
SP-8003 (Double Weight Silica)	23,030	10,455
MXS-198 (Epoxy Novalac Silica)	20,500	9,307
Combination MXS-198/FM-5272 (MXS-198, ϵ = 2.5 to ϵ = 5) (FM 5272, ϵ = 5 to ϵ = 8.515)	19,070	8,657

CONCLUSIONS

Based on the work performed during this program, and on the results and analysis obtained, the following conclusions may be made.

A. LITVC ablation effects must be considered in the design of the nozzle exit cone liner. The following nozzle materials are rated in order of performance with LITVC, both N_2O_4 and Freon injectants.

1. FM-5504 - high silica phenolic
2. SP-8030 - double weight silica phenolic
3. MXS-198 - epoxy novalac silica
4. FM-5272 - crepe paper phenolic
5. KF-418 - canvas duck phenolic

B. The canvas duck phenolic, KF-418, exhibited excessive ablation for both TVC and non-TVC and was the only material tested that had a chemical reaction with the N_2O_4 injectant. This material is not recommended for use with LITVC.

C. The crepe paper phenolic, FM-5272, exhibited ablation rates on the order of 3 times that of the three silica materials at low area ratios in the nozzle, and is recommended for use only above area ratios of 5.

D. Both of the low cost silica materials, SP-8030 and MXS-198, are suitable for use in the 260-in. nozzle as described in Contract No. NAS 3-12040 with no increase in the liner thickness. The MXS-198 is recommended due to its low pressure cure, vacuum bag only, for use in fabricating large nozzles.

E. The use of ablation data obtained on subscale motors must include the effects of upstream mass addition due to erosion of the aft closure insulation to accurately predict fullscale nozzle performance.

RECOMMENDATIONS

A. The ablation rates of both the FM-5272, crepe paper phenolic, and the KF-418, canvas duck phenolic, obtained during this program are approximately twice that reported during the previous NASA materials program, Contract No. NAS 3-10288. The only apparent cause for the difference is the higher pressures used during this program. It is recommended that additional evaluation of these two promising low cost materials be conducted to determine if they have a pressure sensitive threshold to ablation.

B. Additional development work should be performed with all of the low cost materials evaluated during this program, to accurately characterize their properties and processing variables to obtain more repeatable results for each.

C. A larger nozzle employing the MXS-198/FM-5272 materials should be evaluated with LITVC to more accurately determine the optimum area ratio interface for the two materials.

APPENDIX

MEASURED LITVC ABLATION DATA

EST-6101 Q1 FM5504 FREON WS/WA=.0136 EI=2.5

STA	A/A*	TVC INFLUENCED B INCH (CM)	C INCH (CM)	D INCH (CM)	E INCH (CM)	F INCH (CM)
2	5.63	0.003	0.008	0.000	-0.001	0.013
		(0.007)	(0.019)	(0.000)	(-0.003)	(0.034)
4	4.61	-0.004	-0.004	-0.007	-0.014	-0.014
		(-0.010)	(-0.010)	(-0.017)	(-0.037)	(-0.037)
6	3.70	-0.010	-0.008	-0.014	-0.004	-0.004
		(-0.025)	(-0.020)	(-0.034)	(-0.010)	(-0.010)
7	3.28	0.017	0.011	0.015	0.036	0.019
		(0.042)	(0.028)	(0.037)	(0.091)	(0.049)
8	2.89	0.078	0.083	0.071	0.100	0.071
		(0.198)	(0.211)	(0.181)	(0.254)	(0.181)
9	2.52	0.165	0.145	0.136	0.145	0.141
		(0.418)	(0.369)	(0.345)	(0.369)	(0.357)
10	2.17	0.222	0.162	0.177	0.180	0.175
		(0.565)	(0.463)	(0.451)	(0.458)	(0.443)
11	1.86	0.256	0.216	0.212	0.216	0.208
		(0.651)	(0.549)	(0.539)	(0.549)	(0.529)

STA	A/A*	NON-TVC A INCH (CM)	G INCH (CM)	TVC AVE INCH (CM)	NON-TVC A-DOT IN/SEC (CM/SEC)	G-DOT IN/SEC (CM/SEC)	TVC AVE-DOT IN/SEC (CM/SEC)
2	5.63	0.030	-0.007	0.005	0.00136	-0.00031	0.00021
		(0.075)	(-0.017)	(0.012)	(0.00346)	(-0.00079)	(0.00053)
4	4.61	0.060	0.002	-0.009	0.00277	0.00008	-0.00040
		(0.153)	(0.005)	(-0.022)	(0.00703)	(0.00021)	(-0.00102)
6	3.70	0.091	0.065	-0.008	0.00417	0.00299	-0.00036
		(0.230)	(0.165)	(-0.020)	(0.01060)	(0.00759)	(-0.00091)
7	3.28	0.109	0.063	0.019	0.00503	0.00292	0.00090
		(0.277)	(0.161)	(0.049)	(0.01278)	(0.00742)	(0.00227)
8	2.89	0.143	0.085	0.081	0.00659	0.00391	0.00372
		(0.363)	(0.215)	(0.205)	(0.01675)	(0.00993)	(0.00946)
9	2.52	0.176	0.115	0.146	0.00811	0.00529	0.00675
		(0.447)	(0.292)	(0.372)	(0.02060)	(0.01345)	(0.01714)
10	2.17	0.223	0.144	0.187	0.01029	0.00664	0.00863
		(0.567)	(0.366)	(0.476)	(0.02613)	(0.01685)	(0.02193)
11	1.86	0.265	0.181	0.222	0.01220	0.00833	0.01022
		(0.673)	(0.459)	(0.563)	(0.03099)	(0.02116)	(0.02596)

EST-6101 Q3 FM5504 FREON WS/WA=.0246 EI=2.5

STA	A/A*	TVC INFLUENCED B INCH (CM)	C INCH (CM)	D INCH (CM)	E INCH (CM)	F INCH (CM)
2	5.63	-0.003 (-0.007)	0.003 (0.007)	-0.004 (-0.010)	-0.006 (-0.015)	0.001 (0.002)
4	4.61	-0.015 (-0.039)	-0.002 (-0.005)	-0.008 (-0.020)	-0.010 (-0.024)	-0.003 (-0.008)
6	3.70	0.004 (0.009)	0.024 (0.060)	0.009 (0.024)	-0.005 (-0.012)	0.016 (0.041)
7	3.28	0.027 (0.069)	0.053 (0.134)	0.036 (0.091)	0.010 (0.025)	0.039 (0.100)
8	2.89	0.098 (0.249)	0.117 (0.298)	0.111 (0.281)	0.066 (0.167)	0.095 (0.242)
9	2.52	0.132 (0.335)	0.153 (0.389)	0.144 (0.365)	0.139 (0.352)	0.153 (0.389)
10	2.17	0.166 (0.422)	0.181 (0.460)	0.183 (0.465)	0.179 (0.455)	0.189 (0.480)
11	1.86	0.198 (0.503)	0.206 (0.522)	0.211 (0.537)	0.217 (0.551)	0.235 (0.597)

STA	A/A*	NON-TVC A INCH (CM)	G INCH (CM)	TVC AVE INCH (CM)	NON-TVC A-DOT IN/SEC (CM/SEC)	G-DOT IN/SEC (CM/SEC)	TVC AVE-DOT IN/SEC (CM/SEC)
2	5.63	-0.008 (-0.020)	0.036 (0.092)	-0.002 (-0.004)	-0.00035 (-0.00090)	0.00167 (0.00424)	-0.00008 (-0.00021)
4	4.61	0.007 (0.017)	0.063 (0.160)	-0.008 (-0.019)	0.00030 (0.00077)	0.00290 (0.00737)	-0.00035 (-0.00088)
6	3.70	0.052 (0.133)	0.086 (0.218)	0.010 (0.024)	0.00241 (0.00613)	0.00395 (0.01004)	0.00044 (0.00112)
7	3.28	0.063 (0.161)	0.106 (0.270)	0.033 (0.084)	0.00292 (0.00742)	0.00490 (0.01245)	0.00152 (0.00386)
8	2.89	0.089 (0.225)	0.139 (0.354)	0.097 (0.247)	0.00408 (0.01038)	0.00642 (0.01630)	0.00449 (0.01140)
9	2.52	0.124 (0.316)	0.178 (0.452)	0.144 (0.366)	0.00573 (0.01456)	0.00820 (0.02082)	0.00664 (0.01687)
10	2.17	0.158 (0.402)	0.231 (0.586)	0.180 (0.456)	0.00730 (0.01853)	0.01064 (0.02703)	0.00828 (0.02103)
11	1.86	0.190 (0.483)	0.271 (0.690)	0.213 (0.542)	0.00877 (0.02227)	0.01251 (0.03177)	0.00983 (0.02498)

EST-6103 Q1 MXS198 FREON WS/WA=.0135 EI=2.5

STA	A/A*	TVC INFLUENCED B INCH (CM)	C INCH (CM)	D INCH (CM)	E INCH (CM)	F INCH (CM)
2	5.64	0.001	0.018	0.007	-0.001	-0.002
		(0.002)	(0.046)	(0.017)	(-0.003)	(-0.005)
4	4.63	-0.017	0.000	0.026	-0.001	-0.005
		(-0.043)	(0.001)	(0.066)	(-0.001)	(-0.014)
6	3.71	0.015	0.017	0.050	0.049	0.052
		(0.039)	(0.044)	(0.126)	(0.124)	(0.131)
7	3.29	0.069	0.046	0.069	0.069	0.120
		(0.174)	(0.116)	(0.176)	(0.176)	(0.305)
8	2.89	0.128	0.135	0.160	0.144	0.175
		(0.326)	(0.343)	(0.406)	(0.365)	(0.445)
9	2.52	0.194	0.209	0.208	0.201	0.197
		(0.493)	(0.532)	(0.527)	(0.510)	(0.500)
10	2.18	0.230	0.239	0.240	0.239	0.240
		(0.585)	(0.607)	(0.609)	(0.607)	(0.609)
11	1.86	0.261	0.259	0.246	0.269	0.263
		(0.662)	(0.657)	(0.626)	(0.684)	(0.667)

STA	A/A*	NON-TVC A INCH (CM)	G INCH (CM)	TVC AVE INCH (CM)	NON-TVC A-DOT IN/SEC (CM/SEC)	G-DOT IN/SEC (CM/SEC)	TVC AVE-DOT IN/SEC (CM/SEC)
2	5.64	-0.019	-0.028	0.004	-0.00090	-0.00130	0.00021
		(-0.049)	(-0.071)	(0.011)	(-0.00228)	(-0.00329)	(0.00052)
4	4.63	0.011	0.032	0.001	0.00051	0.00148	0.00004
		(0.028)	(0.081)	(0.002)	(0.00129)	(0.00377)	(0.00009)
6	3.71	0.055	0.078	0.036	0.00257	0.00364	0.00170
		(0.141)	(0.199)	(0.093)	(0.00654)	(0.00925)	(0.00431)
7	3.29	0.071	0.108	0.075	0.00332	0.00501	0.00347
		(0.181)	(0.273)	(0.190)	(0.00843)	(0.01272)	(0.00882)
8	2.89	0.119	0.163	0.149	0.00553	0.00757	0.00691
		(0.302)	(0.414)	(0.377)	(0.01405)	(0.01924)	(0.01755)
9	2.52	0.152	0.184	0.202	0.00708	0.00854	0.00939
		(0.386)	(0.466)	(0.513)	(0.01797)	(0.02170)	(0.02384)
10	2.18	0.185	0.224	0.238	0.00862	0.01040	0.01105
		(0.471)	(0.568)	(0.603)	(0.02190)	(0.02641)	(0.02806)
11	1.86	0.231	0.272	0.259	0.01074	0.01265	0.01207
		(0.587)	(0.691)	(0.659)	(0.02729)	(0.03214)	(0.03065)

TEST-6103 Q3 SP8030 FREON WS/WA=.0118 EI=2.5

TVC INFLUENCED

STA	A/A*	B INCH (CM)	C INCH (CM)	D INCH (CM)	E INCH (CM)	F INCH (CM)
2	5.63	0.037 (0.093)	0.032 (0.081)	0.032 (0.081)	0.032 (0.081)	0.023 (0.059)
4	4.62	0.029 (0.074)	0.038 (0.096)	0.036 (0.091)	0.040 (0.101)	0.029 (0.074)
6	3.70	0.046 (0.116)	0.067 (0.169)	0.048 (0.123)	0.063 (0.159)	0.044 (0.111)
7	3.29	0.062 (0.157)	0.095 (0.242)	0.067 (0.169)	0.088 (0.223)	0.082 (0.208)
8	2.89	0.116 (0.296)	0.148 (0.376)	0.124 (0.315)	0.142 (0.361)	0.133 (0.337)
9	2.52	0.187 (0.476)	0.192 (0.488)	0.197 (0.500)	0.198 (0.502)	0.180 (0.456)
10	2.18	0.247 (0.629)	0.247 (0.629)	0.246 (0.624)	0.247 (0.626)	0.243 (0.616)
11	1.86	0.250 (0.636)	0.262 (0.665)	0.269 (0.682)	0.260 (0.660)	0.256 (0.651)

STA	A/A*	NON-TVC A INCH (CM)	NON-TVC G INCH (CM)	TVC AVE INCH (CM)	NON-TVC A-DOT IN/SEC (CM/SEC)	NON-TVC G-DOT IN/SEC (CM/SEC)	TVC AVE-DOT IN/SEC (CM/SEC)
2	5.63	0.031 (0.079)	-0.008 (-0.021)	0.031 (0.079)	0.00144 (0.00365)	-0.00038 (-0.00097)	0.00145 (0.00368)
4	4.62	0.086 (0.220)	0.029 (0.074)	0.034 (0.087)	0.00402 (0.01022)	0.00136 (0.00345)	0.00160 (0.00406)
6	3.70	0.142 (0.361)	0.102 (0.259)	0.053 (0.136)	0.00661 (0.01678)	0.00474 (0.01204)	0.00249 (0.00631)
7	3.29	0.163 (0.414)	0.115 (0.293)	0.079 (0.200)	0.00759 (0.01928)	0.00537 (0.01363)	0.00366 (0.00930)
8	2.89	0.168 (0.427)	0.158 (0.400)	0.133 (0.337)	0.00782 (0.01985)	0.00733 (0.01861)	0.00617 (0.01568)
9	2.52	0.210 (0.534)	0.182 (0.463)	0.191 (0.484)	0.00977 (0.02483)	0.00849 (0.02155)	0.00887 (0.02252)
10	2.18	0.245 (0.621)	0.233 (0.592)	0.246 (0.625)	0.01138 (0.02890)	0.01084 (0.02754)	0.01144 (0.02906)
11	1.86	0.270 (0.687)	0.233 (0.592)	0.259 (0.659)	0.01258 (0.03195)	0.01085 (0.02755)	0.01207 (0.03065)

TEST=6104 Q1 FM5504 N204 WS/WA=.0135 EI=2.5,

STA	A/A*	TVC INFLUENCED B INCH (CM)	C INCH (CM)	D INCH (CM)	E INCH (CM)	F INCH (CM)
2	5.62	0.029 (0.073)	0.020 (0.051)	0.022 (0.056)	0.015 (0.039)	0.014 (0.034)
4	4.61	0.043 (0.110)	0.043 (0.110)	0.044 (0.112)	0.031 (0.078)	0.021 (0.054)
6	3.70	0.078 (0.198)	0.078 (0.198)	0.073 (0.186)	0.073 (0.186)	0.040 (0.101)
8	2.89	0.157 (0.399)	0.118 (0.300)	0.157 (0.399)	0.135 (0.344)	0.120 (0.305)
9	2.52	0.149 (0.379)	0.141 (0.357)	0.133 (0.338)	0.124 (0.316)	0.119 (0.301)
10	2.18	0.184 (0.468)	0.182 (0.463)	0.160 (0.407)	0.132 (0.335)	0.124 (0.315)
11	1.86	0.215 (0.547)	0.210 (0.535)	0.182 (0.462)	0.165 (0.418)	0.150 (0.382)

STA	A/A*	NON-TVC A INCH (CM)	G INCH (CM)	TVC AVE INCH (CM)	NON-TVC A-DOT IN/SEC (CM/SEC)	G-DOT IN/SEC (CM/SEC)	TVC AVE-DOT IN/SEC (CM/SEC)
2	5.62	0.005 (0.013)	0.001 (0.003)	0.020 (0.051)	0.00023 (0.00059)	0.00005 (0.00013)	0.00094 (0.00240)
4	4.61	0.041 (0.105)	0.039 (0.098)	0.037 (0.093)	0.00195 (0.00496)	0.00182 (0.00461)	0.00173 (0.00439)
6	3.70	0.057 (0.144)	0.060 (0.152)	0.068 (0.173)	0.00268 (0.00681)	0.00281 (0.00715)	0.00322 (0.00818)
8	2.89	0.116 (0.295)	0.088 (0.222)	0.138 (0.349)	0.00548 (0.01392)	0.00413 (0.01048)	0.00649 (0.01648)
9	2.52	0.148 (0.376)	0.122 (0.311)	0.133 (0.338)	0.00699 (0.01776)	0.00578 (0.01467)	0.00628 (0.01595)
10	2.18	0.187 (0.475)	0.164 (0.417)	0.160 (0.407)	0.00882 (0.02240)	0.00774 (0.01966)	0.00757 (0.01922)
11	1.86	0.228 (0.578)	0.209 (0.530)	0.184 (0.469)	0.01074 (0.02727)	0.00984 (0.02499)	0.00870 (0.02210)

TEST-6104 Q3 FM5504 N204 WS/WA=.0204 EI=2.5

STA	A/A*	TVC INFLUENCED B INCH (CM)	C INCH (CM)	D INCH (CM)	E INCH (CM)	F INCH (CM)
2	5.62	0.020	0.025	0.014	0.018	0.034
		(0.051)	(0.063)	(0.037)	(0.047)	(0.085)
4	4.61	0.040	0.044	0.031	0.038	0.047
		(0.103)	(0.112)	(0.078)	(0.095)	(0.120)
6	3.70	0.091	0.101	0.089	0.078	0.084
		(0.232)	(0.256)	(0.227)	(0.198)	(0.215)
7	3.29	0.103	0.126	0.123	0.120	0.112
		(0.262)	(0.320)	(0.313)	(0.306)	(0.284)
8	2.89	0.178	0.199	0.190	0.190	0.186
		(0.453)	(0.506)	(0.482)	(0.482)	(0.472)
9	2.52	0.148	0.177	0.164	0.181	0.177
		(0.376)	(0.449)	(0.418)	(0.459)	(0.449)
10	2.18	0.172	0.176	0.176	0.179	0.185
		(0.436)	(0.448)	(0.446)	(0.456)	(0.470)
11	1.86	0.205	0.199	0.207	0.209	0.212
		(0.520)	(0.505)	(0.525)	(0.530)	(0.539)

STA	A/A*	NON-TVC A INCH (CM)	G INCH (CM)	TVC AVE INCH (CM)	NON-TVC A-DOT IN/SEC (CM/SEC)	G-DOT IN/SEC (CM/SEC)	TVC AVE-DOT IN/SEC (CM/SEC)
2	5.62	-0.004	0.015	0.022	-0.00017	0.00073	0.00105
		(-0.009)	(0.039)	(0.057)	(-0.00044)	(0.00185)	(0.00267)
4	4.61	0.031	0.045	0.040	0.00146	0.00213	0.00189
		(0.078)	(0.115)	(0.102)	(0.00370)	(0.00542)	(0.00480)
6	3.70	0.052	0.076	0.089	0.00245	0.00358	0.00418
		(0.132)	(0.193)	(0.225)	(0.00623)	(0.00909)	(0.01063)
7	3.29	0.066	0.090	0.117	0.00311	0.00424	0.00552
		(0.168)	(0.228)	(0.297)	(0.00790)	(0.01076)	(0.01401)
8	2.89	0.099	0.114	0.189	0.00467	0.00539	0.00889
		(0.251)	(0.290)	(0.479)	(0.01186)	(0.01369)	(0.02259)
9	2.52	0.129	0.144	0.169	0.00609	0.00681	0.00799
		(0.328)	(0.367)	(0.430)	(0.01547)	(0.01730)	(0.02030)
10	2.18	0.154	0.178	0.178	0.00724	0.00841	0.00838
		(0.390)	(0.453)	(0.451)	(0.01840)	(0.02137)	(0.02128)
11	1.86	0.197	0.216	0.206	0.00930	0.01020	0.00973
		(0.501)	(0.549)	(0.524)	(0.02361)	(0.02590)	(0.02471)

TEST-6106 Q1 MXS198 N204 WS/WA=.013 EI=2.5

STA	A/A*	TVC INFLUENCED B INCH (CM)	C INCH (CM)	D INCH (CM)	E INCH (CM)	F INCH (CM)
2	5.63	0.068	0.047	0.044	0.040	0.030
		(0.173)	(0.120)	(0.112)	(0.100)	(0.076)
4	4.62	0.082	0.080	0.089	0.081	0.062
		(0.208)	(0.203)	(0.227)	(0.205)	(0.157)
6	3.70	0.111	0.137	0.138	0.137	0.090
		(0.281)	(0.349)	(0.351)	(0.349)	(0.230)
7	3.29	0.167	0.172	0.160	0.148	0.106
		(0.424)	(0.436)	(0.407)	(0.376)	(0.269)
8	2.89	0.237	0.252	0.221	0.201	0.150
		(0.601)	(0.640)	(0.560)	(0.512)	(0.381)
9	2.52	0.195	0.199	0.184	0.170	0.164
		(0.495)	(0.505)	(0.468)	(0.432)	(0.417)
10	2.18	0.246	0.223	0.213	0.208	0.206
		(0.624)	(0.566)	(0.541)	(0.529)	(0.524)
11	1.86	0.262	0.250	0.240	0.230	0.230
		(0.665)	(0.636)	(0.609)	(0.585)	(0.585)

STA	A/A*	NON-TVC A INCH (CM)	G INCH (CM)	TVC AVE INCH (CM)	NON-TVC A-DOT IN/SEC (CM/SEC)	G-DOT IN/SEC (CM/SEC)	TVC AVE-DOT IN/SEC (CM/SEC)
2	5.63	-0.003	-0.007	0.046	-0.00017	-0.00035	0.00221
		(-0.009)	(-0.019)	(0.116)	(-0.00043)	(-0.00089)	(0.00562)
4	4.62	0.034	0.020	0.079	0.00164	0.00095	0.00380
		(0.086)	(0.050)	(0.200)	(0.00417)	(0.00241)	(0.00965)
6	3.70	0.100	0.086	0.123	0.00483	0.00414	0.00593
		(0.254)	(0.218)	(0.312)	(0.01228)	(0.01052)	(0.01506)
7	3.29	0.138	0.089	0.151	0.00668	0.00428	0.00727
		(0.351)	(0.225)	(0.382)	(0.01697)	(0.01088)	(0.01847)
8	2.89	0.171	0.148	0.212	0.00826	0.00715	0.01025
		(0.434)	(0.376)	(0.539)	(0.02097)	(0.01816)	(0.02603)
9	2.52	0.219	0.186	0.182	0.01057	0.00900	0.00881
		(0.556)	(0.473)	(0.463)	(0.02684)	(0.02285)	(0.02239)
10	2.18	0.286	0.240	0.219	0.01380	0.01159	0.01059
		(0.726)	(0.609)	(0.557)	(0.03505)	(0.02943)	(0.02690)
11	1.86	0.210	0.262	0.243	0.01016	0.01265	0.01172
		(0.534)	(0.665)	(0.616)	(0.02581)	(0.03213)	(0.02977)

TEST=6106 Q3 SP8030 N204 WS/WA=.012 EI=2.5

STA	A/A*	TVC INFLUENCED B INCH (CM)	C INCH (CM)	D INCH (CM)	E INCH (CM)	F INCH (CM)
2	5.64	0.058	0.058	0.056	0.055	0.052
		(0.148)	(0.148)	(0.143)	(0.140)	(0.133)
4	4.63	0.090	0.095	0.102	0.083	0.091
		(0.229)	(0.241)	(0.258)	(0.212)	(0.231)
6	3.71	0.145	0.153	0.153	0.143	0.138
		(0.369)	(0.388)	(0.388)	(0.364)	(0.352)
7	3.29	0.175	0.166	0.173	0.147	0.158
		(0.446)	(0.421)	(0.438)	(0.373)	(0.402)
8	2.89	0.215	0.224	0.223	0.194	0.215
		(0.547)	(0.569)	(0.566)	(0.494)	(0.547)
9	2.52	0.191	0.187	0.169	0.173	0.176
		(0.486)	(0.474)	(0.430)	(0.440)	(0.447)
10	2.18	0.204	0.214	0.207	0.203	0.210
		(0.517)	(0.544)	(0.527)	(0.514)	(0.534)
11	1.86	0.241	0.240	0.244	0.234	0.253
		(0.613)	(0.609)	(0.621)	(0.594)	(0.643)

STA	A/A*	NON-TVC A INCH (CM)	G INCH (CM)	TVC AVE INCH (CM)	NON-TVC A-DOT IN/SEC (CM/SEC)	G-DOT IN/SEC (CM/SEC)	TVC AVE-DOT IN/SEC (CM/SEC)
2	5.64	0.017	0.014	0.056	0.00082	0.00068	0.00270
		(0.043)	(0.036)	(0.142)	(0.00209)	(0.00174)	(0.00687)
4	4.63	0.058	0.081	0.092	0.00279	0.00389	0.00446
		(0.147)	(0.205)	(0.234)	(0.00708)	(0.00989)	(0.01132)
6	3.71	0.117	0.133	0.146	0.00567	0.00641	0.00708
		(0.298)	(0.337)	(0.372)	(0.01441)	(0.01628)	(0.01797)
7	3.29	0.143	0.146	0.164	0.00691	0.00705	0.00791
		(0.363)	(0.371)	(0.416)	(0.01755)	(0.01790)	(0.02010)
8	2.89	0.148	0.171	0.214	0.00713	0.00828	0.01036
		(0.375)	(0.435)	(0.545)	(0.01811)	(0.02104)	(0.02631)
9	2.52	0.186	0.203	0.179	0.00896	0.00980	0.00866
		(0.471)	(0.515)	(0.455)	(0.02277)	(0.02488)	(0.02200)
10	2.18	0.212	0.222	0.208	0.01025	0.01071	0.01002
		(0.539)	(0.563)	(0.527)	(0.02603)	(0.02720)	(0.02546)
11	1.86	0.237	0.258	0.242	0.01144	0.01245	0.01171
		(0.601)	(0.655)	(0.616)	(0.02905)	(0.03163)	(0.02975)

TEST-6107 Q1 SP8030 WS/WA=.0447 EI=2.5

STA	A/A*	TVC INFLUENCED B INCH (CM)	C INCH (CM)	D INCH (CM)	E INCH (CM)	F INCH (CM)
2	5.64	-0.026 (-0.067)	-0.025 (-0.062)	0.009 (0.023)	-0.017 (-0.043)	-0.015 (-0.038)
4	4.62	-0.001 (-0.004)	0.013 (0.033)	0.013 (0.033)	-0.001 (-0.004)	0.008 (0.021)
5	4.15	0.015 (0.038)	0.034 (0.086)	0.005 (0.013)	0.010 (0.026)	0.020 (0.050)
6	3.70	0.036 (0.091)	0.062 (0.157)	0.012 (0.031)	0.031 (0.079)	0.036 (0.091)
7	3.28	0.067 (0.169)	0.223 (0.566)	0.194 (0.494)	0.215 (0.547)	0.171 (0.435)
8	2.89	0.145 (0.368)	0.169 (0.430)	0.173 (0.440)	0.176 (0.447)	0.203 (0.515)
9	2.52	0.166 (0.422)	0.207 (0.527)	0.203 (0.514)	0.210 (0.534)	0.222 (0.563)
10	2.17	0.201 (0.512)	0.244 (0.621)	0.234 (0.594)	0.253 (0.643)	0.258 (0.655)

STA	A/A*	NON-TVC A INCH (CM)	G INCH (CM)	TVC AVE INCH (CM)	NON-TVC A-DOT IN/SEC (CM/SEC)	G-DOT IN/SEC (CM/SEC)	TVC AVE-DOT IN/SEC (CM/SEC)
2	5.64	-0.087 (-0.220)	0.004 (0.010)	-0.015 (-0.038)	-0.00358 (-0.00909)	0.00017 (0.00043)	-0.00061 (-0.00155)
4	4.62	0.084 (0.215)	0.013 (0.033)	0.006 (0.016)	0.00349 (0.00887)	0.00053 (0.00135)	0.00026 (0.00065)
5	4.15	0.091 (0.232)	0.034 (0.086)	0.017 (0.043)	0.00377 (0.00958)	0.00140 (0.00356)	0.00069 (0.00176)
6	3.70	0.108 (0.273)	0.060 (0.152)	0.035 (0.090)	0.00444 (0.01129)	0.00247 (0.00628)	0.00146 (0.00371)
7	3.28	0.105 (0.266)	1.709 (4.341)	0.067 (0.169)	0.00433 (0.01100)	0.07063 (0.17939)	0.00275 (0.00699)
8	2.89	0.135 (0.344)	1.897 (4.819)	0.145 (0.368)	0.00560 (0.01421)	0.07840 (0.19915)	0.00599 (0.01521)
9	2.52	0.176 (0.446)	2.086 (5.297)	0.166 (0.422)	0.00726 (0.01843)	0.08618 (0.21890)	0.00686 (0.01743)
10	2.17	0.221 (0.560)	2.274 (5.775)	0.201 (0.512)	0.00911 (0.02315)	0.09396 (0.23865)	0.00832 (0.02114)

TEST-6017 Q3 SP8030 N204 WS/WA=.0426 FI=3.5

STA	A/A*	TVC INFLUENCED B INCH (CM)	C INCH (CM)	D INCH (CM)	E INCH (CM)	F INCH (CM)
2	5.64	0.039	0.028	0.023	0.030	0.042
		(0.100)	(0.071)	(0.059)	(0.076)	(0.107)
3	5.12	0.051	0.020	0.050	0.047	0.060
		(0.130)	(0.052)	(0.127)	(0.120)	(0.151)
4	4.62	0.075	0.043	0.070	0.063	0.088
		(0.190)	(0.110)	(0.178)	(0.161)	(0.224)
5	4.15	0.091	0.059	0.101	0.036	0.141
		(0.232)	(0.149)	(0.256)	(0.217)	(0.358)
6	3.70	0.133	0.117	0.155	0.131	0.184
		(0.339)	(0.297)	(0.394)	(0.334)	(0.467)
7	3.28	0.124	0.135	0.127	0.143	0.133
		(0.315)	(0.344)	(0.322)	(0.363)	(0.339)
8	2.89	0.166	0.207	0.203	0.210	0.222
		(0.422)	(0.527)	(0.514)	(0.534)	(0.563)
9	2.52	0.201	0.244	0.234	0.253	0.258
		(0.512)	(0.621)	(0.594)	(0.643)	(0.655)
10	2.17	0.000	0.000	0.000	0.000	0.000
		(0.000)	(0.000)	(0.000)	(0.000)	(0.000)

STA	A/A*	NON-TVC A INCH (CM)	G INCH (CM)	TVC AVE INCH (CM)	NON-TVC A-DOT IN/SEC (CM/SEC)	G-DOT IN/SEC (CM/SEC)	TVC AVE-DOT IN/SEC (CM/SEC)
2	5.64	0.004	0.023	0.033	0.00017	0.00096	0.00135
		(0.010)	(0.059)	(0.083)	(0.00043)	(0.00244)	(0.00342)
3	5.12	0.011	0.059	0.046	0.00045	0.00242	0.00189
		(0.028)	(0.149)	(0.116)	(0.00114)	(0.00615)	(0.00479)
4	4.62	0.018	0.084	0.068	0.00073	0.00349	0.00281
		(0.045)	(0.215)	(0.173)	(0.00185)	(0.00887)	(0.00714)
5	4.15	0.044	0.091	0.095	0.00184	0.00377	0.00394
		(0.113)	(0.232)	(0.242)	(0.00467)	(0.00958)	(0.01002)
6	3.70	0.069	0.098	0.144	0.00287	0.00405	0.00596
		(0.176)	(0.249)	(0.366)	(0.00728)	(0.01029)	(0.01514)
7	3.28	1.709	0.114	0.132	0.07063	0.00472	0.00547
		(4.341)	(0.290)	(0.336)	(0.17939)	(0.01200)	(0.01390)
8	2.89	1.897	0.150	0.000	0.07840	0.00619	0.00000
		(4.819)	(0.380)	(0.000)	(0.19915)	(0.01572)	(0.00000)
9	2.52	2.086	0.193	0.000	0.08618	0.00797	0.00000
		(5.297)	(0.490)	(0.000)	(0.21890)	(0.02023)	(0.00000)
10	2.17	2.274	0.232	0.000	0.09396	0.00959	0.00000
		(5.775)	(0.589)	(0.000)	(0.23865)	(0.02435)	(0.00000)

TEST-6108 Q1 MXS198 N204 WS/WA=.0435 EI=2.5

STA	A/A*	TVC INFLUENCED B INCH (CM)	C INCH (CM)	D INCH (CM)	E INCH (CM)	F INCH (CM)
2	5.65	-0.046	0.000	0.000	-0.014	-0.027
		(-0.116)	(0.000)	(0.000)	(-0.036)	(-0.068)
4	4.63	-0.053	-0.024	0.002	-0.007	0.004
		(-0.134)	(-0.061)	(0.004)	(-0.018)	(0.009)
5	4.16	-0.048	-0.025	-0.018	-0.008	0.025
		(-0.121)	(-0.063)	(-0.046)	(-0.019)	(0.063)
6	3.71	-0.025	-0.015	-0.010	-0.001	0.055
		(-0.062)	(-0.038)	(-0.026)	(-0.002)	(0.139)
7	3.29	0.039	0.087	0.003	0.059	0.150
		(0.098)	(0.222)	(0.009)	(0.149)	(0.380)
8	2.89	0.139	0.195	0.123	0.154	0.237
		(0.354)	(0.495)	(0.313)	(0.390)	(0.601)
9	2.52	0.297	0.345	0.354	0.345	0.324
		(0.755)	(0.876)	(0.900)	(0.876)	(0.823)

STA	A/A*	NON-TVC A INCH (CM)	G INCH (CM)	TVC AVE INCH (CM)	NON-TVC A-DOT IN/SEC (CM/SEC)	G-DOT IN/SEC (CM/SEC)	TVC AVE-DOT IN/SEC (CM/SEC)
2	5.65	-0.032	0.010	-0.017	-0.00131	0.00039	-0.00070
		(-0.082)	(0.024)	(-0.044)	(-0.00333)	(0.00099)	(-0.00178)
4	4.63	0.000	0.012	-0.016	-0.00001	0.00049	-0.00064
		(-0.001)	(0.031)	(-0.040)	(-0.00003)	(0.00124)	(-0.00162)
5	4.16	0.021	0.031	-0.015	0.00085	0.00124	-0.00060
		(0.053)	(0.078)	(-0.037)	(0.00216)	(0.00314)	(-0.00152)
6	3.71	0.063	0.066	0.001	0.00256	0.00268	0.00003
		(0.161)	(0.168)	(0.002)	(0.00651)	(0.00680)	(0.00009)
7	3.29	0.113	0.099	0.068	0.00458	0.00400	0.00274
		(0.288)	(0.251)	(0.172)	(0.01164)	(0.01017)	(0.00695)
8	2.89	0.171	0.166	0.169	0.00692	0.00672	0.00686
		(0.434)	(0.422)	(0.430)	(0.01757)	(0.01707)	(0.01743)
9	2.52	0.283	0.299	0.333	0.01145	0.01211	0.01348
		(0.718)	(0.760)	(0.846)	(0.02908)	(0.03075)	(0.03425)

TEST-6108 Q3 MXS198 N204 WS/WA=.0449 EI=3.5

STA	A/A*	TVC INFLUENCED B INCH (CM)	C INCH (CM)	D INCH (CM)	E INCH (CM)	F INCH (CM)
2	5.65	-0.017	-0.043	-0.010	-0.007	-0.011
		(-0.043)	(-0.109)	(-0.026)	(-0.017)	(-0.029)
4	4.63	0.043	-0.019	-0.005	0.004	0.033
		(0.108)	(-0.049)	(-0.013)	(0.011)	(0.084)
5	4.16	0.088	0.045	-0.017	0.047	0.074
		(0.223)	(0.114)	(-0.044)	(0.119)	(0.187)
6	3.71	0.138	0.121	0.079	0.097	0.140
		(0.350)	(0.306)	(0.200)	(0.246)	(0.355)
7	3.29	0.154	0.164	0.157	0.171	0.178
		(0.392)	(0.416)	(0.399)	(0.436)	(0.453)
8	2.89	0.176	0.214	0.229	0.228	0.229
		(0.446)	(0.543)	(0.582)	(0.579)	(0.582)
9	2.52	0.307	0.383	0.412	0.345	0.335
		(0.779)	(0.973)	(1.046)	(0.876)	(0.852)

STA	A/A*	NON-TVC A INCH (CM)	G INCH (CM)	TVC AVE INCH (CM)	NON-TVC A-DOT IN/SEC (CM/SEC)	G-DOT IN/SEC (CM/SEC)	TVC AVE-DOT IN/SEC (CM/SEC)
2	5.65	0.000	-0.024	-0.018	0.00000	-0.00096	-0.00072
		(0.000)	(-0.060)	(-0.045)	(0.00001)	(-0.00245)	(-0.00182)
4	4.63	0.004	0.014	0.011	0.00018	0.00057	0.00045
		(0.011)	(0.036)	(0.028)	(0.00046)	(0.00144)	(0.00115)
5	4.16	0.007	0.037	0.047	0.00027	0.00151	0.00191
		(0.017)	(0.095)	(0.120)	(0.00068)	(0.00383)	(0.00485)
6	3.71	0.046	0.082	0.115	0.00187	0.00334	0.00464
		(0.117)	(0.209)	(0.291)	(0.00474)	(0.00847)	(0.01179)
7	3.29	0.083	0.130	0.165	0.00335	0.00528	0.00668
		(0.210)	(0.331)	(0.419)	(0.00850)	(0.01341)	(0.01697)
8	2.89	0.135	0.214	0.215	0.00545	0.00866	0.00871
		(0.342)	(0.543)	(0.546)	(0.01383)	(0.02198)	(0.02212)
9	2.52	0.259	0.279	0.356	0.01048	0.01130	0.01443
		(0.658)	(0.709)	(0.905)	(0.02663)	(0.02869)	(0.03665)

TEST-6109 01 FM5272 N204 WS/WA=.0435 EI=2.5

STA	A/A*	TVC INFLUENCED B INCH (CM)	C INCH (CM)	D INCH (CM)	E INCH (CM)	F INCH (CM)
2	5.64	0.240 (0.611)	0.281 (0.713)	0.276 (0.701)	0.300 (0.761)	0.252 (0.640)
4	4.63	0.284 (0.721)	0.317 (0.806)	0.351 (0.891)	0.349 (0.886)	0.301 (0.765)
5	4.15	0.281 (0.714)	0.324 (0.823)	0.376 (0.956)	0.357 (0.908)	0.324 (0.823)
6	3.71	0.278 (0.706)	0.321 (0.815)	0.378 (0.960)	0.364 (0.924)	0.352 (0.895)
7	3.29	0.275 (0.698)	0.294 (0.746)	0.356 (0.904)	0.342 (0.868)	0.366 (0.928)
8	2.89	0.341 (0.867)	0.362 (0.921)	0.367 (0.933)	0.358 (0.908)	0.420 (1.066)
9	2.52	0.498 (1.265)	0.464 (1.180)	0.527 (1.337)	0.507 (1.289)	0.486 (1.235)
10	2.18	0.500 (1.269)	0.552 (1.402)	0.552 (1.402)	0.533 (1.354)	0.457 (1.160)

STA	A/A*	NON-TVC A INCH (CM)	G INCH (CM)	TVC AVE INCH (CM)	NON-TVC A-DOT IN/SEC (CM/SEC)	G-DOT IN/SEC (CM/SEC)	TVC AVE-DOT IN/SEC (CM/SEC)
2	5.64	0.071 (0.179)	0.099 (0.252)	0.270 (0.685)	0.00285 (0.00725)	0.00401 (0.01020)	0.01092 (0.02774)
4	4.63	0.079 (0.200)	0.093 (0.236)	0.320 (0.814)	0.00319 (0.00809)	0.00377 (0.00956)	0.01298 (0.03296)
5	4.15	0.123 (0.313)	0.138 (0.350)	0.333 (0.845)	0.00499 (0.01269)	0.00557 (0.01416)	0.01346 (0.03419)
6	3.71	0.278 (0.706)	0.230 (0.585)	0.339 (0.860)	0.01125 (0.02857)	0.00932 (0.02366)	0.01371 (0.03482)
7	3.29	0.313 (0.795)	0.318 (0.807)	0.326 (0.829)	0.01267 (0.03219)	0.01287 (0.03268)	0.01321 (0.03356)
8	2.89	0.391 (0.993)	0.482 (1.224)	0.370 (0.939)	0.01583 (0.04022)	0.01951 (0.04955)	0.01497 (0.03802)
9	2.52	0.441 (1.119)	0.517 (1.313)	0.497 (1.261)	0.01784 (0.04530)	0.02093 (0.05316)	0.02010 (0.05106)
10	2.18	0.428 (1.087)	2.271 (5.769)	0.519 (1.317)	0.01733 (0.04401)	0.09195 (0.23354)	0.02100 (0.05334)

TEST=6109 Q3 FM5272 N204 WS/WA=.0457 EI=3.5

STA	A/A*	TVC INFLUENCED B INCH (CM)	C INCH (CM)	D INCH (CM)	E INCH (CM)	F INCH (CM)
2	5.64	0.309	0.247	0.290	0.286	0.311
		(0.786)	(0.628)	(0.737)	(0.727)	(0.790)
4	4.63	0.383	0.260	0.410	0.301	0.288
		(0.974)	(0.661)	(1.042)	(0.765)	(0.731)
5	4.15	0.343	0.278	0.460	0.327	0.265
		(0.871)	(0.706)	(1.167)	(0.830)	(0.672)
6	3.71	0.289	0.316	0.437	0.348	0.292
		(0.735)	(0.803)	(1.111)	(0.883)	(0.742)
7	3.29	0.351	0.463	0.523	0.389	0.370
		(0.892)	(1.176)	(1.329)	(0.989)	(0.941)
8	2.89	0.425	0.434	0.520	0.453	0.415
		(1.078)	(1.103)	(1.321)	(1.151)	(1.054)
9	2.52	0.431	0.441	0.507	0.479	0.460
		(1.095)	(1.119)	(1.289)	(1.216)	(1.168)
10	2.18	0.437	0.437	0.495	0.485	0.418
		(1.111)	(1.111)	(1.257)	(1.232)	(1.063)

STA	A/A*	NON-TVC A INCH (CM)	G INCH (CM)	TVC AVE INCH (CM)	NON-TVC A-DOT IN/SEC (CM/SEC)	G-DOT IN/SEC (CM/SEC)	TVC AVE-DOT IN/SEC (CM/SEC)
2	5.64	0.004	0.042	0.289	0.00015	0.00169	0.01169
		(0.009)	(0.106)	(0.734)	(0.00038)	(0.00430)	(0.02970)
4	4.63	0.249	0.078	0.329	0.01007	0.00315	0.01330
		(0.632)	(0.197)	(0.834)	(0.02557)	(0.00799)	(0.03378)
5	4.15	0.343	0.123	0.334	0.01389	0.00499	0.01354
		(0.871)	(0.313)	(0.849)	(0.03527)	(0.01269)	(0.03439)
6	3.71	0.373	0.216	0.337	0.01512	0.00874	0.01362
		(0.948)	(0.548)	(0.855)	(0.03840)	(0.02219)	(0.03460)
7	3.29	0.480	0.313	0.419	0.01944	0.01267	0.01698
		(1.220)	(0.795)	(1.065)	(0.04937)	(0.03219)	(0.04313)
8	2.89	0.530	0.405	0.449	0.02144	0.01641	0.01819
		(1.345)	(1.030)	(1.141)	(0.05446)	(0.04169)	(0.04621)
9	2.52	0.536	0.450	0.463	0.02170	0.01822	0.01876
		(1.362)	(1.143)	(1.177)	(0.05512)	(0.04629)	(0.04766)
10	2.18	0.543	0.395	0.455	0.02196	0.01597	0.01841
		(1.378)	(1.002)	(1.155)	(0.05579)	(0.04057)	(0.04676)

TEST-6110 Q1 FM5272 N204 WS/WA=.0137 EI=2,5 (P=750)

STA	A/A*	TVC INFLUENCED B INCH (CM)	C INCH (CM)	D INCH (CM)	E INCH (CM)	F INCH (CM)
2	5.64	0.639	0.489	0.502	0.517	0.483
		(1.623)	(1.242)	(1.276)	(1.314)	(1.227)
4	4.63	0.657	0.665	0.720	0.591	0.560
		(1.670)	(1.689)	(1.828)	(1.500)	(1.423)
5	4.16	0.657	0.698	0.777	0.618	0.585
		(1.668)	(1.773)	(1.974)	(1.569)	(1.486)
6	3.71	0.631	0.669	0.660	0.615	0.568
		(1.603)	(1.701)	(1.676)	(1.562)	(1.443)
7	3.29	0.617	0.633	0.702	0.593	0.548
		(1.568)	(1.609)	(1.784)	(1.507)	(1.391)
8	2.90	0.596	0.584	0.641	0.575	0.536
		(1.513)	(1.484)	(1.629)	(1.459)	(1.362)
9	2.53	0.434	0.485	0.487	0.485	0.482
		(1.103)	(1.232)	(1.237)	(1.232)	(1.225)
10	2.18	0.424	0.439	0.447	0.434	0.449
		(1.077)	(1.114)	(1.136)	(1.102)	(1.141)

STA	A/A*	NON-TVC A INCH (CM)	G INCH (CM)	TVC AVE INCH (CM)	NON-TVC A-DOT IN/SEC (CM/SEC)	G-DOT IN/SEC (CM/SEC)	TVC AVE-DOT IN/SEC (CM/SEC)
2	5.64	0.066	0.059	0.526	0.00268	0.00241	0.02147
		(0.167)	(0.150)	(1.336)	(0.00682)	(0.00613)	(0.05454)
4	4.63	0.046	0.068	0.639	0.00189	0.00279	0.02606
		(0.118)	(0.173)	(1.622)	(0.00480)	(0.00708)	(0.06620)
5	4.16	0.043	0.138	0.667	0.00174	0.00564	0.02722
		(0.109)	(0.351)	(1.694)	(0.00443)	(0.01433)	(0.06914)
6	3.71	0.178	0.243	0.629	0.00725	0.00990	0.02567
		(0.451)	(0.616)	(1.597)	(0.01842)	(0.02515)	(0.06519)
7	3.29	0.272	0.335	0.619	0.01112	0.01366	0.02526
		(0.692)	(0.850)	(1.572)	(0.02825)	(0.03469)	(0.06415)
8	2.90	0.347	0.409	0.586	0.01417	0.01671	0.02393
		(0.882)	(1.040)	(1.489)	(0.03600)	(0.04244)	(0.06079)
9	2.53	0.385	0.449	0.475	0.01571	0.01832	0.01938
		(0.977)	(1.140)	(1.206)	(0.03989)	(0.04652)	(0.04922)
10	2.18	0.388	0.449	0.439	0.01583	0.01833	0.01790
		(0.985)	(1.141)	(1.114)	(0.04022)	(0.04655)	(0.04546)

TEST-6110 03 FM5272 N204 WS/WA=.0137 EI=2.5 (P=280)

STA	A/A*	TVC INFLUENCED B INCH (CM)	C INCH (CM)	D INCH (CM)	E INCH (CM)	F INCH (CM)
2	5.64	0.242 (0.616)	0.244 (0.621)	0.267 (0.679)	0.376 (0.955)	0.398 (1.011)
4	4.63	0.364 (0.925)	0.320 (0.814)	0.383 (0.974)	0.455 (1.156)	0.471 (1.197)
5	4.16	0.401 (1.018)	0.358 (0.909)	0.435 (1.106)	0.490 (1.244)	0.481 (1.222)
6	3.71	0.441 (1.121)	0.391 (0.992)	0.483 (1.227)	0.521 (1.322)	0.499 (1.266)
7	3.29	0.473 (1.202)	0.454 (1.153)	0.521 (1.323)	0.540 (1.371)	0.513 (1.303)
8	2.90	0.503 (1.277)	0.514 (1.307)	0.529 (1.343)	0.541 (1.374)	0.522 (1.326)
9	2.53	0.501 (1.273)	0.530 (1.346)	0.495 (1.256)	0.481 (1.222)	0.509 (1.293)
10	2.18	0.472 (1.199)	0.467 (1.187)	0.434 (1.102)	0.463 (1.177)	0.453 (1.150)

STA	A/A*	NON-TVC A INCH (CM)	G INCH (CM)	TVC AVE INCH (CM)	NON-TVC A-DOT IN/SEC (CM/SEC)	G-DOT IN/SEC (CM/SEC)	TVC AVE-DOT IN/SEC (CM/SEC)
2	5.64	-0.016 (-0.042)	0.039 (0.099)	0.306 (0.776)	-0.00067 (-0.00169)	0.00159 (0.00405)	0.01248 (0.03169)
4	4.63	0.046 (0.118)	0.075 (0.190)	0.399 (1.013)	0.00189 (0.00480)	0.00306 (0.00777)	0.01628 (0.04135)
5	4.16	0.079 (0.201)	0.119 (0.303)	0.433 (1.100)	0.00323 (0.00819)	0.00486 (0.01235)	0.01767 (0.04489)
6	3.71	0.215 (0.546)	0.225 (0.573)	0.467 (1.186)	0.00877 (0.02228)	0.00920 (0.02337)	0.01905 (0.04840)
7	3.29	0.320 (0.813)	0.325 (0.826)	0.500 (1.270)	0.01307 (0.03320)	0.01327 (0.03370)	0.02041 (0.05185)
8	2.90	0.422 (1.071)	0.406 (1.032)	0.522 (1.325)	0.01721 (0.04372)	0.01659 (0.04214)	0.02130 (0.05410)
9	2.53	0.447 (1.135)	0.428 (1.086)	0.503 (1.278)	0.01824 (0.04633)	0.01746 (0.04435)	0.02054 (0.05217)
10	2.18	0.419 (1.065)	0.412 (1.046)	0.458 (1.163)	0.01712 (0.04348)	0.01681 (0.04269)	0.01869 (0.04746)